DAM-BREAK SOLUTIONS FOR A PARTIAL BREACH

A thesis

submitted in partial fulfilment

of the requirements for the Degree

of

Doctor of Philosophy in Civil Engineering

at the

University of Canterbury

by

Salahudin Gozali

University of Canterbury
Christchurch, New Zealand

May 1991

ABSTRACT

Four different numerical models are developed to simulate the flow resulting from a breached dam. The models are a level-reservoir-approximation model, an explicit method-of-characteristics model, an implicit method-of-characteristics model and a linearized implicit finite-difference model. The first model is based upon the storage form of the continuity equation, and the other models are based upon the complete St. Venant equations.

Laboratory experiments are performed to investigate the flow characteristics and to verify the validity of the numerical models. Comparisons between model results and experiment are used to evaluate the accuracy of the numerical models. These comparisons show that the explicit method-of-characteristics model always gives a more accurate solution than the other models. Computational problems, computer requirements and model robustness are also evaluated to assess ease-of-use of the models.

Finally, the experimental and numerical results were used to construct a simplified numerical model to compute dam-break outflow hydrographs. The outflow hydrographs computed by this simplified model agree relatively closely with the corresponding results computed by the explicit method-of-characteristics model for any breach size. This suggests that the simplified model can be used for a wide range of breach sizes and gives a maximum practical level of accuracy.

ACKNOWLEDGEMENTS

The research presented herein was conducted in the Department of Civil Engineering, University of Canterbury.

First and foremost, I would like to thank my supervisor Dr. B.W. Hunt for his invaluable supervision, helpful guidance and encouragement throughout this study.

My gratitude is also extended to Dr. M.G. Webby for his friendly advice and help.

I am also grateful to the technical staff of the Civil Engineering Department for their contribution to this project. Mr. Alan Poynter who skilfully constructed the laboratory equipments that were used for the experimental work, Mr. Ian Sheppard who was also involved in the technical aspects of the work. Their friendship and help is appreciated.

My thanks to Mr. Gordon Grey for his electronic expertise, Mrs. Val Grey for skilfully drawing some of the figures and Mr. Lionel Gardner for developing the photographs.

I would like to thank my wife, Nila Liswara, for her love, patience, understanding, encouragement and constant support during the past years.

I wish to express my deep gratitude to my parents for their constant support and encouragement.

Finally, I would like to thank the Parahyangan Catholic University, Bandung, Indonesia, for providing the scholarship which enabled me to study in New Zealand.

TABLE OF CONTENTS

CHAPTER			Page
ABSTRACT			i
ACKNOWLEDGMENTS			ii
TABLE OF CONTENTS			iii
LIST OF FIGURES			vi
1.	INTRODUCTION		1
	1.1	Thesis Objective	2
	1.2	Thesis Outline	4
2.	LITERATURE REVIEW		
	2.1	Introduction	5
	2.2	Dam-Break Flood Models for Total Failure	6
	2.3	Dam-Break Flood Models for Partial Failure	9
	2.4	Conclusions	14
3.	ANALYSIS OF UNSTEADY FLOW IN A RESERVOIR		
	3.1	Introduction	15
	3.2	Simplified Routing Analysis	16
	3.3	Dynamic Routing Analysis	20
		3.3.1 Method of Characteristics	23
		(a) Explicit Schemes	27
		(b) Implicit Schemes	30
		3.3.2 Preissmann Finite-Difference Scheme	34
	3.4	Surge Analysis	37

4. MODEL DEVELOPMENT

4.1 Introduction 40

4.2 Breach Simulation 41

4.3 Stage-Discharge at the Breach 43

4.4 Numerical Models 46

4.4.1 The Level-Reservoir-Approximation Model 47

4.4.2 The Method-of-Characteristic Models 48

(a) The Explicit Model 49

(b) The Implicit Model 57

4.4.3 Linearized Implicit Finite-Difference Model 61

5. EXPERIMENTAL EQUIPMENT AND PROCEDURES

5.1 Introduction 67

5.2 The Flume 68

5.3 The Dam 69

5.4 Unsteady Water Depth Measurements 71

5.5 Test Conditions and Procedures 72

6. COMPARISON OF MODEL RESULTS WITH EXPERIMENT

6.1 Introduction 75

6.2 Experimental Model I 75

6.3 Experimental Model II 77

6.4 Experimental Model III 80

6.5 Experimental Model IV 81

6.6 Conclusions 83

7. EVALUATION OF THE NUMERICAL MODELS

7.1 Introduction 98

7.2 The Level-Reservoir-Approximation Model 99

7.3 The Explicit Method-of-Characteristic Model 100

7.4 The Implicit Method-of-Characteristic Model 102

7.5 The Implicit Finite-Difference Model 104

7.6 Accuracy Test of the Dynamic Models 106
7.7 Conclusions 107

8. APPROXIMATE SOLUTIONS
8.1 Introduction 113
8.2 Initial Breach Discharges 114
8.3 Effect of Flow Resistance Within the Reservoir on the Outflow Hydrograph 120
8.4 Dam-Break Outflow Hydrographs 123
8.5 Conclusions 131

9. GENERAL CONCLUSIONS 132
9.1 Wave Propagation 132
9.2 The Numerical Models 133
9.3 The Approximate Solutions 134

REFERENCES 135

APPENDICES
A. DERIVATION OF THE CHARACTERISTIC EQUATIONS 144
B. THE TWO COMPABILITY EQUATIONS IN THE IMPLICIT MOC MODEL 146
C. THE TWO LINEAR EQUATIONS IN THE IMPLICIT FINITE-DIFFERENCE MODEL 149

LIST OF FIGURES

Figure No.		Page
2.1	Sketch of dam-break problem in dry channel	6
2.2	Pattern of characteristic lines for the Ritter solution	6
3.1	Characteristic lines in the (x,t)-plane	24
3.2	A specified time interval scheme for the Hartree method	27
3.3	A specified time interval scheme for the time-line interpolations	30
3.4	A specified time interval scheme for an implicit scheme	31
3.5	Computational grid for the Preissmann schemes	34
3.6	Path of a bore separating two continuous flow regions	37
3.7	Characteristics in the neighbourhood of the surge	39
4.1	Breach formation: (a) rectangular, triangular or trapezoidal; (b) parabolic	43
4.2	Characteristics for the specified time-interval scheme	50
4.3	Characteristics at the upstream boundary condition for $Q_{inp} > 0$, subcritical flow	51
4.4	Upstream boundary condition for $Q_{inp} = 0$: (a) longitudinal cross section of the reservoir; (b) grid net for subcritical flow	52
4.5	Characteristics for downstream boundary condition	54
4.6	The surge path and the characteristics C^+ and C^-: (a) for $U_1 > U_2 > v$ and $A_1 < A_2$; (b) for $v > U_1 > U_2$ and $A_1 > A_2$	55
4.7	The implicit scheme of the method of characteristics	57
4.8	Double-sweep algorithm for the implicit scheme	58

5.1	Schematic diagram of channels: (a) prismatic channel; (b) nonprismatic channel	68
5.2	Dam-breach mechanism: (a) partial breaches; (b) gradual breaches	70
6.1	Computed and measured depth hydrographs for test condition 1.1	85
6.2	Computed and measured depth hydrographs for test condition 1.2	86
6.3	Computed and measured depth hydrographs for test condition 1.3	87
6.4	Computed and measured depth hydrographs for test condition 2.1	88
6.5	Computed and measured depth hydrographs for test condition 2.2	89
6.6	Computed and measured depth hydrographs for test condition 2.3	90
6.7	Computed and measured depth hydrographs for test condition 3.1	91
6.8	Computed and measured depth hydrographs for test condition 3.2	92
6.9	Computed and measured depth hydrographs for test condition 3.3	93
6.10	Computed and measured depth hydrographs for test condition 4.1	94
6.11	Computed and measured depth hydrographs for test condition 4.2	95
6.12	Computed and measured depth hydrographs for test condition 4.3	96
6.13	Computed and measured depth hydrographs for test condition 4.4	97
7.1	Reservoir outflow hydrographs computed by the numerical models for experimental model I	108

7.2 Reservoir outflow hydrographs computed by the numerical models for experimental model II 109

7.3 Reservoir outflow hydrographs computed by the numerical models for experimental model III 110

7.4 Reservoir outflow hydrographs computed by the numerical models for experimental model IV 111

7.5 Reservoir outflow hydrographs computed by the numerical models for small breach sizes: (a) assumed a reservoir of experimental model II; (b) assumed a reservoir of experimental model III 112

8.1 Scheme for the derivation of initial breach discharge equation 115

8.2 Relationship of the relative height of the initial hydraulic head (β) to the relative of opening height (α) of rectangular breaches of the same width as the reservoir 117

8.3 Relationship of the initial breach discharges to the relative of opening height of rectangular breaches of the same width as the reservoir 118

8.4 Comparison of initial breach discharges computed by Eq. 8.7 with the corresponding results computed by the explicit MOC model, for rectangular breaches of the same width as the reservoir 119

8.5 Effect of bed roughness on the outflow hydrographs, assumed for a prismatic rectangular channel with a sloping bed and a rectangular breach of the same width as the channel 121

8.6 Effect of bed roughness and breach sizes on the outflow hydrographs, assumed for a prismatic-rectangular channel with a sloping bed and rectangular breaches of the same width as the channel 122

8.7 Scheme to approximate the difference in the reservoir volume during the time interval Δt 124

8.8 Scheme for derivation of the discharge Q_{acc} in case of movement of the steep negative wave 125

8.9 Comparisons between reservoir outflow hydrograph computed by the simplified model and the corresponding result computed by the explicit MOC model, assumed for a prismatic-rectangular channel with $S_0=0.02$, $n=0.04$ and rectangular breaches of the same width as the channel 129

8.10 Comparisons between reservoir outflow hydrograph computed by the simplified model and the corresponding result computed by the explicit MOC model, assumed for a prismatic-rectangular channel with $S_0=0.02$, $n=0.02$ and rectangular breaches of the same width as the channel 130

CHAPTER 1

INTRODUCTION

A dam with its impounded water possesses a catastrophic flood potential for people and property downstream in the case of a dam breach. Floods from failure of dams are much more devastating than floods from precipitation-runoff floods. This is because dam-break floods have a great peak discharge magnitude and a very short time base when compared to precipitation-runoff floods. The time to peak may have values ranging from only a few minutes to usually no more than a few hours. Due to those facts, dam-break flood analyses are much more difficult to analyze with the common techniques which have worked well for precipitation-runoff floods.

Most previous efforts to predict downstream flooding due to dam failures were based on the assumptions of complete and instantaneous collapse. The resulting floods are the most dangerous cases of dam-break floods, but they lead to unrealistic flood-plain management requirements since most dams do not tend to collapse completely and instantaneously. Therefore, research has also begun on dam-break flood waves due to partial and gradual collapse of a dam.

A dam may fail because of one or more combinations of the following reasons: overtopping of the dam when the spillway is insufficient during large inflows to the reservoir from heavy precipitation runoff or when the gates are not operated properly; seepage through the dam or along internal conduits; landslide-generated waves within the reservoir; dam slope embankment slides; and earthquake damages and liquefaction of earth-dams from earthquakes.

Johnson and Illes (1976) review 300 dam failures and Serafim and Countinho-Rodrigues (1989) summarize 142 dam failures throughout the world. Past dam failures showed that flash-floods created by dam failures had caused large losses

in human life and property in large areas downstream. For example, for the Teton Dam in U.S.A. (1976) the inundation downstream killed 14 persons and caused $400 million in property damage with some estimates running as high as $ 1 billion, and the Tous Dam failure in Spain (1982) caused the deaths of 15 people in the 90,000ha of inundated valley below. In the last three decades more than 59 dams have collapsed throughout the world (Serafim and Countinho-Rodrigues, 1989). This relatively high frequency of dam failures has motivated a greatly increased public and government agencies interest in dam-break flood forecasting. In the last two decades dam-break routing models have been and continue to be developed to predict the inundation downstream. This forecasting is very important for evacuation planning and safe management of reservoir operations. Therefore, it is desirable to have an accurate dam-break flood model which is convenient to use.

1.1 Thesis Objective

The protection of life and property from a flash flood caused by a failure of a dam depends primarily on accuracy in predicting magnitude and arrival time of the flash flood at a location downstream from the dam. As generalized mathematical models have been and continue to be developed, it is hoped that better decisions can be made to advise the public of downstream flooding when there is a dam failure. It is in this spirit that this study was carried out. The objective of this study is to investigate accurate numerical models which are convenient to use for estimating dam-break flood waves.

Flood wave computations resulting from a dam breach can be divided into two distinct phases: (1) computing the reservoir outflow hydrograph; and (2) routing the flood downstream from the breach. The determination of the reservoir outflow hydrograph consists of simulating the dam-breach and routing the reservoir inflow and water stored in the reservoir through the breach. Both reservoir and downstream routings can be accomplished by either hydrologic routing or dynamic routing methods. Thus, a mathematical model developed to

calculate the reservoir outflow hydrograph can be used to route the flood wave downstream by using appropriate upstream and downstream boundary conditions. Therefore, this research work considers only the possibility and accuracy of mathematical models to determine the reservoir outflow hydrographs.

In order to get a comprehensive numerical model to determine the reservoir outflow hydrograph, four numerical models were investigated. The models are a level-reservoir-approximation model, an explicit method-of-characteristics model, an implicit method-of-characteristics model and a linearized implicit finite-difference model.

Because rapidly-varied unsteady flow which follows the partial collapse of a dam is very complex, the validity of mathematical models to simulate this flow has often been questioned. In order to verify the validity of the numerical models, the results from four experimental models are compared with the corresponding results from the numerical models. These comparisons are also used to evaluate the accuracy of each of the numerical models. Besides the validity and accuracy of the numerical model, computer problems, computer requirements and robustness are evaluated to assess ease-of-use of the models.

A more complete numerical model is generally complex, time consuming and expensive to use. Therefore, it is also intended to investigate a less complete but relatively accurate numerical model (a simplified model) for computing dam-break outflow hydrographs. This simplified model is developed by using hydrologic storage routing and taking into consideration the effect of the movement of the negative waves and flow resistance. Results computed by the simplified model are compared with the corresponding results computed by the more complete numerical models to assess the accuracy and validity of the simplified model.

1.2 Thesis Outline

In chapter 2 a review of dam-break solutions is described. Chapter 3 presents theoretical analyses of unsteady flow in a reservoir. Chapter 4 describes model development of four numerical models. The models are a level-reservoir-approximation model, an explicit method-of-characteristics model, a linearized implicit method-of-characteristics model and a linearized implicit finite-difference model. The experimental equipment and procedures used in the study are described in chapter 5. In chapter 6 results of the numerical models are compared with the corresponding results of the laboratory experiments. A comprehensive evaluation of the numerical models is presented in chapter 7. A practical procedure for computing dam-break outflow hydrographs is described in chapter 8. The major conclusions drawn from this investigation are presented in Chapter 9.

CHAPTER 2

LITERATURE REVIEW

2.1 Introduction

Dam-break flood analysis is one of the classical problems of unsteady open channel flow which has been of theoretical interest to hydraulic engineers for well over a century. Solutions for dam-break flood problems are obtained by solving the partial differential equations of continuity and momentum which govern gradually varied unsteady flow in open channel (De St. Venant, 1871).

Early studies of dam-break flood analyses were based on the assumption that the dam collapsed entirely and instantaneously. This assumption is easier and more convenient when applying certain mathematical techniques for analyzing dam-break flood waves, and for a very simple case the De Saint-Venant equations can be solved analytically (Ritter, 1892).

Since most dams do not tend to collapse entirely and instantaneously, research has also begun on dam-break flood waves due to partial and gradual collapse of a dam. Mathematical models for these problems can not be solved analytically. Therefore, early studies for these problems, such as Schocklitsch (1917) and Army Corps of Engineers (1960, 1961), were based on experiments with physical models, since numerical solutions for the De St. Venant equations were not practical at that time.

During the last two decades, solution of the complete De St. Venant equations has become practical using numerical methods and high-speed computers. Various explicit and implicit finite difference schemes and explicit method of

characteristics schemes have been used to solve the equations for dam-breach wave simulation. Therefore, the more complete mathematical models of dam-break flood waves have occurred during this time.

2.2 Dam-Break Flood Models for Total Failure.

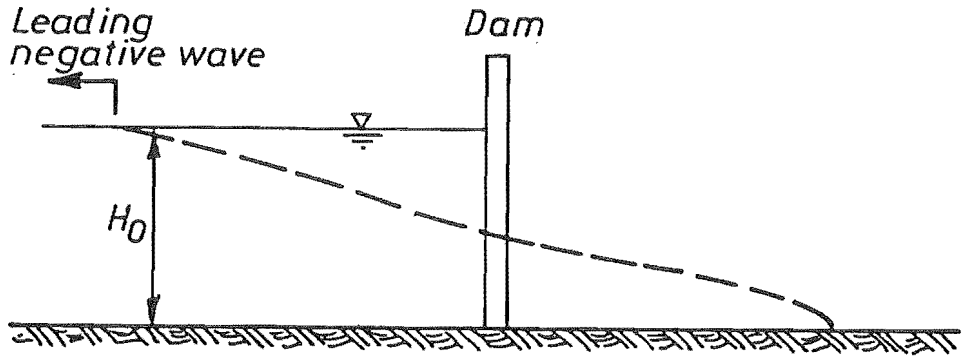

Fig. 2.1 Sketch of dam-break problem in dry channel

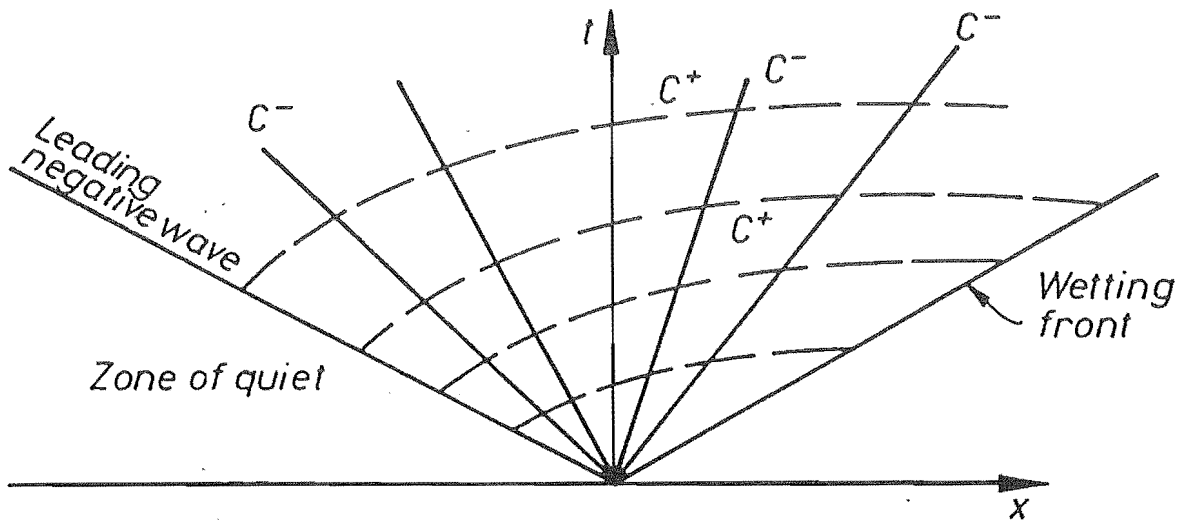

Fig. 2.2 Pattern of characteristic lines for the Ritter solution.

The first theoretical solution of the dam-break problem was made by Ritter (1892). He used the method of characteristics to obtain a closed-form solution for the flooding from a total instantaneous dam failure with unlimited upstream storage on a horizontal bed with a dry downstream channel and zero bed

resistance, as shown in Fig. 2.1. Since the leading negative-wave propagation speed is independent of the bed roughness, the Ritter solution will give accurate results in the region of the negative wave. However near the positive wave front, the Ritter solution becomes unrealistic for large values of time since the effect of resistance is gradually to decrease the wave speed and increase depths.

Dressler (1952) used a perturbation procedure to obtain a first-order correction for resistance. In order to verify his theoretical results, he also conducted a series of experiments in a glass-wall, horizontal flume 65 m long and 0.255 m wide with three different bed roughnesses ranging from smooth to very rough. For the case with resistance, he noted that the Ritter solution agreed closely with his results only for small values of time. Thus, bed roughness does not have significant effect at the early stage of dam-break flooding, and the Ritter solution can be used as an initial condition in the vicinity of the dam for a subsequent numerical computation.

However, the Ritter solution does not yield a very practical initial condition for subsequent numerical solution of the De Saint-Venant equations. This is because the very low depths with finite velocities lead to great values of friction slope which causes extreme curvature of the characteristics curves and extreme variation of quantities along these curves near the positive wave front.

Whitham (1955) showed how the initial effects of channel resistance could be found analytically. He treated the positive wave front as a growing boundary-layer region and assumed that: all resistance effects are restricted to this growing tip region. Thus, the Ritter solution is valid in the region behind the tip, and the water velocity within the growing tip region is equal to the wave propagation speed. However, because the width of the boundary-layer region grew very rapidly with time, Whitham noted that his solution might not apply for large values of time.

Dressler and Whitham used a channel of infinite width to simplify their analyses. In order to include both the effects of resistance and channel cross section on

the waves of sudden release, Su and Barnes (1970) extended Dressler's theoretical study to include channel cross-sectional geometry. They showed that the effect of channel cross-sectional shape is significant for the case without resistance but is less significant for the case with resistance.

Sakkas and Strelkoff (1973) extended the Ritter solution by including the effects of bed resistance for a sloping prismatic channel with a general parabolic cross section. The generalized parabolic cross section is described by a formula of the type, $B = C\, y^{M}$, in which B is the top width and C and M are constants. Rectangular, triangular and parabolic cross sections are specified by setting the parameter M equal to zero, one and between zero and one, respectively. A generalized Ritter solution for a prismatic channel of general parabolic cross section was used as an initial condition for starting the method of characteristics computation. Difficulties were encountered where flow depths approached zero near the wave front and near the upstream end of the finite-length reservoir. In order to avoid these problems, Sakkas and Strelkoff used a fictitious stream with sufficiently small depth at the upstream end and terminated the numerical calculations at a distance close to the wave front. They then extended the solution to the wave front by using Whitham's analytical solution.

All dam-break solutions discussed above use an assumption that the downstream side of the dam is initially dry. Stoker (1957) generalized the Ritter solution by including the effect of varying depth of water on the downstream side of the dam. In this case, Stoker showed that the sudden release of water from the reservoir will form a hydraulic bore (a shock) which then constitutes the front of dam-break flood wave. If the water is assumed at rest on both sides of the dam initially and all assumptions leading to the Ritter solution are carried over for this case, an analytical solution is possible. Stoker related the depths and velocities on both sides of the bore by using the continuity and momentum equations for steady flow in a coordinate system moving with the bore.

Terzidis and Strelkoff (1970) and Martin and Zovne (1971) demonstrated the applicability of the De St. Venant equations to simulate bore propagation in

channels with more general cross-sectional shapes. For simplicity, they assumed that the bore had a vertical face, and they neglected the effects of the bottom slope and bed shear.

Chen and Armbruster (1980) presented a solution for a more general dam-break problem with a shock in a sloping bed, a nonprismatic channel and a base flow. They formulated the dam-break problem as a boundary-value problem with a moving boundary (the shock) imposed at the wave front. An inflow hydrograph was specified for the upstream boundary condition. In the case of zero inflow, a fictitious flow with finite depth was assumed both upstream and downstream from the reservoir to let the computation continue. Chen and Ambruster used the Rankine-Hugoniot equations with an explicit method of characteristics scheme and a specified time interval to solve for flow depths and velocities at the advancing shock front.

2.3 Dam-Break Flood Models for Partial Failure.

Assumption of total and instantaneous failure of a dam is the simplest but least likely type of a dam failure. If only the upper part of the dam collapses, the remaining dam forms a weir.

Schocklitsch (Army Corps of Engineers, 1960) recognized the need to assume partial rather than complete breaches. He conducted a series experiments and derived empirical peak-flow equations for instantaneous partial failures of a dam. The maximum discharge for partial-width partial-depth breaches was determined by :

$$Q_{max} = \frac{8}{27} W_b \left(\frac{W_d}{W_b}\right)^{0.25} \left(\frac{H_0}{D_b}\right)^{0.33} \sqrt{g D_b^3} \qquad (2.1)$$

in which W_b is breach width, W_d is dam width, D_b is breach depth and H_0 is water depth at the dam before breach.

The Army Corps of Engineers (1960, 1961) conducted an extensive series of physical experiments to investigate the flood magnitudes of instantaneous partial failures. Their experimental results verified the Schoklitsch relationship, and then they presented a dimensionless plot of Q_{max} against the breach dimensions. From this curve, the following relationship of Q_{max} as a function of rectangular breach dimensions was derived :

$$Q_{max} = 0.29\ W_b \sqrt{g D_b^3} \left(\frac{W_d}{W_b} \frac{H_0}{D_b} \right)^{0.28} \qquad (2.2)$$

The Corps suggested that the term within the parentheses should be between one and twenty and that the accuracy of prediction would improve as the term within the parentheses approaches one.

Menendez and Navarro (1990) conducted a series of laboratory experiments to investigate the flow characteristics for gradual collapse of a dam. The experiments were conducted in a glass-horizontal flume 0.31 m wide, 0.38 m high and 30 m long. The model dam was a plate and was situated approximately at the middle of the flume length. To simulate gradual collapse, the plate was moved down through a slot at constant speed. Based on the experimental results, they presented a complete and coherent physical description of the flow characteristics associated with the finite removal time.

Due to the development and accessibility of large-capacity high-speed digital computers in the last two decades, the emphasis of dam-break flood-routing models has shifted toward numerical models. Dam-break flood-routing computations for partial failure can be divided into the two tasks : (1) computation of the outflow hydrograph through the breach; and (2) routing the

flood wave through the downstream valley. These two tasks can be modelled separately because the dam breach acts as a flow control.

The determination of the reservoir outflow hydrographs involves two problems: (1) simulating the dam-breach and; (2) routing of the reservoir inflow and water stored in the reservoir through the breach. Since mathematical models for the flow that follows the collapse of a dam in a nonprismatic channel is very complex, solutions of dam-break routing models can be obtained only as approximations of different degrees of accuracy. The approximations can be accomplished by either hydrologic routing methods based on the conservation of mass equation or dynamic routing methods based on the De St. Venant equations.

Yevjevich (1975) used a hydrologic routing method to obtain practical procedures for computing the outflow from the reservoir through instantaneous small, medium and large breaches. Approximations to the outflow hydrographs were as follows: (1) for a small breach, the outflow hydrograph was determined by using the mass-conservation differential equation and by neglecting the effects of movement of steep negative waves, flow resistance and tail water; (2) for a medium breach, the first approximation of the outflow hydrograph was computed by neglecting the effect of steep negative waves and flow resistance. The second and third approximations include the additional effects of the steep negative wave and flow resistance, respectively; (3) for a large breach, the first approximation of the outflow hydrograph was determined by taking into account the submergence effect but by neglecting movement of steep negative waves and flow resistance. The second approximation was obtained by using a fictitious inflow hydrograph that takes into account the movement of steep negative waves, the inflow hydrograph, flow resistance and submergence.

Price, et al. (1977) developed a mathematical model to compute outflow hydrographs caused by either instantaneous complete or instantaneous partial failure of a dam and compared the results with the corresponding results estimated by the classical dam-break equations. The mathematical model was

verified by using well-documented floods which have occurred in a particular reservoir. Because flows caused by failure of a dam were larger in magnitude than historical flood flows, the model was calibrated against a standard-step backwater model which used the same geometric river or reservoir description as the unsteady flow model. For a partial failure, the solution upstream from the dam breach was calculated independently from the solution downstream from the breach. An inflow hydrograph and a rating curve were assumed known for the upstream and downstream boundary conditions, respectively. The discharge through the breach was determined by using a rating curve based on scaled model tests of the failed structure. The partial differential equations were approximated by a centred finite-difference scheme proposed by Stoker that can be solved by digital computer. They concluded that: the gradually varied flow equations provide a practical solution for obtaining the complete hydrographs from a dam breach; and the maximum discharge computed by using the classical dam-break equation (equation 2.1) and that computed by using the mathematical model were in remarkable agreement.

Rajar (1978) developed a mathematical model to simulate dam-break flood waves due to total, partial or gradual collapse of a dam in nonprismatic channels. In case of partial collapse of a dam, a special procedure was used that introduced a discontinuity in water levels at the dam site. He used two cross sections at the dam site, one of which was the cross section of the partly collapsed dam. This cross section was not explicitly expressed in the mathematical model but was taken into account in the weir discharge formula. For a gradual collapse, he assumed that the size and form of the destroyed part as a function of time was known. Thus, the calculation could be executed by the same program for partial collapse. In order to establish the error due to inaccuracy of the numerical methods, he used two explicit finite-difference schemes, the diffusive scheme and the Lax-Wendroff scheme, to approximate the dynamic equations. He compared the results of the mathematical models with the corresponding results of four physical models and concluded that the maximum error was ± 20% for the rather irregular valley but was less than ±15% for the other part of the model and that the Lax-Wendroff scheme was

preferable in most cases because of its better accuracy.

Fread (1977, 1984) presented a dam-break forecasting model (DAMBRK) which then gained international acceptance as a state-of-the-art model (Wurbs, 1987). The DAMBRK model was tested on five historical dam-break floods: 1976 Teton Dam, 1972 Buffalo Creek Coal-Waste Dam, 1889 Johnstown Dam, 1977 Toccoa (Kelly Barnes) Dam and the 1977 Laurel Run Dam. The DAMBRK model consists of three basic components: (1) a component describing the geometrical and temporal description of the breach, (2) a component describing the reservoir outflow hydrograph and (3) a component routing the flood wave through the downstream valley. For reasons of simplicity and uncertainty in the actual failure mechanism of the breach, it was assumed that the breach size and shape (rectangular, triangular or trapezoidal) as a function of time were known. The flow through the breach was treated as flow over a broad crested weir for an overtopping failure or as flow through an orifice for a piping failure. Both hydrologic routing and dynamic routing methods were used to determine the reservoir outflow hydrographs. The Preissmann finite-difference scheme was used to obtain approximate solutions of the dynamic equations. Because reservoir dynamic routing must deal with decreasing flow depths, the computation became unstable when flow depths approached a value less than the normal depth at the upstream boundary. Fread avoided this problem by monitoring the upstream depth. The location of the upstream boundary condition was shifted downstream one node at a time if the upstream depth was less than the normal depth.

Wurbs (1987) showed some comparative evaluations of alternative state-of-the-art methods to predict the flood wave resulting from a breached dam. He concluded that: the various available dam-breach flood models gave a wide range of trade-offs between accuracy and ease-of-use; a dynamic routing model should be used in order to obtain a maximum practical level of accuracy; computational problems caused by rapidly rising hydrographs were the main factor that made dynamic routing models much more difficult to use than the other models; and, in general, dam-breach flood wave modelling was still not

highly accurate. Therefore, more robust dynamic routing algorithms are needed so that subcritical and supercritical flow under all situations can be handled.

2.4 Conclusions

Early attempts to predict dam-break flood waves were based on the assumption that the flow was in a prismatic channel and that the dam failed completely and instantaneously. In this case, most of the models used the explicit method of characteristics to solve the De St. Venant equations.

General mathematical models for partial collapse of a dam were developed in the last two decades. Because the dam breach acts a flow control, calculations upstream and downstream from the breach are usually carried out separately. Outflow hydrographs at the dam breach are computed by using a weir discharge formula together with either a hydrologic routing method or a more accurate but more difficult dynamic routing method. For partial failure, most of the models used either explicit or implicit finite-difference methods to approximate the dynamic equations. Wurbs (1987) concluded that, in general, dam-breach flood wave modelling was still not highly accurate.

To the writer's knowledge there is no satisfactory model available in the literature that simulates accurately wave formations within a reservoir. Thus, bore propagation which may be formed within a reservoir and propagation of a drying front at the upstream end in case of zero inflow have not been modelled previously, and no direct comparison of the method of characteristics (supposedly the most accurate) and finite-difference methods has been made for the partial collapse of a dam. Thus, in order to obtain maximum practical accuracy, there is a need to develop a more complete mathematical representation of the physical situation. Then this model can be compared with the less complete numerical models to determine when these less complete models can be used with confidence.

CHAPTER 3

ANALYSIS OF UNSTEADY FLOW IN A RESERVOIR

3.1 Introduction

Analysis of unsteady flow in a reservoir can be performed either by a simplified routing analysis, which is based only on the mass-conservation differential equation, or by a dynamic routing analysis, which is based on the complete De St. Venant equations.

A simplified routing analysis assumes that the water surface within the reservoir is level and that the flow rate through the breach is given by one of the formulae for flow over a weir. The friction factor does not enter into these calculations. These assumptions are suitable for gradually formed breaches with no significant reservoir inflow hydrograph and for wide, flat reservoirs with gradual changes in water-surface elevations. As long as the basic assumptions are valid, a simplified routing is as reliable as a dynamic routing and is easier to use.

However, when there is a wave progressing within the reservoir, such as a negative wave caused by sudden a reservoir drawdown or a positive wave caused by a significant reservoir inflow, a dynamic routing analysis has to be used for better accuracy.

A dynamic routing method is better for a long, narrow reservoir with rapid water-level changes at the breached dam. Water surface profiles within the reservoir can be produced as well as the outflow hydrograph.

Generally the flow in the reservoir is subcritical, at least until the negative wave reaches the upstream limit of the reservoir. After that time, a surge (an abrupt change in water surface level) may form within the reservoir. Whether or not the surge forms depends on the bed slope, the breach characteristics, the outflow through the breach and the reservoir inflow.

When the surge occurs, the basic equations of dynamic routing based on the De St. Venant differential equations are not valid in the neighbourhood of the surge. Thus, a surge analysis is carried out by using control volume forms of the momentum and continuity equations across the surge, and the De St. Venant equations are used for all other portions of the flow.

3.2 Simplified Routing Analysis

The simplified routing analysis through a reservoir is a hydrologic routing with an assumption of a horizontal free surface elevation. It may be used for certain conditions in determination of the outflow hydrograph.

The differential equation which is based on the conservation of volume can be expressed as :

$$(Q_{inp} - Q_{out}) = \frac{dS}{dt} \qquad (3.1)$$

in which Q_{inp} is the inflow, Q_{out} is the outflow, dt is the time period, and dS is the difference in volume in the reservoir.

In order to calculate the outflow hydrograph through the breach, the storage capacity and the inflow hydrograph must be known. If these functions can be approximated by integrable expressions, the analytical integration of this equation is possible.

The outflow through the breach is a function of the breach geometry and the reservoir water surface elevation above the breach crest. This function can be expressed as :

$$Q_{out} = \beta\, h^n \tag{3.2}$$

in which h is the reservoir water surface elevation above the breach bottom at time t, and the coefficient ß and exponent n depend on the breach characteristics. The range of n is 1.5 to 2.5.

The volume of a reservoir can be related to its surface to develop an elevation-storage curve. It can be approximated by the function

$$S = \alpha\, H^m + S_0 \tag{3.3}$$

in which S is the storage volume, S_0 is a constant, H is the elevation of the water surface above a reference level, and the coefficient α and exponent m can be determined from the elevation-storage curve. For majority of natural valleys the range of m is 1 to 4 (Yevjevich, 1975)

Since both the outflow and the storage are functions of the reservoir water surface level, it is possible to use the same reference level for measuring h and H. Then h=H, and eliminating h between equations (3.2) and (3.3) gives

$$S = \varphi\, Q_{out}^k + S_0 \tag{3.4}$$

in which $k = m/n$ and $\varphi = \alpha/(\beta^k)$

It is possible to fit some parts of a recorded inflow hydrograph by mathematical expressions. However, for practical purposes (such as the inflow is nearly constant or can be neglected for a short period of time during the outflow through the dam breach), it is more convenient to approximate the inflow hydrograph with a simple mathematical expression. The simplest forms of the function $Q_{inp} = f(t)$ are Q_{inp} = constant and $Q_{inp} = 0$.

In case of zero inflow $Q_{inp} = 0$, equation (3.1) becomes

$$- Q_{out} = \frac{dS}{dt} \tag{3.5}$$

inserting equation (3.4) in equation (3.1) gives

$$-dt = \varphi \; k \; Q_{out}^{(k-2)} \; dQ \tag{3.6}$$

integrating this equation leads to the result

$$Q_t^{(k-1)} = Q_0^{(k-1)} - \frac{(k-2)\; t}{\varphi \; k} \tag{3.7}$$

in which Q_t is the outflow at $t=t$ and Q_0 is the outflow at $t=0$. Thus, the outflow hydrograph can be determined for each time t.

Since a dam-break study for a partial breach has to be made for different sizes

and shapes of breaches, the analytical approach may have some advantages in comparison with the numerical procedures of reservoir routings. The analytical solution is easier to use and can lead to a better understanding of the role of different variables for small dam breaches.

However, there are some difficulties in analytically integrating the differential equation (especially in case the inflow changes with time) and in fitting the elevation-storage curve of natural reservoirs with tractable mathematical expressions. For engineering purposes, most of the solutions are numerical solutions obtained by using digital computers.

The equation (3.1) can be expressed in finite-difference form as :

$$\frac{\Delta S}{\Delta t} + \frac{(Q_{out1} + Q_{out2})}{2} - \frac{(Q_{inp1} + Q_{inp2})}{2} = 0 \qquad (3.8)$$

in which Δ is the approximated differential, the subscript 1 and 2 indicate values at the time t - Δt and t, respectively.

Inserting equations (3.3) and (3.2) in equation (3.8) result in the following expression

$$\frac{\alpha (h_2 - h_1)^m}{\Delta t} + \frac{h_1^n + h_2^n}{2} - \frac{Q_{inp1} + Q_{inp2}}{2} = 0 \qquad (3.9)$$

Since all terms are known except h_2, equation (3.9) can be solved for the unknown h_2 by using an iterative method. After h_2 is obtained, the corresponding outflow Q_{out} can be obtained by using equation (3.2). In this way the outflow hydrograph Q(t) can be determined for each time t, as t goes from zero to a terminating value.

3.3 Dynamic Routing Analysis

The basic theory for a dynamic routing analysis consists of two partial differential equations firstly derived by De St. Venant in 1871. Although the unsteady flow equations can be expressed in two or three dimensions, and a reservoir geometry is in three-dimensions, the unsteady flow in a reservoir is assumed to be one-dimensional flow in the sense that the flow characteristics are considered to vary only with the longitudinal coordinate and time.

Unsteady flow in a nonprismatic channel can be expressed by the continuity and the conservation of momentum equations, respectively:

$$\frac{\partial A}{\partial t} + \frac{\partial (UA)}{\partial x} = 0 \tag{3.10}$$

$$\frac{\partial (UA)}{\partial t} + \frac{\partial (U^2 A)}{\partial x} + gA\frac{\partial h}{\partial x} = gA(S_0 - S_f) \tag{3.11}$$

Calculating the derivatives in equations (3.10) and (3.11) gives

$$B\frac{\partial h}{\partial t} + U\left(\frac{\partial A}{\partial x}\right)_h + UB\frac{\partial h}{\partial x} + A\frac{\partial U}{\partial x} = 0 \tag{3.12}$$

$$\frac{\partial U}{\partial t} + U\frac{\partial U}{\partial x} + g\frac{\partial h}{\partial x} = g(S_0 - S_f) \tag{3.13}$$

in which A = flow area, B = surface width, t = time, U = mean velocity, h = flow depth, g = gravitational constant, x = horizontal distance , S_0 = bed slope, S_f = friction slope and $(\partial A/\partial x)_h$ is the rate of change of A with respect to x when h is held constant.

The friction slope can be evaluated from Manning's equation for uniform, steady flow

$$S_f = \frac{n^2 |Q| Q}{A^2 R^{4/3}} \tag{3.14}$$

in which n = Manning's resistance coefficient and R = the hydraulic radius

In most cases the partial differential equations cannot be solved by analytical methods, but they may be solved to obtain approximate solutions by numerical methods using digital computers. The continuous region in which the solution is desired is replaced by a set of points or nodes in the time-space domain. The flow parameters are calculated at these nodal points, and intermediate values are determined by an interpolation process. The type of interpolation process influences the quantities at the nodal points. In principle, the accuracy increases as the accuracy of the interpolation increases.

In general, a numerical analysis of unsteady flow in a reservoir has to be able to deal either with zones of supercritical and subcritical flow separated by a discontinuity (a shock) or with flows that are entirely subcritical. In the current technical literature, there are two classes of numerical solutions for one-dimensional flow ,i.e., (1) the method of characteristics based on the characteristic form of the equations and (2) the finite-difference methods based on algebraic finite-difference relationships of the partial difference equations.

The method of characteristics is extremely helpful in interpreting the physics of flows, and it also has the advantages of stability, accuracy and easily imposed boundary and initial conditions. It has the capability of dealing easily with

problems in which a transition from subcritical to supercritical flow occurs. This set of conditions is often encountered in a dam-break flow. The characteristic methods can be handled either by the grid of characteristics scheme or the specified time interval scheme (the rectangular grid scheme). Because of its many advantages, the latter has been the preferred scheme in most unsteady-flow applications.

In the finite-difference method, the dependent variables in the x-t region are calculated at a rectangular net of discrete points. Of the various finite-difference schemes, the Preissmann or the weighted four-point finite-difference scheme is the one currently used in most unsteady-flow analyses (see, for example, Chaudhry and Contractor (1973), Liggett and Cunge (1975), and the National Weather Service (Fread, 1984)).

In the method of characteristics with a rectangular grid scheme or in the finite difference method, it is possible to use either an explicit or an implicit scheme.

Explicit schemes solve the equations for one point at a time. The values of the dependent variables at one time can be expressed as explicit functions of the values of the dependent variables at an earlier time. These schemes are easy to program and give the solution directly. In cases in which the dependent variables are changing rapidly, such as a dam-break flow, small distance steps (Δx) must be used in order to maintain accuracy. If the dependent variables are changing slowly, the distance steps (Δx) can be increased in order to take advantage of larger time steps (Δt). If the time steps become too large explicit schemes then become unstable.

A stable solution in a rectangular grid explicit formulation can be obtained by selecting the distance step (Δx) and the time step (Δt) in such a way that

$$\Delta t \leq \frac{\Delta x}{U \pm C} \tag{3.15}$$

This is called Courant-Friedrichs-Lewy (CFL) condition. The implicit schemes were developed because of the Courant constraint imposed on the explicit schemes. Implicit schemes eliminate this constraint on the time step, but they are more difficult to program and require much more computation.

Implicit schemes solve for a group of points at a time. The values of the dependents variables are calculated by solving a set of simultaneous equations that contain values of the dependent variables at two different time levels. Although implicit schemes are inherently stable, computational problems (accuracy and non-convergence) can arise for large time steps when implicit schemes are applied to rapidly rising hydrographs, such as the dam-break outflow hydrograph. However, these problems can be overcome by proper selection of the time step.

3.3.1 Method of Characteristics

Integration by the method of characteristics means that the two basic partial difference equations (3.12) and (3.13) are replaced by four ordinary differential equations. The partial difference equations are transformed into the characteristic forms by using a linear combination of the two basic equations and a combination factor $\lambda = \pm C/A$ (see appendix A). After their transformation, the characteristic forms are :

$$\frac{dU}{dt} + \frac{g}{C}\frac{dh}{dt} = g\,(S_0 - S_f) - \frac{U}{A}\,C\left(\frac{\partial A}{\partial x}\right)_h \qquad (3.16)$$

along the forward characteristic C^+

$$\frac{dx}{dt} = U + C \tag{3.17}$$

and

$$\frac{dU}{dt} - \frac{g}{C}\frac{dh}{dt} = g\,(S_0 - S_f) + \frac{U}{A}\,C\left(\frac{\partial A}{\partial x}\right)_h \tag{3.18}$$

along the backward characteristic C^-

$$\frac{dx}{dt} = U - C \tag{3.19}$$

in which $C = \sqrt{gA/B}$ is the celerity of a small-amplitude wave in still water and $(\partial A/\partial x)_h$ is the rate of change of A with respect to x when h is held constant.

Either a characteristics grid or a rectangular grid is generally used in placing equations (3.16-3.19) in a form suitable for numerical solution. The dependent variables at every point in the (x,t)-plane are defined at the intersections of the forward (C^+) and the backward (C^-) characteristics.

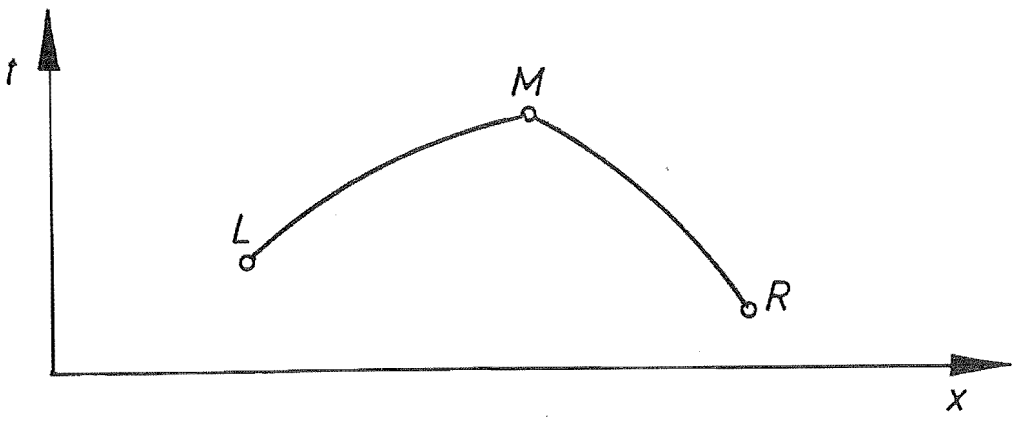

Fig. 3.1 Characteristic lines in the (x,t)-plane

Let us assume that the dependent variables at points L and R are known, and the solution is extended to point M (Fig. 3.1).

The unknown values at point M are found by solution of equations (3.16-3.19). Integration along the characteristics are as follows :

$$x_M - x_L + \int_{t_L}^{t_M} (U + C)\, dt \tag{3.20}$$

$$U_M - U_L - g\int_{h_L}^{h_M} \frac{dh}{C} + \int_{t_L}^{t_M} \left(g(S_0 - S_f) - \frac{U}{A} C \left(\frac{\partial A}{\partial x} \right)_h \right) dt \tag{3.21}$$

$$x_M - x_R + \int_{t_R}^{t_M} (U - C)\, dt \tag{3.22}$$

$$U_M - U_R + g\int_{h_R}^{h_M} \frac{dh}{C} + \int_{t_R}^{t_M} \left(g(S_0 - S_f) + \frac{U}{A} C \left(\frac{\partial A}{\partial x} \right)_h \right) dt \tag{3.23}$$

Equations (3.20-3.23) are four equations with four unknowns, i.e., t_M, x_M, U_M and h_M. No approximations have been made. A numerical approximation appears in evaluating the integrals. For example, the trapezoidal rule of integration leads to equations:

$$x_M - x_L + \frac{1}{2}(t_M - t_L)(U_M + C_M + U_L + C_L) \tag{3.24}$$

$$(U_M-U_L)+\frac{g}{2}\left(\frac{1}{C_M}+\frac{1}{C_L}\right)(h_M-h_L) =$$

$$\frac{1}{2}(t_M-t_L)\left(g[(S_{0M}-S_{fM})+(S_{0L}-S_{fL})]-\left(\frac{U_M}{A_M}C_M+\frac{U_L}{A_L}C_L\right)\left(\frac{A_{(x_M,h_L)}-A_{(x_L,h_L)}}{x_M-x_L}\right)\right) \quad (3.25)$$

$$x_M = x_R + \frac{1}{2}(t_M-t_R)(U_M-C_M+U_R-C_R) \quad (3.26)$$

$$(U_M-U_R)-\frac{g}{2}\left(\frac{1}{C_M}+\frac{1}{C_R}\right)(h_M-h_R) =$$

$$\frac{1}{2}(t_M-t_R)\left(g[(S_{0M}-S_{fM})+(S_{0R}-S_{fR})]+\left(\frac{U_M}{A_M}C_M+\frac{U_R}{A_R}C_R\right)\left(\frac{A_{(x_M,h_R)}-A_{(x_R,h_R)}}{x_M-x_R}\right)\right) \quad (3.27)$$

Equations (3.24-3.27) are non-linear algebraic equations and an iteration method must be used for their solution. The accuracy of the solution of the equations for t_M, x_M, U_M and h_M is increased by increasing the number of iterations, and the accuracy of approximations of these equations is increased by decreasing the intervals L-M and R-M.

In the grid of characteristics scheme, the solutions are projected directly to the next points so that the (x,t)-plane is filled with characteristics and all the dependent variables are determined at the intersections. The grid of characteristics scheme forms an irregular grid. Values of the results at any desired location must be interpolated between the points of the characteristics net.

The desire to avoid the irregular grid and interpolation of results has led to the

development of specified time interval schemes. In these schemes, the intersection points of the forward (C^+) and the backward (C^-) characteristics are made to coincide with a point on a rectangular grid system with specified time intervals dt. The values of the dependent variables at time row i are assumed known, and the solutions are advanced to row i+1. In the specified time interval scheme, it is possible to use either an explicit or an implicit formulation.

a. Explicit Schemes

An explicit scheme solves the equations for one grid point at a time. The values of dependent variables are known at grid intersection points on the time row i from earlier calculations or from initial conditions. The values of dependent variables at grid points on the next time row i+1 are sought.

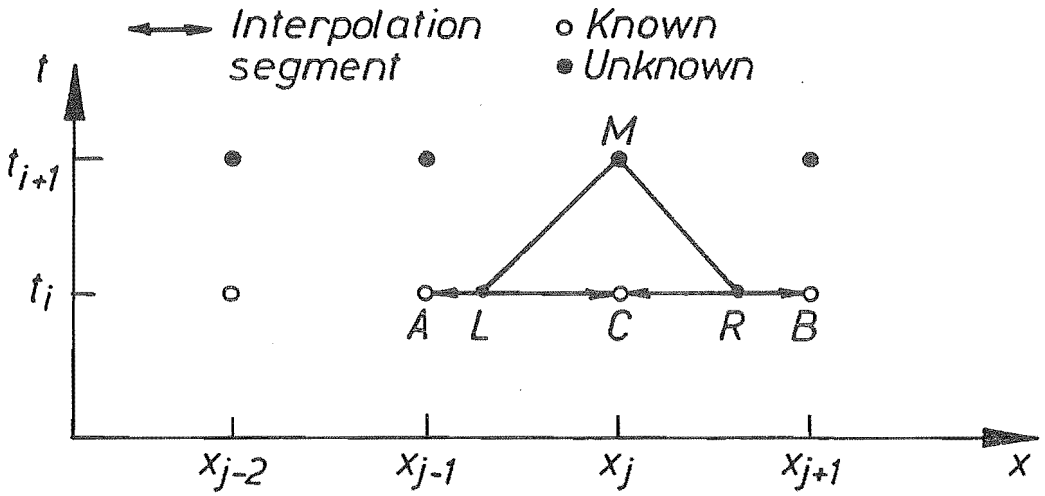

Fig. 3.2 A specified time interval scheme for the Hartree method.

The Hartree method (1952) is commonly used with the specified time interval schemes. The forward and the backward characteristics are made to coincide with a grid point such as M (Fig. 3.2) on the time row i+1. These characteristics usually do not coincide with grid points on the time row i but instead intersect time row i at intermediate points such as L and R . Thus, this procedure requires interpolations. A linear interpolation between two adjacent grid points in the x-direction is usually used to find the values of dependent variables at L

and R. These values are used as known values in the characteristic equations (3.25) and (3.27) to obtain the solutions at point M. Since the location of L and R are a function of the solution at point M, this implies an iterative solution.

The Newton-Raphson iteration method and other iteration methods can be used to solve the non-linear equations, but the following is the simplest procedure :

(1) For the first iteration, the locations of X_L and X_R are determined by using the characteristics directions known at point C

$$x_L = x_C - (U_C + C_C)\,\Delta t \tag{3.28}$$

$$x_R = x_C - (U_C - C_C)\,\Delta t \tag{3.29}$$

(2) Values for U and h at L and R are determined by linear interpolation

$$U_L = U_A + \frac{(U_C - U_A)\,(x_L - x_A)}{\Delta x} \tag{3.30}$$

$$U_R = U_B + \frac{(U_C - U_B)\,(x_B - x_R)}{\Delta x} \tag{3.31}$$

$$h_L = h_A + \frac{(h_C - h_A)\,(x_L - x_A)}{\Delta x} \tag{3.32}$$

$$h_R = h_B + \frac{(h_C - h_B)\,(x_B - x_R)}{\Delta x} \tag{3.33}$$

(3) Equations (3.25) and (3.27) are used to obtain values at point M. The trapezoidal integration is used by using values at points L and R, respectively.

(4) Points L and R are relocated by using the new characteristic directions at point M

$$x_{LN} = x_M - 0.5\,(U_M + C_M + U_L + C_L)\,\Delta t \tag{3.34}$$

$$x_{RN} = x_M - 0.5\,(U_M - C_M + U_R - C_R)\,\Delta t \tag{3.35}$$

Step 2 through 4 are repeated until changes in the values of X_L, X_R, U_M and C_M from one cycle to the next are insignificant.

As an alternative to the interpolations in the x-direction, the forward and the backward characteristics can be extended back beyond the present time level so that they intersect with vertical time lines at points L' and R' as shown in Fig.3.3. This scheme was initiated by Wylie (1980).

The values of dependent variables at points L' and R' are determined by using a linear interpolation in the time direction (a line of constant x). Thus, a linear interpolation between points A and D (E and F) can provide the variables at point L' (R'). These variables are used as known variables in the characteristic equations (3.25) and (3.27) to obtain the values of dependent variables at point M.

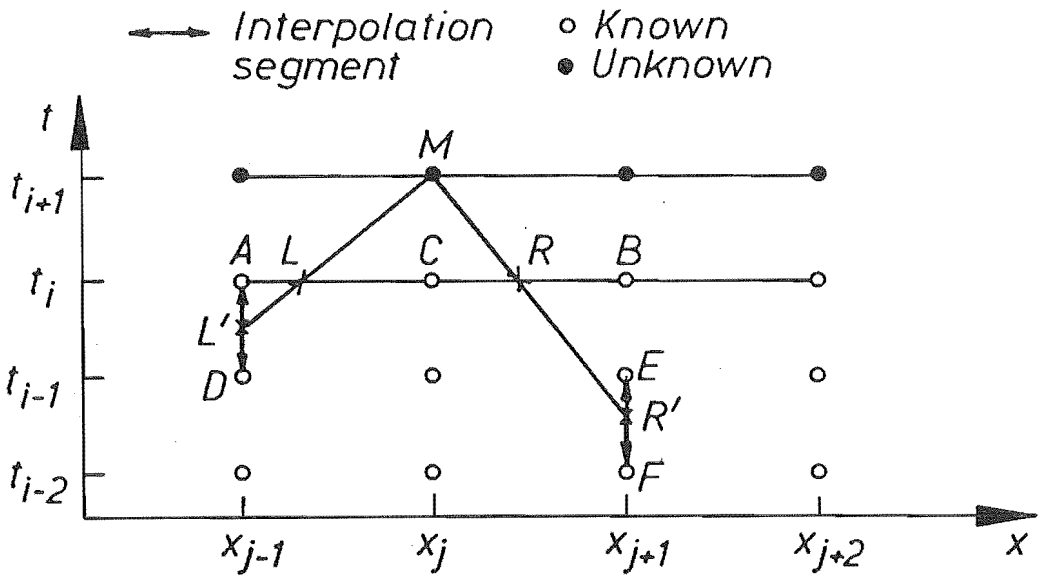

Fig. 3.3 A specified time interval scheme for the time-line interpolations

Although these are explicit schemes, their solutions can not be obtained directly as an iterative procedure must be used to calculate simultaneously both the solution at M and the location of points L and R or L' and R'. Thus, interpolation errors along one time level will be propagated into the next time level. In order to minimize these interpolation errors, a Courant number (Cr) less than or equal one is used to ensure that L lies between A and C and that R lies between C and B in figures (3.2) and (3.3).

b. Implicit Schemes

An implicit scheme solves for a group of points at the advance time t_{i+1}. Schmitz and Edenhofer (1983) first applied this scheme to flood routing and named it the implicit method of characteristics.

In this scheme, the characteristics from point M_j are made to intersect the adjacent time lines at L_j and R_j as shown in Fig. 3.4. For L and R to always lie within the present time step Δt, it is necessary that the Courant number be

greater than one. The values of dependent variables at point M_j are then expressed in terms of unknowns at points M_{j-1} and M_{j+1} as well as the known values at points N_{j-1}, N_j, and N_{j+1}. This procedure leads to a system of nonlinear algebraic equations.

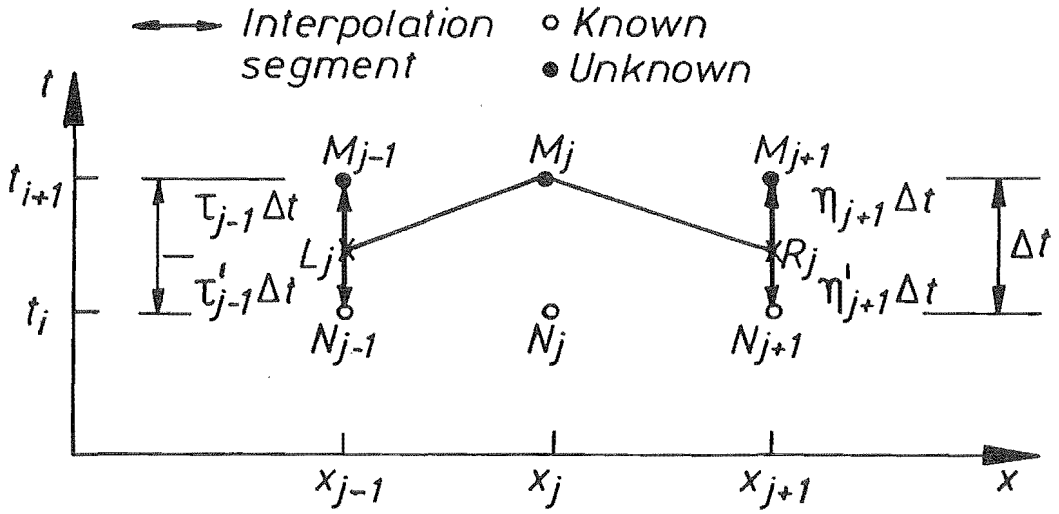

Fig. 3.4 A Specified time interval scheme for an implicit scheme

The algebraic equations for this scheme can be developed as follows:

(1) The locations of L_j and R_j can be determined by using the forward (C^+) and the backward (C^-) characteristics

$$\tau_{j-1} = \frac{\dfrac{(x_j - x_{j-1})}{\Delta t}}{0.5\left[(U+C)_{L_j} + (U+C)_{M_j}\right]} \tag{3.36}$$

$$\tau'_{j-1} = 1.0 - \tau_{j-1} \tag{3.37}$$

$$\eta_{j+1} = \frac{\dfrac{-(x_{j+1}-x_j)}{\Delta t}}{0.5\,[(U-C)_{R_j}+(U-C)_{M_j}]} \tag{3.38}$$

$$\eta'_{j+1} = 1.0 - \eta_{j+1} \tag{3.39}$$

(2) The variables (U and h) at the intersection points L_j and R_j can be interpolated linearly between points N_{j-1} and M_{j-1} and N_{j+1} and M_{j+1}, respectively :

$$U_{L_j} = \tau_{j-1}\, U_{N_{j-1}} + \tau'_{j-1}\, U_{M_{j-1}} \tag{3.40}$$

$$h_{L_j} = \tau_{j-1}\, h_{N_{j-1}} + \tau'_{j-1}\, h_{M_{j-1}} \tag{3.41}$$

$$U_{R_j} = \eta_{j+1}\, U_{N_{j+1}} + \eta'_{j+1}\, U_{M_{j+1}} \tag{3.42}$$

$$h_{R_j} = \eta_{j+1}\, h_{N_{j+1}} + \eta'_{j+1}\, h_{M_{j+1}} \tag{3.43}$$

(3) The two compatibility equations from point M_j can be determined by substituting equations (3.36), (3.40) and (3.41) into equation (3.25), and equations (3.38),(3.42) and (3.43) into equation (3.27). The result of these substitutions can be expressed in the following form:

$$\frac{g}{C_{L_jM_j}}\left(h_{M_j}-(\tau_{j-1}h_{N_{j-1}}+\tau'_{j-1}h_{M_{j-1}})\right)$$

$$+U_{M_j}-(\tau_{j-1}U_{N_{j-1}}+\tau'_{j-1}U_{M_{j-1}})=(F+)_{L_jM_j}\tau_{j-1}\Delta t \qquad (3.44)$$

$$\frac{g}{C_{R_jM_j}}\left(-h_{M_j}+(\eta_{j+1}h_{N_{j+1}}+\eta'_{j+1}h_{M_{j+1}})\right)$$

$$+U_{M_j}-(\eta_{j+1}U_{N_{j+1}}+\eta'_{j+1}U_{M_{j+1}})=(F-)_{R_jM_j}\eta_{j+1}\Delta t \qquad (3.45)$$

in which

$$(F\pm)=\left(g(S_0-S_f)\mp\frac{U}{A}C\left(\frac{\partial A}{\partial x}\right)_h\right) \qquad (3.46)$$

Equations (3.44) and (3.45) can be written for each interior node at time t_{i+1}. At the left-hand boundary node, equation (3.45) and a second equation expressing the left-hand boundary condition are written. Likewise, at the right-hand boundary node, equation (3.44) and a second equation expressing the right-hand boundary condition are written. Since two equations have been written for each node at time t_{i+1}, and since there are two unknowns at each of these nodes, the total number of equations equals the total number of unknowns. Since these simultaneous equations are nonlinear, they are usually solved with iterative techniques at the end of each time step.

3.3.2 Preissmann Finite-Difference Scheme

Numerical solution by the method of finite differences means that the partial differential equations are replaced by algebraic finite-difference relationships. Of the various implicit methods of finite differences that have been developed, the Preissmann-type schemes (the weighted four-point schemes) appear most advantageous since they have the following salient features :

- They use the same computational grid points to compute both unknown flow variables (Fig. 3.5);
- They can be used readily with unequal space intervals (Δx) since they link flow variables at only two adjacent sections;
- Their stability-convergence properties can be controlled easily with a weighting coefficient θ.

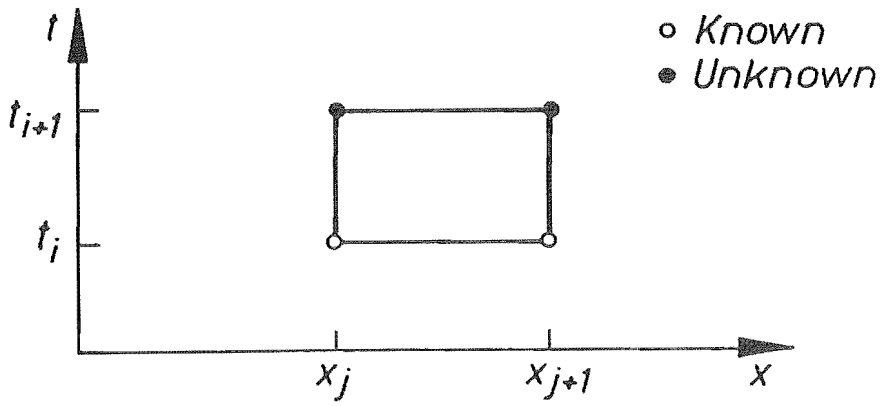

Fig. 3.5 Computational grid for the Preissmann schemes

According to Preissmann, the discretization of dependent variables and its derivatives are :

$$f(x,t) \approx \frac{\theta}{2}\left(f_{j+1}^{i+1} + f_j^{i+1}\right) + \frac{1-\theta}{2}\left(f_{j+1}^{i} + f_j^{i}\right) \tag{3.47}$$

$$\frac{\partial f}{\partial x} \approx \theta \frac{f_{j+1}^{i+1} - f_j^{i+1}}{\Delta x} + (1-\theta)\frac{f_{j+1}^{i} - f_j^{i}}{\Delta x} \tag{3.48}$$

$$\frac{\partial f}{\partial t} \approx \frac{f_{j+1}^{i+1} - f_{j+1}^{i} + f_j^{i+1} - f_j^{i}}{2\Delta t} \tag{3.49}$$

in which f is a variable, and θ , $0 \le \theta \le 1$, is a weighting coefficient.

In finite-difference schemes, the flow rate Q rather than the average velocity U is the preferred dependent variable in the dynamic equations (Amein and Chu, 1975). This is because Q is,in general, a smoother function of x and t. For example, the area and the average velocity may vary significantly between two adjacent sections, but the value of Q = U A may change smoothly.

If the velocity U is replaced by Q/A in equations (3.10) and (3.11), then the dynamic equations become

$$\frac{\partial z}{\partial t} + \frac{1}{B}\frac{\partial Q}{\partial x} = 0 \tag{3.50}$$

$$\frac{\partial Q}{\partial t} + \frac{1}{\partial x}\left(\frac{Q^2}{A}\right) + gA\frac{\partial z}{\partial x} + gA\frac{Q|Q|}{K^2} = 0 \tag{3.51}$$

in which

$$K^2 = \frac{Q|Q|}{S_f} \tag{3.52}$$

The application of the finite-difference operators defined by equations (3.47), (3.48) and (3.49) to replace the derivatives and other variables in equations (3.50) and (3.51) leads to a system of two non-linear algebraic equations:

$$\left(\frac{z_{j+1}^{i+1}-z_{j+1}^{i}+z_j^{i+1}-z_j^{i}}{2\Delta t}\right)+\frac{2}{\Delta x}\left\{\frac{\theta(Q_{j+1}^{i+1}-Q_j^{i+1})+(1-\theta)(Q_{j+1}^{i}-Q_j^{i})}{\theta(B_j^{i+1}+B_{j+1}^{i+1})+(1-\theta)(B_j^{i}+B_{j+1}^{i})}\right\} \tag{3.53}$$

$$\frac{1}{2\Delta t}(Q_{j+1}^{i+1}-Q_{j+1}^{i}+Q_j^{i+1}-Q_j^{i})+\frac{\theta}{\Delta x}\left[\left(\frac{Q^2}{A}\right)_{j+1}^{i+1}-\left(\frac{Q^2}{A}\right)_j^{i+1}\right]+\frac{(1-\theta)}{\Delta x}\left[\left(\frac{Q^2}{A}\right)_{j+1}^{i}-\left(\frac{Q^2}{A}\right)_j^{i}\right]$$

$$+\frac{g}{2}\left[\theta(A_{j+1}^{i+1}+A_j^{i+1})+(1-\theta)(A_{j+1}^{i}+A_j^{i})\right]\left\{\left(\frac{\theta}{\Delta x}(z_{j+1}^{i+1}-z_j^{i+1})+\frac{(1-\theta)}{\Delta x}(z_{j+1}^{i}-z_j^{i})\right)\right.$$

$$\left.+\left(\frac{\theta[Q_{j+1}^{i+1}|Q_{j+1}^{i+1}|+Q_j^{i+1}|Q_j^{i+1}|]+(1-\theta)[Q_{j+1}^{i}|Q_{j+1}^{i}|+Q_j^{i}|Q_j^{i}|]}{\theta[(K_{j+1}^{i+1})^2+(K_j^{i+1})^2]+(1-\theta)[(K_{j+1}^{i})^2+(K_j^{i})^2]}\right)\right\}=0 \tag{3.54}$$

Equations (3.53) and (3.54) are not sufficient to find the values of z_j^{i+1}, z_{j+1}^{i+1}, Q_j^{i+1} and Q_{j+1}^{i+1}, since for these four unknowns only two equations are available. However, if equations (3.53) and (3.54) are applied for every pair of computational points (j,j+1), then for N computational points there will be 2(N-1) of such equations for 2 N unknowns. As the upstream and the downstream boundary conditions will provide two additional equations, there will be a system of 2 N algebraic equations for 2 N unknowns. Thus, this system can be solved by an iterative procedure for any time step Δt.

3.4 Surge Analysis

A surge is a moving steep wave front which brings an abrupt change in water surface levels. Sudden reservoir drawdown caused by partial breach of a dam can create a surge within the reservoir.

When the surge occurs, the De St. Venant differential equations are not valid in the neighbourhood of the surge. The zone which is affected by the surge is very narrow, usually narrower than the distance between two computational grid points (Δx). Thus, it is reasonable to assume that the surge (discontinuity) is a boundary between two continuous flow regions (Fig. 3.6), and it is necessary to treat the discontinuity separately from the rest of the flow region.

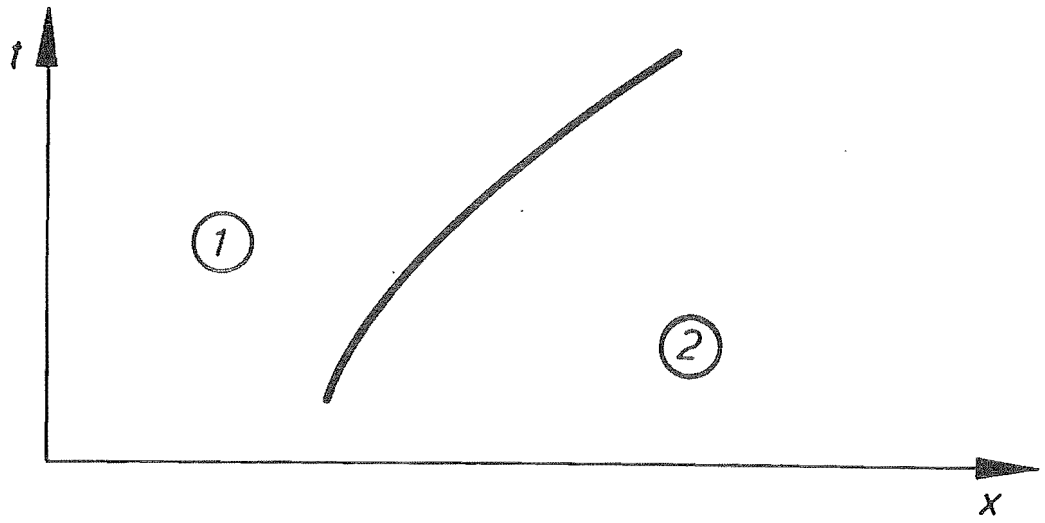

Fig. 3.6 Path of a bore separating two continuous flow regions

If the surge is considered as a simple discontinuity of the water surface height, it is possible to establish two relationships valid across the surge by using control-volume forms of the momentum and continuity equations.

The momentum and continuity equations for a moving hydraulic jump (surge) for a rectangular channel are :

$$\frac{h_1}{h_2} = \frac{1}{2}\left\{\sqrt{1+\frac{8(v-U_2)^2}{gh_2}} - 1\right\} \tag{3.55}$$

$$(v-U_1)\,h_1 = (v-U_2)\,h_2 \tag{3.56}$$

in which 1 and 2 denote the sections upstream and downstream of the surge, respectively, and v is the celerity of the surge.

The location of the surge path on the (x,t)-plane is found by integrating the equation

$$\frac{dx}{dt} = v \tag{3.57}$$

The surge celerity, which is the slope of the surge path, is different from the celerity, C, of small-amplitude waves ($C = \sqrt{gh}$). Thus, if the surge celerity, v, is smaller than the propagation speed $dx/dt = U_1+C_1$ in the region 1 and greater than $dx/dt = U_2+C_2$ in the region 2, then the positive characteristics from region 1 will overtake the surge, while all positive characteristics of region 2 are overtaken. Thus, the positive characteristics from region 1 can be made to intersect with a pair of characteristics from region 2 at the surge path, as shown in Fig. 3.7.

The flow variables in the neighbourhood of the surge can be determined, since for nine unknowns,i.e., h_{M1}, U_{M1}, h_{M2}, U_{M2}, v, $x_{L'}$, x_M, x_L and x_R, there are nine equations available , i.e, two differential equations (3.16) and (3.17) or (3.18) and (3.19) corresponding to each of the characteristics L'M, LM and RM, two

algebraic relationships across the discontinuity and one equation of the surge path. These nonlinear algebraic equations can be solved by an iterative method.

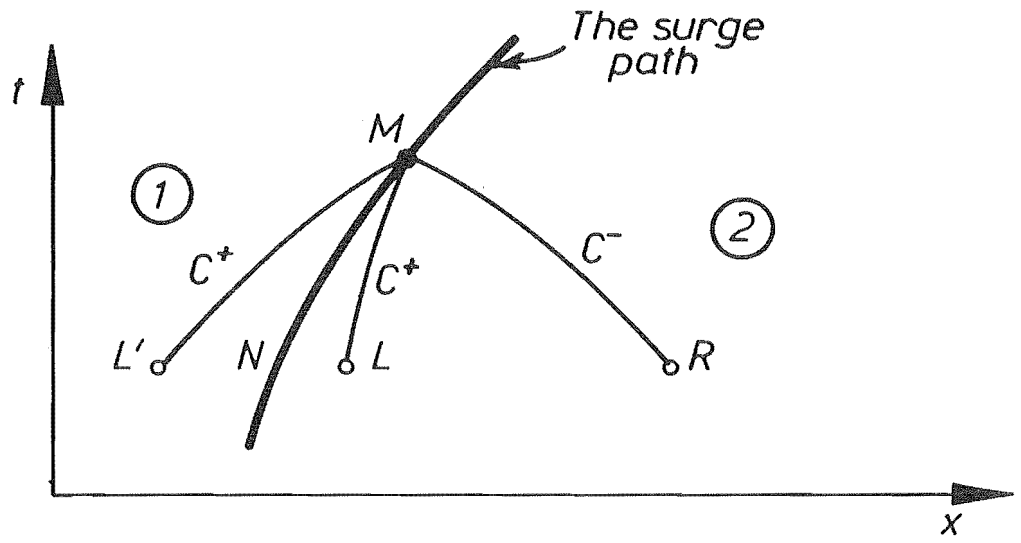

Fig. 3.7 Characteristics in the neighbourhood of the surge

CHAPTER 4

MODEL DEVELOPMENT

4.1 Introduction

Mathematical models were developed to calculate the reservoir outflow hydrograph caused by a dam failure. Velocities and depths within the reservoir were calculated by applying boundary conditions at the upstream end of the reservoir and at the dam breach. Thus, it was necessary to specify both the geometry and time history of the breach development together with the reservoir inflow, controlled outflow and reservoir geometry.

In practice, both the geometry and time history of breach development depend upon the time history of the reservoir inflow and outflow and, possibly, upon other external factors such as seismic movements. Present-day technology, however, is too limited to consider a model that calculates the breach development as part of the problem solution. Therefore, it was decided to specify the geometry and time history of the breach development independently of the breach outflow.

The outflow through dam-breaches and outlet structures are computed as a function of reservoir water surface elevation by using empirical weir or orifice equations. Thus, the dam breach is assumed to act as a flow control, and any influence of the downstream flow upon outflow through the breach is neglected.

In order to get a comprehensive numerical model for routing of the reservoir inflow and water stored in the reservoir through the breach, four numerical methods were investigated. The numerical methods are a simplified method, an

explicit method of characteristics, a linearized implicit method of characteristics and a linearized implicit finite-difference method. The simplified method is based upon continuity and the level-reservoir approximation, and the other methods involve solution of the complete De St. Venant equations.

4.2 Breach Simulation

The reservoir outflow hydrograph is governed largely by the geometry of the breach and the development of the breach with time. In the past it has usually been assumed that the dam collapsed entirely and instantaneously because it was easier and more convenient when applying certain mathematical techniques for analyzing dam-break flood waves. These assumptions may be relevant for concrete arch-type dams, but they are not appropriate for earth-dams and concrete gravity dams, which tend to have a partial breach.

Overtopping and internal piping are the main causes of failure for earth-dams. A piping failure occurs when initial breach formation takes place some point below the top of the dam, and, as the erosion proceeds, a larger and larger opening is formed until the structure above the pipe collapses. An overtopping failure starts with the formation of one or several notches. Then the discharging water erodes the notches until either the reservoir water is depleted or the breach resists further erosion. Although the main modes of failure for earth-dams have been identified, the mechanics of failure have never been accurately described analytically, and little is understood about the definition of the size and shape of the incipient breach.

The failures of concrete dams are less predictable than failures of earth-dams, and the final shape of the breach depends on many structural and geological parameters. The logical way to simulate the failure of a gravity dam is to assume that one or more of the monolithic sections formed during the construction of the dam are displaced, as their joints may be considered relatively weaker than other parts of the dam. Thus, there is a sequence of monolith removals.

In the last 20 years a number of mathematical models have been developed for the simulation of earth-dam breach erosion. The models considered critical flow conditions at the breach and used sediment transport formulae to determine the rate of erosion at the breach. The breach morphology is usually taken as rectangular, triangular or trapezoidal. Most of the models require the specification of reservoir, dam geometry and physical characteristics of the dam, i.e., mean particle diameter, resistance to erosion, angle of internal friction, and cohesion.

Regardless of the level of the model sophistication, there is a degree of uncertainty of the result. This is because the range of values of parameters involved is very wide, and the models require specification of the critical unknown parameters, i.e., initial size, shape and erosive patterns of the breach. Thus, for reasons of simplicity, most of the models assumed that breach patterns were rectangular, triangular, trapezoidal or parabolic.

Since the actual failure mechanics are not well understood for concrete dams, and since there are some doubts about the results of earth-dam breach erosion models, the breach parameters are specified herein independently of the outflow through the breach. Thus, the user has to specify a breach failure time, an initial size and shape of the breach, and an enlargement rate of the breach with time.

An enlargement rate and a breach shape for a rectangular, triangular, or trapezoidal shape (see Fig. 4.1a) can be specified by parameters $b_b(t)$, $h_b(t)$, and $z(t)$, in which $b_b(t)$ is the breach bottom width, $h_b(t)$ is the breach height, and $z(t)$ is the side slope of the breach, i.e., 1 vertical : z horizontal slope,. For example, $b_b(t)>0$, $h_b(t)>0$, and $z=0$. produces a rectangular shape. An enlargement for a parabolic shape (see Fig. 4.1b) is specified by a parameter $h_b(t)$. This type of breach simulation allows the user to update the breach parameters with the latest capabilities for estimating the breach parameters.

Selection of the failure time, size and shape of the breach in forecasting dam-break floods introduces a varying degree of uncertainty in the model results.

Johnson and Illes (1976) stated that the fully formed breach in an earth-dam is between one and three times as wide as it is deep. Singh, V.P. and Scarlatos, P.D. (1988) collected 52 historical dam-cases and noticed that the breach shape for practical purposes can be approximated as trapezoidal. The ratio of the breach width at the top and the bottom ranges from 1.06-1.74 with mean value of 1.29 and standard deviation of 0.180. The failure time for most cases was between half an hour and 12 hours. For a concrete gravity dams, failure is expected to be fairly rapid.

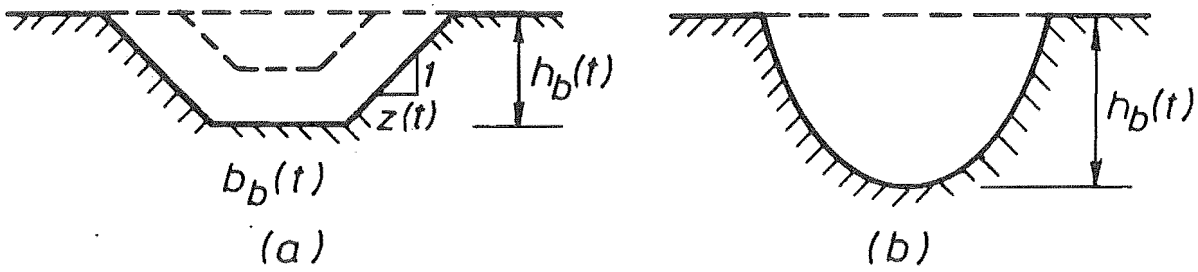

Fig. 4.1 Breach Formation: (a) rectangular, triangular or trapezoidal;
(b) parabolic

For forecasting a dam-break flood wave, it is possible to establish a theoretical upper limit on the peak outflow from the dam breach by selecting the failure time in the lower range and the breach size in the upper range.

4.3 Stage-Discharge at the Breach

Discharge through the breach is assumed to be a function of the breach geometry and the instantaneous upstream hydraulic head. The breach geometry as a function of time is given as input data, and the hydraulic head is the head a short distance upstream where streamline curvatures are relatively small. Thus, the breach opening at the dam is assumed to be a flow control, and the breach acts as a broad-crested weir.

The breach outflows (Q_b) are computed as follows:

Breach geometry	Discharge equation	
Parabolic	$Q_b = C_d \sqrt{0.75fg}\ H^2$	(4.1)
Rectangular	$Q_b = \frac{2}{3} C_d \sqrt{\frac{2g}{3}}\ b_b\ H^{1.5}$	(4.2)
Triangular	$Q_b = \frac{16}{25} C_d \sqrt{\frac{2g}{5}}\ z\ H^{2.5}$	(4.3)
Trapezoidal	$Q_b = C_d\ (b_b Y_c + z Y_c)\ \sqrt{2g}\ (H - Y_c)$	(4.4)

where

b_b = instantaneous breach bottom width
C_d = coefficient of discharge
f = a focal distance for a parabolic shape
g = gravity
h = upstream head above the breach
H = upstream hydraulic head relative to breach level
= h + U^2/g
Y_c = critical depth at the breach
z = the horizontal slope of the breach

The discharge equations are derived from the Bernoulli equation. The coefficient of discharge (C_d) is introduced to account for centripetal forces in the zone of accelerations, non-uniform velocity distributions, viscous effects, and turbulence, all of which are neglected in derivation of the discharge equations. Singer (1964) deduced that the coefficient of discharge is a function of two ratios: H/L and H/(H+P), where L is the length of the crest in the flow

direction, and P is the lowest crest level above the bed level. Bos (1976) showed that C_d is in the range of 0.848 to 1.052 and 0.85 to 1.00 for rectangular broad-crested weirs and triangular broad-crested weirs, respectively.

In the literature, the discharge equation for a trapezoidal weir is sometimes computed as the sum of the discharge equations for rectangular and triangular weirs. This is appropriate for a sharp-crested weir but not for a broad-crested weir. Bos (1976) gave two reasons why the superposition of various discharge equations for a broad-crested weir is not correct. The first reason is the difference of simultaneous critical depth values,i.e., $Y_c=(2/3)H$ for a rectangular and $Y_c=(4/5)H$ for a triangular control section, and the second reason is significant difference in mean flow velocities through the rectangular and triangular portions of the control section. Thus, superposition of discharge equations for broad-crested weirs will lead to an incorrect value for C_d.

Broad-crested weirs are not sensitive to the effects of tail-water level. The weirs can tolerate ratio of total heads upstream and downstream of the weir of up to 0.66 without the critical conditions on the weir being drowned out. Thus, it is reasonable to assume that the breach outflow is independent of downstream conditions. When the depth of flow downstream starts to cause the head on the weir to increase, the submergence effects cannot be neglected and the breach outflow computation requires specification of downstream conditions.

Depletion of the reservoir storage by the outflow tends to cause the discharge to decrease, and any inflow to the reservoir tends to cause the hydraulic head and discharge to increase. In order to determine the outflow hydrograph, a reservoir routing technique must be used to account for the simultaneous effects of the reservoir inflow, the reservoir storage characteristics and the breach characteristics.

4.4 Numerical Models

Four numerical models were developed for computing dam-break outflow hydrographs. They are a level-reservoir-approximation model, an explicit method-of-characteristics model, a linearized implicit method-of- characteristics model, and a linearized implicit finite-difference model. The first model is based upon the storage form of the continuity equation, and the other models are based upon the complete De St. Venant equations.

The level-reservoir-approximation model assumes that the water surface elevation within the reservoir is level. This model is easy and cheap to execute on a digital computer, but it is only suitable for breach widths that are small compared to both lateral dimensions of the reservoir. In this case the reservoir will empty slowly enough to allow the free surface to be approximated with a horizontal plane.

The method of characteristics models are based upon the characteristic form of the De St. Venant equations. Both explicit and implicit approximations of the method of characteristics with specified time intervals were developed. The method of characteristics tends to give relatively accurate numerical solutions and, therfore, is useful for checking the accuracy of other numerical models.

Because the De St. Venant equations are not valid in the neighbourhood of a surge, a mathematical model with special surge equations is incorporated in the method of characteristics models. Thus, the models can describe closely the wave formations in the reservoir. They can establish the time and place of surge generation, and they can track the surge whether it is propagating under subcritical, supercritical, or mixed flow conditions in either prismatic or nonprismatic channels.

The linearized implicit finite-difference model is based upon the De St. Venant equations. The Preissmann scheme was used to discretize the partial differential

equations. The resulting nonlinear algebraic equations were linearized, and the linear algebraic equations were solved simultaneously.

The main advantage of the linearized implicit finite-difference model is its high efficiency. This is because the time step is no longer subject to the Courant constraint. Nevertheless, this model is unable to include either a surge or supercritical flow in its solution, even though the time step used is much smaller than the Courant condition. Thus, special conditions concerning the inception and propagation of a surge are not furnished by this model.

4.4.1 The Level-Reservoir-Approximation Model

The level-reservoir-approximation model uses the storage form of continuity equation with an assumption of a horizontal free surface. Thus, the difference in volume of a reservoir (ΔS) during the time interval Δt can be expressed as :

$$\Delta S = \frac{h_2 - h_1}{2} (A_{s_2} + A_{s_1}) \qquad (4.5)$$

in which the subscript 1 and 2 indicate values at the time t-Δt and t, respectively, h is the reservoir water surface elevation above a reference level, and A_s is the reservoir surface area at an elevation h.

Inserting equations (3.2) and (4.5) in equation (3.8) results in the following expression :

$$\frac{(h_2 - h_1)\ (A_{s2} + A_{s1})}{2\,\Delta t} + \frac{\beta\ (h_2^n + h_1^n)}{2} - \frac{Q_{inp2} + Q_{inp1}}{2} = 0 \qquad (4.6)$$

The reservoir water surface area (A_s) can be calculated for every elevation h from the input data of the reservoir geometry. The coefficient β and the exponent n are determined from the breach geometry. The reservoir inflow (Q_{inp}) as a function of time is known from the input data. Thus, the only unknown variable is h_2 which can be obtained by using the Newton-Raphson iteration.

Having obtained h_2 at time (t), the corresponding reservoir outflow can be obtained by using the discharge equation through the breach. The reservoir outflow hydrograph Q(t) can be developed by computing the reservoir outflow for each time (t), which goes from zero to a terminating value. A numerical integration error in equation (4.6) can be reduced by decreasing the time interval Δt.

4.4.2 The Method-of-Characteristic Models

The specified-time-interval numerical schemes have been the preferred schemes in most unsteady flow applications. There are two basic types of these numerical schemes ,i.e., the explicit and implicit method of characteristic schemes. To implement these schemes, the explicit method-of-characteristics model and the linearized implicit method-of-characteristics model were developed.

Solutions of the gradually-varied flow in a nonprismatic channel are used as the initial condition for the flow. Boundary conditions at the upstream end of the reservoir and at the dam breach are specified for all times.

The explicit model can be applied to the subcritical, supercritical or mixed flow conditions. A surge, which may form in the reservoir, is formulated as the internal boundary condition. The Froude number is used as a parameter to locate the surge initial point, and the propagation of the surge is traced by using the shock fitting method.

In principle, the explicit model is believed to be more accurate than the other models, since the explicit model can deal with any flow conditions and can simulate closely the propagation of waves in the reservoir at any time. For better accuracy, the time steps (Δt) are selected so that Courant numbers computed in the flow model are always less than one.

The time steps (Δt) used in the explicit model are often too small for practical purposes because Courant numbers must be always less than one. The time steps (Δt) used in the implicit model are not subject to the Courant condition. However, the implicit model can be applied only when subcritical flow exists throughout the entire solution domain.

The system of nonlinear equations in the implicit model is linearized by using locally constant coefficients for the unknown variables. Then this system of linear equations is solved by using the double sweep method, which is very efficient with respect to computing time and storage.

a. The Explicit Model

The model has exterior boundary conditions at the upstream end of reservoir and at the dam breach. The surge which may form within the reservoir is formulated as an internal boundary condition.

The initial depths and velocities within the reservoir are solutions of the gradually-varied steady-flow equation for nonprismatic channels:

$$\frac{dh}{dx} = \frac{S_0 - S_f + \dfrac{Q_0^2 A_x^h}{gA^3}}{1 - \dfrac{Q_0^2 T}{gA^3}} \qquad (4.7)$$

in which Q_0 = steady discharge at the dam at t = 0, x = distance measured from the breach with x<0 in the upstream direction, h = flow depth , S_0 = bed slope, S_f = friction slope, g = gravitational constant, and A = flow area. Given Q_0, the initial flow depths (h_0) at t=0 for all grid points are calculated by integrating equation (4.7) numerically. Then initial velocities are calculated from $U_0 = Q_0/A_0$. If Q_0 = 0, then S_f = 0 and simplification of equation (4.7) leads to a level water surface in the reservoir. Thus, $h_0 = S_0 x$ and U_0 = 0.

In addition to initial conditions, boundary conditions at the upstream end of the reservoir and at the dam breach must be specified for all times. The reservoir inflow hydrograph Q(t) and the breach characteristics provide the necessary boundary conditions at the upstream and downstream boundaries, respectively.

There are a number of numerical methods for solving the characteristic equations (equations (3.25) and (3.27)). For convenience and simplicity, the method of characteristics with specified time intervals is used (Fig. 4.2).

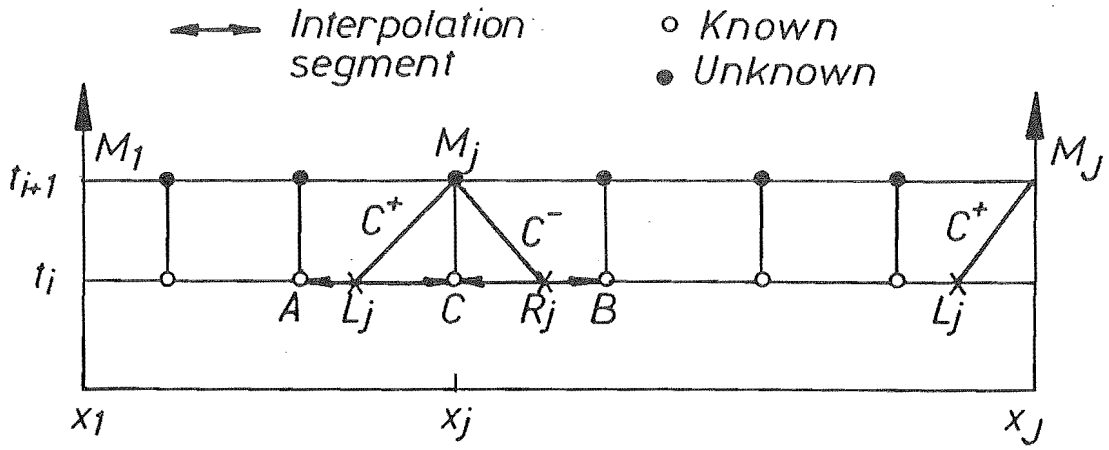

Fig. 4.2 Characteristics for the specified time-interval scheme

Values of U_{Mj} and C_{Mj} at all interior grid points (M_2-M_{J-1}) are solved by using the characteristic equations (equations (3.25) and (3.27)) along the characteristics L_j-M_j and R_j-M_j, respectively. Values of depths and velocities at L_j and R_j are interpolated linearly between two adjacent grid points (A-C and C-B). Care must be taken to choose the correct pair of two adjacent points,

since for supercritical flow $x_{Rj} < x_j$. Thus, for supercritical flow the interpolation points have to be adjusted accordingly.

The upstream boundary condition, the inflow hydrograph (Q_{inp}), which may or may not change with time, is given as input data. Depending upon the given discharge, slope, roughness, and reservoir geometry, the flow at the upstream end may vary from subcritical to supercritical flow or vice versa. For subcritical flow, $Q_{inp} = A_1U_1$ and equation (3.27) along the backward characteristic R_1-M_1 are solved simultaneously to obtain the value of U_{M1} and C_{M1} at point M_1 (Fig. 4.3). Values of U and C at point R_1 are obtained by interpolating linearly between points C and B.

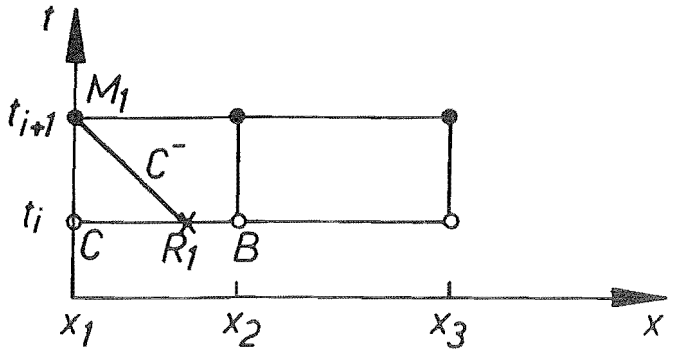

Fig. 4.3 Characteristics at the upstream boundary condition for $Q_{inp} > 0$, subcritical flow

For supercritical flow, both families of characteristics slope downstream so that the flow depth must be specified. Thus, the depth remains unchanged from its value at t=0 and no computation is made at the upstream boundary. In this case, a surge will occur within the reservoir.

In case that $Q_{inp}=0$, the front of the negative wave serves as the upstream computational boundary as long as it is propagating upstream. Thus, both U=0 and the water depth are known at this upstream moving boundary. As water starts to leave the reservoir, small depths and very low velocities at the upstream end lead to computational problems in an area of little practical interest. To avoid these problems the upstream boundary condition is applied at a node where the depth is small but finite. This depth is constantly monitored

(Fig. 4.4a), and when the depth becomes small enough, the location of the upstream boundary is shifted downstream one node.

Since both the depth and velocity at the upstream boundary are very small, the volume of water will decrease slowly at the upstream end. Thus, the water surface can be approximated with a horizontal plane (Fig. 4.4a).

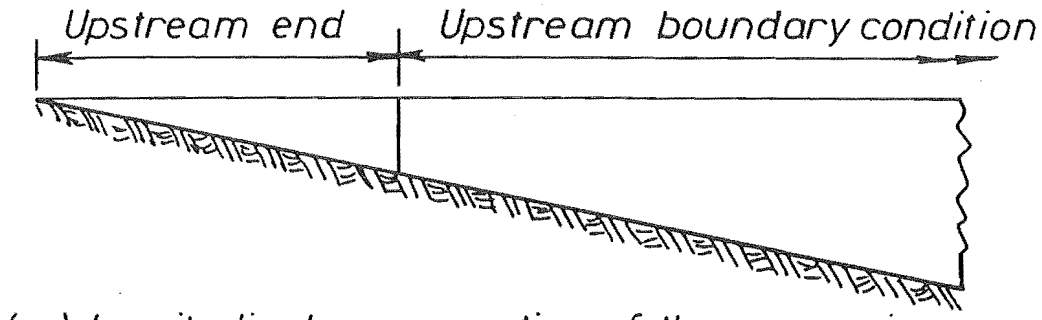

(a) Longitudinal cross section of the reservoir

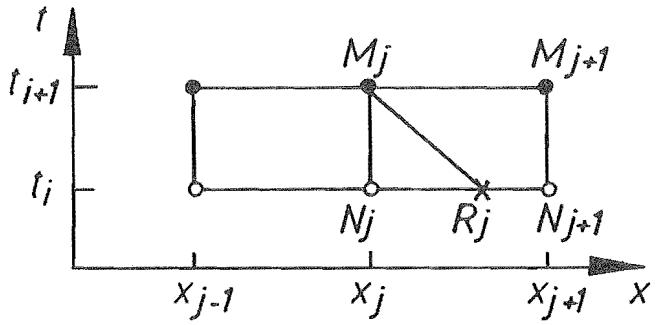

(b) Grid net for subcritical flow

Fig. 4.4 Upstream boundary condition for $Q_{inp} = 0$

Inserting equation (4.5) in equation (3.8) for $Q_{inp}=0$, the storage form of the continuity equation becomes :

$$\frac{(h_M - h_N)\,(A_{s_M} + A_{s_N})}{2\,\Delta t} + (Q_{out_M} + Q_{out_N}) = 0 \qquad (4.8)$$

in which the subscripts M and N indicate values at the time t_{i+1} and t_i , respectively, and A_s is the area of the horizontal free surface upstream from the boundary node.

For subcritical flow, h_{Mj} and U_{Mj} can be found by using equation (4.8) and equation (3.27) along the backward characteristic R_j-M_j (Fig. 4.4b), where values at point R_j are interpolated linearly between points N_j and N_{j+1}. The procedure described above is not suitable for supercritical flow, since the negative waves cannot travel upstream (U-C > 0). Then both U and h must be specified for the upstream boundary condition, and another equation in addition to equation (4.8) is needed. To satisfy this requirement, Manning's formula is used to calculate the flow rate at grid point ($M_{j,i+1}$) by assuming that values of the energy slope (S_f) at grid points ($M_{j,i+1}$) and ($M_{j+1,i+1}$) are equal. This procedure requires that dependent variables at grid points ($M_{j+1,i+1}$) be computed first.

Inserting equation (3.14) in equation (4.8) gives:

$$\frac{(h_M - h_N)\ (A_{s_M} + A_{s_N})}{2\ \Delta t} + \frac{\left(\frac{1}{n} R^{\frac{2}{3}} S_f^{\frac{1}{2}} A\right)_M + Q_{out_N}}{2} = 0 \qquad (4.9)$$

The water surface area (A_s), the hydraulic radius (R), and the flow area (A) can be calculated for every elevation h. Since all terms are known except h_M, equation (4.9) can be solved by using the Newton-Raphson iteration. Then U_{Mj} can be obtained by using Manning's formula (equation 3.14).

At the downstream boundary, the breach geometry as a function of time is given as input data. The discharge equation and equation (3.27) along the forward characteristic L_J-M_J are used to find values of velocities and depths at point M_J (Fig. 4.5). Values for U and h at point L_J are obtained by interpolating linearly between points A and C.

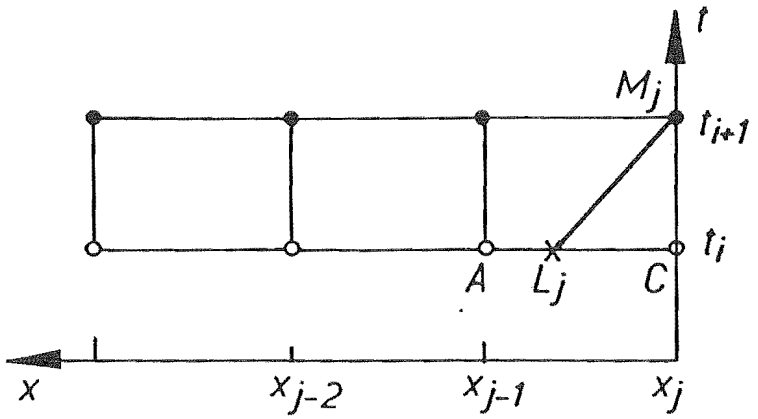

Fig. 4.5 Characteristics for downstream boundary condition.

The surge (discontinuity) appears when there is an intersection of two characteristics of the same family, which leads to multiple-valued results. Since the method of characteristics with specified time intervals uses linear interpolation for values of depths and velocities between grid points, the intersection of the characteristics of the same family will not appear in the computation. In view of the fact that the regions upstream and downstream of the surge will be supercritical and subcritical flow or vice versa, the surge is assumed to start midway between the first two nodes where the Froude number changes from less than one to more than one.

The momentum and continuity equations for a moving hydraulic jump give the following two relations:

$$U_1 - U_2 + \left[g \frac{A_1 - A_2}{A_1 A_2} (A_1 \eta_1 - A_2 \eta_2) \right]^{\frac{1}{2}} \tag{4.10}$$

$$v = \frac{A_1 U_1 - A_2 U_2}{A_1 - A_2} \tag{4.11}$$

in which 1 and 2 denote the section upstream and downstream of the surge, respectively, and η is the depth of the centroid of the cross section beneath the water surface.

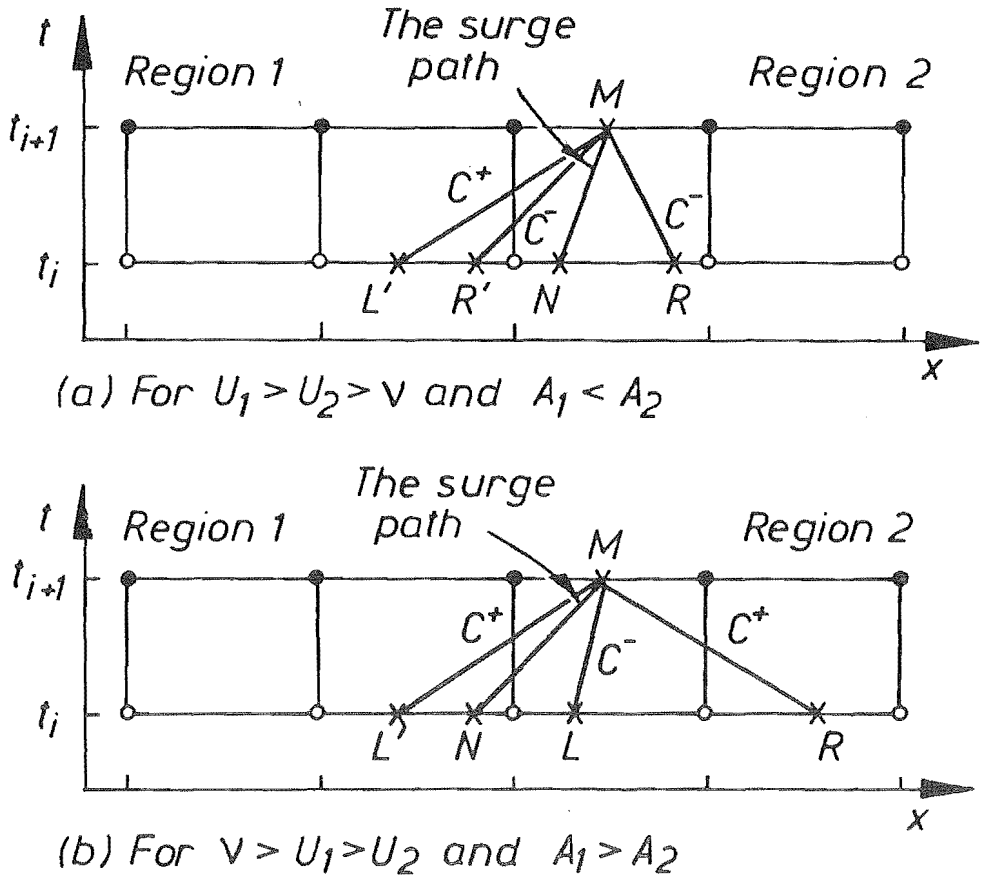

Fig. 4.6 The surge path and the characteristics C^+ and C^-

Figure 4.6 depicts two cases which will arise in the internal boundary condition. Figure 4.6a shows the only case that arises in this particular problem. In this case, the surge front computation proceeds as follows :

(1) For the first iteration, the location of the surge front at time t_{i+1} is determined by using the surge celerity (v) at time t_i.

$$x_M = x_N + v_N \Delta t \tag{4.12}$$

(2) Values of U_2 and C_2 at M are computed by using equations (3.25) and (3.27) along the characteristics L'-M and R'-M, respectively.

(3) Values of v_M, U_{2M}, and C_{2M} are determined by solving simultaneously equation (3.27) along the characteristic L-M and the surge equations (equations (4.10) and (4.11)).

(4) Point M is relocated by using the new value of v_M

$$x_M = x_N + \frac{(v_M + v_N)\,\Delta t}{2} \tag{4.13}$$

Step 2 through 4 are repeated until changes in the values of x_M from one cycle to the next are insignificant.

Since the outflow causes water depths to decrease in the reservoir, the surge will diminish and eventually vanish as h_2/h_1 approaches unity.

The solution at time t_{i+1} depends upon the interpolated solution at time t_i. Thus, any errors will accumulate with time. To increase the accuracy of the scheme, the time interval (Δt) is calculated from the smallest of the Courant numbers computed for all grid points at time t_i.

$$\Delta t \le \frac{\Delta x}{(U_j + C_j)_{max}} \tag{4.14}$$

The selection of the interval Δx depends upon the length of the reservoir. If Δx is chosen very small, there will be a large number of grid points that require a corresponding large amount of computer time for a solution. Furthermore, there is a limit beyond which we cannot decrease Δx further. If Δx is decreased further

at this stage, the error will increase because of round-off errors in the computation. On the other hand, a large Δx will not provide the desired accuracy in the result. Thus, selection of Δx requires engineering judgment.

b. The Implicit Model

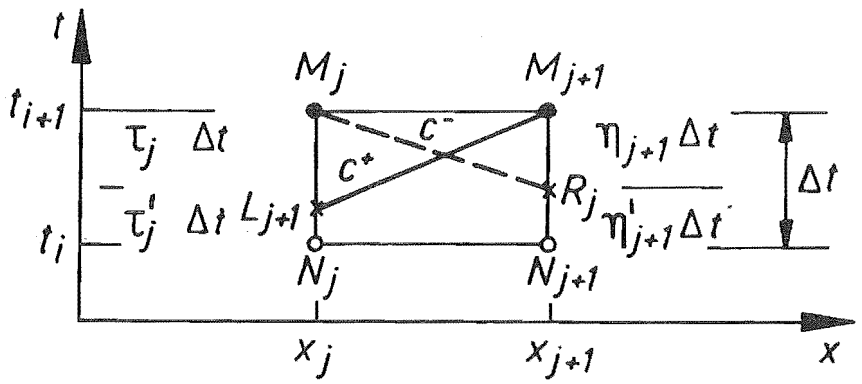

Fig. 4.7 The implicit scheme of the method of characteristics

This implicit model applies only to subcritical flow conditions. The model is based on equations (3.44) and (3.45) along the forward and backward characteristics, respectively. For any pair of grid points (j,j+1) as shown in Fig. 4.7, an equation along the characteristic L_{j+1}-M_{j+1} and an equation along the characteristic R_j-M_j can be written in finite-difference forms as:

$$A h_{j+1}^{i+1} + B U_{j+1}^{i+1} + C h_j^{i+1} + D U_j^{i+1} + G = 0 \qquad (4.15)$$

$$A' h_{j+1}^{i+1} + B' U_{j+1}^{i+1} + C' h_j^{i+1} + D' U_j^{i+1} + G' = 0 \qquad (4.16)$$

where the coefficients A,B,C,D,...,G' (see appendix B) are functions of known and unknown variables at time t_i and t_{i+1}, respectively. For simplicity, superscripts of the unknown variables will be dropped from the following analysis.

For N grid points, there are 2(N+1) non-linear equations that can be organized for 2(N+1) unknowns. This system of equations can be linearized by using locally constant variables for coefficients A,B,C,...G'. The matrix of this linear system of equations is sparse and banded. A double-sweep method uses the matrix structure of the linear system of equations to compute the solution. A computation point in the double-sweep method is linked only to adjacent points. For example, a point j is linked only to adjacent points j-1 and j+1. Thus for a given number of points, N, the number of operations to solve the system of the linear equations is proportional to N rather than N^3. The method was first applied to open channel hydraulics by Preissmann and Cunge (1961). Lai (1988) applied the double-sweep method to the implicit scheme of the method of characteristics.

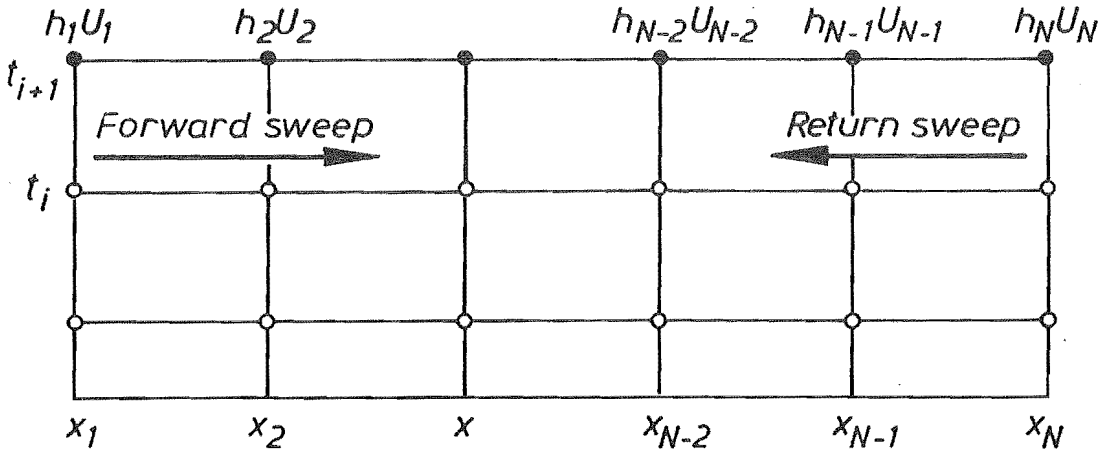

Fig. 4.8 Double-sweep algorithm for the implicit scheme.

At the upstream boundary, j=1, the inflow hydrograph, $Q_{inp} = Q(t)$, is given as input data. A value of h_1 is assumed, and the corresponding value of U_1 can be found. Since the value of U_1 is known, two other linear relationships can be obtained from equations (4.15) and (4.16) :

$$h_1 = L_1 h_2 + M_1 U_2 + N_1 \tag{4.17}$$

$$h_1 = L_1' h_2 + M_1' U_2 + N_1' \tag{4.18}$$

in which

$$L_1 = \frac{-A_1}{C_1} \quad , \quad M_1 = \frac{-B_1}{C_1} \quad , \quad N_1 = \frac{-(D_1 U_1 + G_1)}{C_1}$$

$$L_1' = \frac{-A_1'}{C_1'} \quad , \quad M_1' = \frac{-B_1'}{C_1'} \quad , \quad N_1' = \frac{-(D_1' U_1' + G_1')}{C_1'}$$

Another relationship is obtained by eliminating h_1 from equations (4.17) and (4.18) :

$$U_2 = E_2 h_2 + F_2 \tag{4.19}$$

in which

$$E_2 = \frac{-(L_1 - L_1')}{(M_1 - M_1')} \quad , \quad F_2 = \frac{-(N_1 - N_1')}{(M_1 - M_1')}$$

The same procedure can be repeated and, in general, between points j and j+1 there are two linear relationships which can be written as follows :

$$h_j = L_j h_{j+1} + M_j U_{j+1} + N_j \tag{4.20}$$

$$U_{j+1} = E_{j+1} h_{j+1} + F_{j+1} \tag{4.21}$$

in which

$$j = 2, N-1$$

$$L_j = \frac{-A_j}{C_j + D_j E_j} \qquad M_j = \frac{-B_j}{C_j + D_j E_j}$$

$$N_j = \frac{-(G_j + D_j F_j)}{(C_j + D_j E_j)}$$

$$E_{j+1} = \frac{-(L_j - L_j')}{(M_j - M_j')} \qquad F_{j+1} = \frac{-(N_j - N_j')}{(M_j - M_j')}$$

All coefficients L_j, M_j, N_j, E_{j+1} and F_{j+1} (j=1, N-1) can be calculated in the forward sweep (Fig. 4.8).

At the downstream boundary, j=N, the stage-discharge relation is given as input data ($Q_N = f(h_N)$). Assuming h_N by extrapolating from the previous values of h_N, U_N can be calculated by using equation (4.21). In the return sweep, values of variables h_j and U_j for j=N-1 through 1 can be computed. At j=1, the computed value of h_1 is compared with the assumed value of h_1, and the whole process is repeated until satisfactory agreement is obtained.

An iteration procedure for the system of nonlinear equations proceeds as follows: (1) the system of non-linear equations is linearized by using locally constant coefficients for the unknown variables; (2) then, the linearized system of equations is solved by using the double sweep method; (3) after one complete double-sweep, the newly computed variables at time t_{i+1} are used to improve values of coefficients A,B,...,G'. Step 2 and 3 are repeated until changes in the computed variables from one cycle to the next are insignificant.

The initial depths and velocities must be known at all cross sections of the channel. If the initial condition is gradually-varied steady-flow, equation (4.7) is used to calculate the initial depths, and the initial velocities are calculated from $U_0 = Q_0/A_0$.

The time intervals, Δt, are selected by using the Courant constraint as a guide. Since the implicit model becomes explicit when the Courant number is less than one, the time interval Δt is chosen so that Courant numbers are greater than one for all grid points at all times.

The distance steps (Δx) are not necessarily of the same length. They can be varied in order to get better accuracy. For instance, Δx can be reduced in regions of severe expansions or contractions and also in other regions of rapidly varied flow.

4.4.3 The Linearized Implicit Finite-Difference Model

The linearized implicit finite-difference model is based on two non-linear algebraic equations in terms of z_j^{i+1}, Q_j^{i+1}, z_j^i, and Q_j^i (equations (3.53) and (3.54)). Since all functions f(z,Q) in the equations are known at time t_i and are differentiable with respect to z and Q, then z_j^{i+1} and Q_j^{i+1} can be substituted in the form of a Taylor series

$$f_j^{i+1} = f_j^i + \Delta f = f_j^i + \frac{\partial f_j}{\partial z}\Delta z_j + \frac{\partial f_j}{\partial Q}\Delta Q_j + \frac{\partial^2 f_j}{\partial z^2}\frac{\Delta z_j^2}{2} + \ldots \qquad (4.22)$$

where Δz, ΔQ are z and Q increments during the time step Δt. This substitution leads to a system of two non-linear algebraic equations in terms of Δz_j, ΔQ_j, Δz_{j+1}, ΔQ_{j+1}. Then the equations are linearized by developing the terms in power series and keeping only the first-order in terms of unknowns Δz_j and ΔQ_j,

j=1,2,...,N, (Liggett and Cunge, 1975). For any pair of grid points (j,j+1), the system of two linearized algebraic equations can be written as follows :

$$A\,\Delta z_{j+1} + B\,\Delta Q_{j+1} + C\,\Delta z_j + D\,\Delta Q_j + G = 0 \qquad (4.23)$$

$$A'\,\Delta z_{j+1} + B'\,\Delta Q_{j+1} + C'\,\Delta z_j + D'\,\Delta Q_j + G' = 0 \qquad (4.24)$$

where the coefficients A,B,C,D,...,G' (see appendix C) are calculated from the known values at time t_i.

The linearized model will only give a good approximation for the solution of the system of nonlinear equations when $\Delta f << f$. If this condition is not satisfied for a given Δt, then the ratio $\Delta f/f$ must be decreased by decreasing the time step Δt, thus satisfying the requirement $\Delta f << f$.

The linearized system of equations (4.23) and (4.24) for N points are solved by using the double sweep method. This method uses the banded matrix structure of the linear system of equations. Thus, for a number of points N the number of operations to solve the system is proportional to N rather than N^3, which is required for the standard method of matrix inversion. The method was first applied to open-channel hydraulics by Preissmann and Cunge (1961). More details on the double sweep method as applied to the Preissman scheme are given by Liggett and Cunge (1975).

The application of the method to the Preissmann scheme can be described briefly as follows : assume, in equations (4.23) and (4.24), that for a point j there is a linear relationship :

$$\Delta Q_j = E_j \Delta z_j + F_j \tag{4.25}$$

If this is true, then one can write the relationship for the next point j+1:

$$\Delta Q_{j+1} = E_{j+1} \Delta z_{j+1} + F_{j+1} \tag{4.26}$$

Equation (4.25) is substituted into equations (4.23) and (4.24) to eliminate the unknown Δz_j, then express ΔQ_{j+1} as a function of Δz_{j+1}. The results are :

$$\Delta Q_{j+1} = f(E_j)\ \Delta z_{j+1} + f(E_j,F_j) \tag{4.27}$$

Thus, there are two recurrence relationships as defined by equation (4.27):

$$E_{j+1} = f(E_j) \tag{4.28}$$

$$F_{j+1} = f(E_j,F_j) \tag{4.29}$$

If E_1 and F_1 are known at the boundary j=1, then both coefficients E_j and F_j can be computed for any point j (j=2,N).

The third relationship can be obtained by eliminating ΔQ_j from equations (4.23) and (4.24) :

$$\Delta z_j = L_j \Delta z_{j+1} + M_j \Delta Q_{j+1} + N_j \qquad (4.30)$$

where coefficients L_j, M_j and N_j can be computed for all points j (j=1,N-1). If Δz_N is known at boundary j=N, then ΔQ_N and Δz_{N-1} can be computed by using equations (4.27) and (4.30), respectively.

Thus, the algorithm of the double sweep method can be explained as follows: (1) the forward sweep computes all coefficients E_{j+1}, F_{j+1}, L_j, M_j and N_j (j=1,N-1); (2) then the return sweep computes values of Δz_j, ΔQ_j, z_j^{i+1} and Q_j^{i+1} (j=N-1,1).

The boundary conditions must be linearized in terms of Δz and ΔQ. Coefficients E_1 and F_1 must be known at boundary j=1, and values of Δz_N must be specified at boundary j=N.

At the upstream boundary, j=1, the inflow hydrograph ($Q_{inp}=Q(t)$) is given as input data. Values of coefficients E_1 and F_1 are determined by using the relationship:

$$\Delta Q_1 = E_1 \Delta z_1 + F_1 \qquad (4.31)$$

Let $E_1 = 0$ and $F_1 = Q(t_i+\Delta t) - Q(t_i)$. Thus, whatever the computed value of Δz_1, $\Delta Q_1 = Q(t_i+\Delta t) - Q(t_i)$.

At the downstream boundary, j=N, the stage-discharge relation is given as input data. Since $Q_N = f(z_N)$ is given, then

$$f(z_N^i) + \frac{df}{dz}\Delta z_N = E_N \Delta z_N + F_N + Q_N^i \qquad (4.32)$$

$$\Delta z_N = \frac{f(z_N^i) - F_N - Q_N^i}{E_N - \frac{df}{dz}} \qquad (4.33)$$

The initial depths and velocities, associated with steady flow, are calculated from equation (4.7) and $U_0=Q_0/A_0$, respectively.

Martin and Zovne (1971) showed that it may not always be necessary to impose special conditions concerning the inception and propagation of a surge in a channel. Thus, special conditions concerning the inception and propagation of a surge are not furnished in this model.

The stability-convergence properties of the Preissmann scheme can be controlled easily with a weighting coefficient θ. Baltzer and Lai (1968) used $\theta=1$ which yields the backward difference scheme. Amein and Fang (1970) used $\theta=0.5$ which yields the so called "box scheme". Fread (1974) examined the influence of the weighting coefficient on the accuracy of the computation and concluded that the accuracy decreases as θ departs from 0.5 and approaches 1.0. This effect becomes more pronounced as the magnitude of the computational step increases. In this model, θ is specified in the input data.

The distance steps (Δx) can be varied within the length of the reservoir. In order to maintain a stable and accurate solution, Δx can be reduced in regions of rapidly varied flow, such as immediately upstream from the breach.

Even though the implicit finite-difference scheme is unconditionally stable and is not subject to the Courant constraint, rapidly rising outflow hydrographs can cause computational problems. If Δt is too large, truncation errors increase and can even lead to the calculation of negative depths. This computational problem can be treated by reducing the time step Δt by a factor of 0.5. In order to maintain accuracy, values of the time step Δt are maintained within the Courant conditions in the early part of the computations. Then the time step can be increased as the computation advances in time.

CHAPTER 5

EXPERIMENTAL EQUIPMENT AND PROCEDURES

5.1 Introduction

Rapidly-varied unsteady flow caused by partial collapse of a dam is very complex. Near the dam site highly curved streamlines cause the basic equations to be violated. In the case of zero inflow, there is no a single analytical solution which can analyze the movement drying at the upstream end. Since a surge may form within a reservoir, the water surface cannot be assumed continuous at any time. Therefore, experimental results will be used to verify the validity of approximations used to overcome these difficulties.

The experiments were conducted in a tilting-glass flume. Four experimental models were constructed in this flume. Model I used a prismatic channel with a horizontal bed, model II used a prismatic channel with a sloping bed, and models III and IV used a nonprismatic channel with a sloping bed.

Partial instantaneous breaches of a dam were simulated by model I, II and III, and gradual breaches of a dam were simulated by model IV. The model dam was a calibrated sharp-crested weir. Various size of breaches were created in the model dam in order to obtain either rapid or gradual changes in water-surface elevations.

Unsteady water depths were measured at four predetermined locations along the channel for all test conditions. A video-recording system, which had a speed of 25 frames per second, was used to record the water depth versus time at a predetermined location. Repeated runs were necessary in order to record at all selected locations. After each recording had been completed, the water depths and times were read frame by frame from a video monitor. These data were then plotted to obtain graphs of water depth versus time.

5.2 The Flume

The experiments were conducted in a glass-tilting flume 0.56 m wide, 0.46 m high and 12.64 m long. A model dam and a barrier were put at the downstream and upstream ends of the flume, respectively.

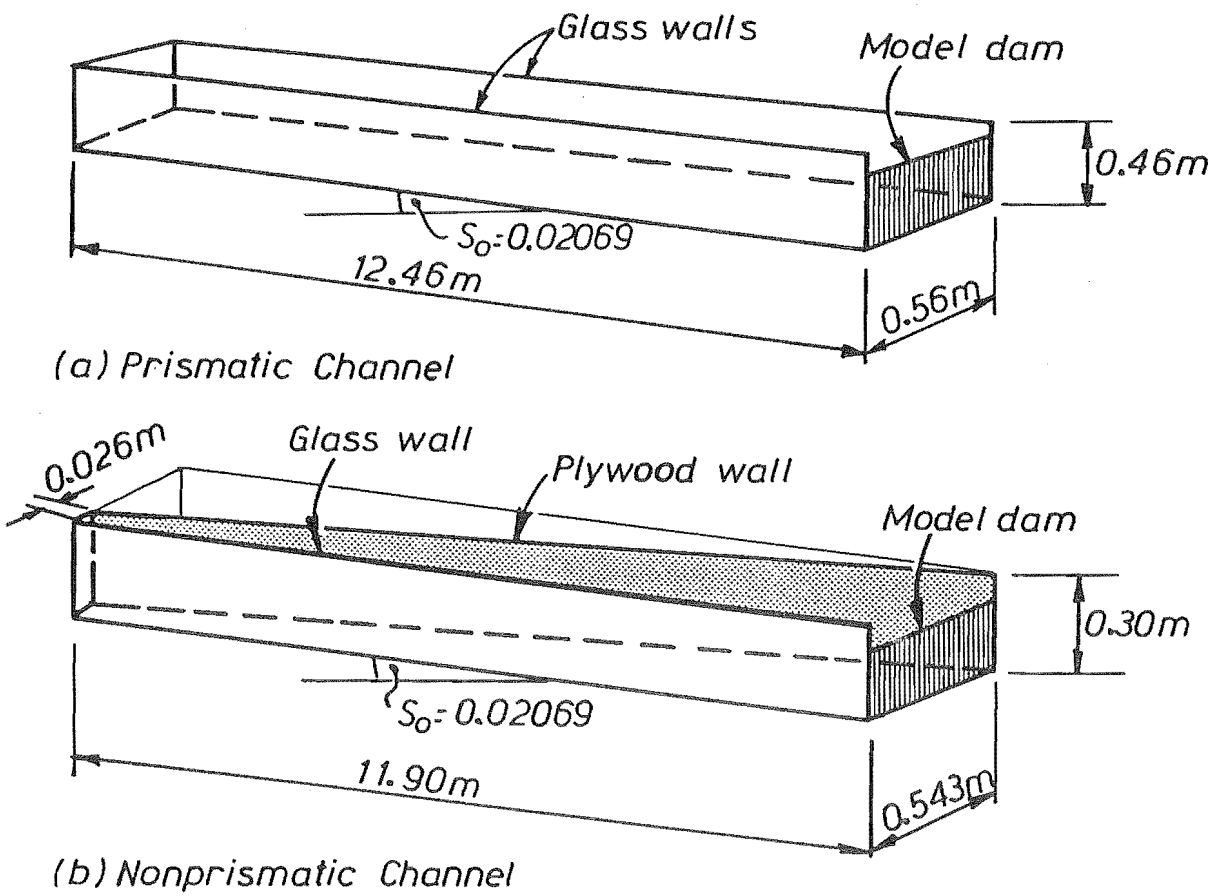

Fig. 5.1 Schematic diagram of channels

Four experimental models were used in this flume. Model I used a prismatic channel with a horizontal bed, model II used a prismatic channel with a sloping bed, and models III and IV used a nonprismatic channel with a sloping bed. The sloping bed models all had a slope equal to 0.02069.

The nonprismatic channel was constructed by placing a plywood wall between the side walls of the flume. Thus, the channel width varied linearly from 0.026m at the upstream end to 0.543 m at the downstream end.

The coefficient of roughness was measured for both the prismatic and nonprismatic channels. Thus, the coefficient of roughness (n) was calculated from Manning's equation :

$$n = \frac{R^{\frac{2}{3}} S_f^{\frac{1}{2}} A}{Q} \tag{5.1}$$

in which Q is the discharge, R is the hydraulic radius, S_f is the friction slope, and A is the flow area. A number of test runs were conducted to evaluate the coefficient of roughness. The various discharges used to calibrate the channels roughness were measured by using a calibrated electromagnetic flow meter. The results indicated that the channels roughness can be assumed to be 0.009 for both the prismatic and nonprismatic channels.

5.3 The Dam

The model dams were sharp-crested weirs. A large number of runs were conducted to evaluate values for the discharge coefficient (C_d) as a function of H/P, in which H is energy head over the weir and P is height of weir crest above the flume bed. The various discharges used to calibrate the weirs were measured by using a calibrated pit, which was 1.67 m wide, 5.48 m long and 1.54 m high.

Partial instantaneous breaches of a dam were simulated by instantaneously removing a gate that was placed behind the dam. The gate-removing mechanism is shown in (Fig. 5.2a). The video movie of this system showed that the gate was fully opened in 0.08 seconds and lost contact with the water almost instantaneously.

Gradual breaches of a dam were simulated by moving the dam vertically downward as a function of time (Fig. 5.2b). A video-camera and a graphics

generator, which was used to place a reference clock on the video recordings, were used to record the movement of dam. The resulting pictures were read frame by frame every 0.04 seconds to obtain the dam height as a function of time. The failure times were from 0.82 to 3.32 seconds.

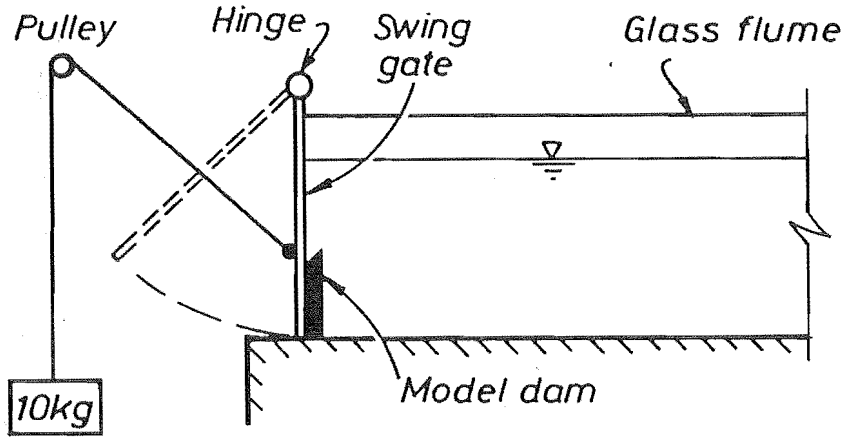

(a) Partial breaches

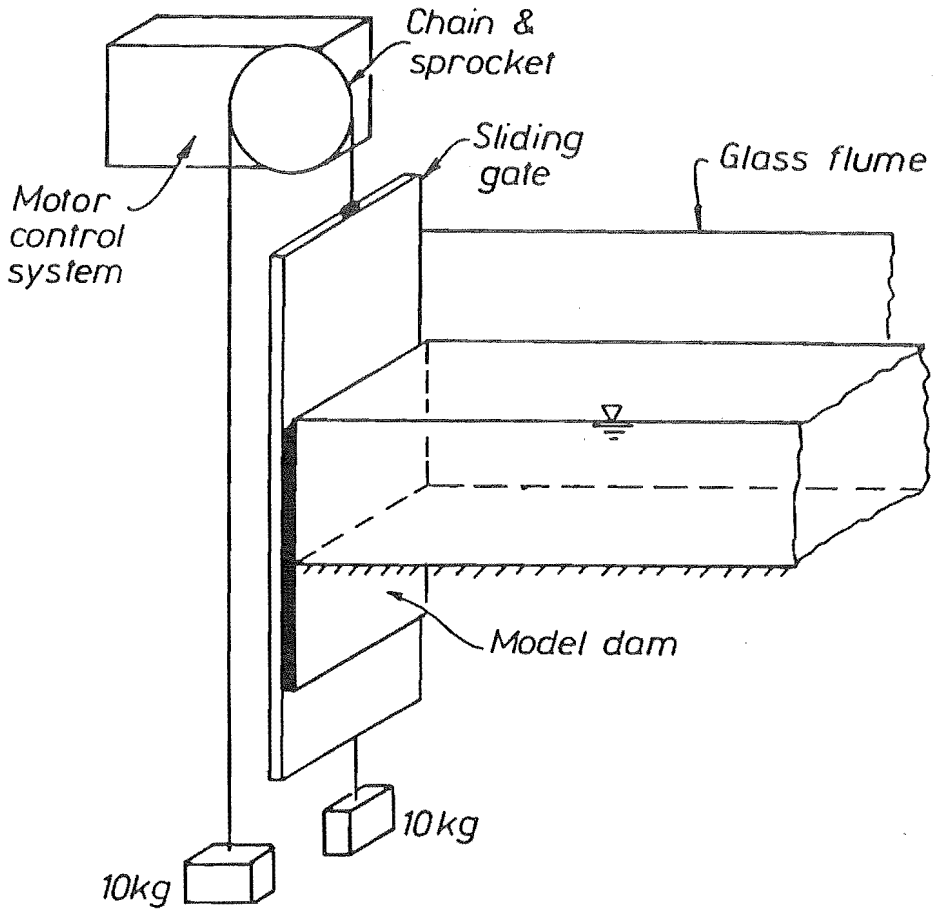

(b) Gradual breaches

Fig. 5.2 Dam-breach mechanism

5.4 Unsteady Water Depth Measurements

Measurements of water depths along the channel as a function of time were used to verify the numerical models. Under all test conditions, these measurements were made at four different locations. Three different techniques to measure water depths versus time were investigated. These three techniques used capacitance gauges, pressure transducers and a video-recording system. The first and second techniques used a computer to record the data. Capacitance gauges or pressure transducers were connected to an amplifier and a computer. The readings from the gauges or pressure transducers were sent to a computer via a DASH-16F A/D board. A program was used to record these data on a hard disk. The data file was later retrieved, manipulated and plotted by another program so that a graph of water depth versus time could be obtained.

The capacitance gauge and pressure transducer systems read data from four different locations simultaneously. The computer then constructed graphs of water depth versus time. Comparison of these graphs with data from a video-recording system showed that the gauges and pressure transducers were not sensitive to either rapid or small changes in water depths. For example, depth changes of 5 cm in 0.04 seconds and small changes of the order 0.5-1.0 mm were not recorded accurately. Thus, their results were not satisfactory and the capacitance gauge and pressure transducer systems were abandoned.

The video-recording system did not require calibration and gave water depths directly with an accuracy of about 0.5 mm. A video camera, recorder and monitor were used to record the water depths. The camera was set level with the water surface and mounted on a tripod, which was about 1.5 m from the flume. The water surface was recorded through the glass wall of the flume. As a reference for the water depth, a transparent ruler was attached to the outside of the glass wall. A graphics generator was used to place a reference clock on the video recordings. The water depths and times were read frame by frame from the video monitor. Then these data were used as input on a computer to obtain a graph of water depth versus time.

Since the video-recording system could only cover one location, repeated runs were necessary in order to record all specified locations. Reproducibility of repeated runs showed that the data obtained were in remarkable agreement.

5.5 Test Conditions and Procedures

Four experimental models were used to verify the capability of the numerical models. Partial instantaneous breaches of a dam were simulated by models I, II and III, and gradual breaches of a dam were simulated by model IV. Three test conditions were used in each of models I, II and III by generating full-width partial breaches in the model dam. Four test conditions were employed in model IV by using two different failure times in two full-width gradual breaches of the model dam. The test conditions are identified and described in table 5.1, and the breach heights as a function of time are described in table 5.2. The decimal system is used in numbering the test conditions; the whole number refers to the identification number of the experimental models, which are described in section 5.2, while the decimal refers to the test conditions (various size of breaches or duration of a breach).

The general procedures used to conduct the experiments are listed below :

1) The video camera was set up at a predetermined location. For model I, unsteady water depths were recorded at 0.20 m, 0.40 m, 5.70 m and 11.40 m behind the dam. For models II, III and IV, the water depths were recorded at 0.36m, 1.00 m, 4.50 m and 5.50 m behind the dam.

2) The model dam was put into place, and the water was impounded in the channel to the top of the model dam. The water was left undisturbed for a sufficient period of time to permit any current present in the channel to subside.

3) The video camera was started at about 40 seconds before a partial instantaneous or gradual breach was simulated at the dam.

4) The video recording system timer and the breach simulation were started simultaneously, and the video camera was operated continuously until the discharge through the breach was insignificant. The recording intervals varied from test to test because of the difference in the channel and breach sizes, but, in general, the camera was operated from 40 seconds to 90 seconds.

Table 5.1

Description of Test Conditions

Test conditions	Dam height (cm)	Dam width (cm)	Breach height (cm)	Breach width (cm)	Coef. of discharge C_d	Duration of a breach (sec.)
1.1	40.00	56.00	29.92	56.00	0.7237	0.00
1.2	40.00	56.00	24.84	56.00	0.6874	0.00
1.3	40.00	56.00	20.02	56.00	0.6661	0.00
2.1	25.90	56.00	15.82	56.00	0.8121	0.00
2.2	25.90	56.00	10.60	56.00	0.6950	0.00
2.3	25.90	56.00	5.89	56.00	0.6762	0.00
3.1	24.62	54.30	14.62	54.30	0.8121	0.00
3.2	24.62	54.30	9.41	54.30	0.6950	0.00
3.3	24.62	54.30	4.19	54.30	0.6762	0.00
4.1	24.80	54.30	14.80	54.30	0.6988	0.82
4.2	24.80	54.30	14.80	54.30	0.6988	3.32
4.3	24.80	54.30	9.70	54.30	0.6658	0.56
4.4	24.80	54.30	9.70	54.30	0.6658	2.16

Table 5.2

Breach Heights as a Function of Time

Test condition 4.1		Test condition 4.2		Test condition 4.3		Test condition 4.4	
Time (sec.)	Breach height (cm)	Time (sec.)	Breach height (cm)	Time (sec.)	Breach height (cm)	Time (sec.)	Breach height (cm)
0.00	0.00	0.00	0.00	0.00	0.00	0.00	0.00
0.10	0.03	0.33	1.72	0.06	0.40	0.21	0.96
0.20	0.54	0.66	3.41	0.12	1.33	0.43	1.99
0.30	2.42	0.92	4.62	0.18	2.61	0.64	3.02
0.40	5.17	1.25	6.22	0.21	3.52	0.85	4.05
0.50	8.14	1.84	9.05	0.25	4.36	1.02	4.82
0.55	9.56	2.16	10.61	0.30	5.65	1.24	5.85
0.60	10.84	2.49	12.16	0.39	7.31	1.49	7.04
0.70	12.90	2.76	13.39	0.46	8.44	1.70	8.00
0.76	14.10	3.02	14.32	0.50	9.05	1.92	8.99
0.82	14.80	3.32	14.80	0.56	9.70	2.13	9.70

CHAPTER 6

COMPARISON OF MODEL RESULTS WITH EXPERIMENT

6.1 Introduction

It is very important to understand wave formations in the channel caused by a dam-break. This information can be interpreted from water depth hydrographs measured at predetermined locations along the channel. It is believed that a numerical model which can simulate closely the wave formations in the channel will compute outflow hydrographs accurately.

In order to assess the ability and accuracy of the explicit method-of-characteristics model, the implicit method-of-characteristics model and the implicit finite-difference model to simulate wave formations in the channel, computed water depths at predetermined locations along the channel were compared with the corresponding results from four experimental models.

6.2 Experimental Model I

Experimental model I was a prismatic channel with a horizontal bed. The channel was 0.56 m wide, 11.40 m long and had a Manning n of 0.009. The initial water depth in the channel was 0.40 m. Three full-width partial breaches were generated in the model dam. The breach parameters are shown in table 5.1.

Comparisons between computed and measured depth hydrographs at four selected locations for test conditions 1.1, 1.2 and 1.3 are shown in figures 6.1, 6.2 and 6.3, respectively.

From these figures, it is obvious that there are only two distinct steep waves in the channel after the dam break: a steep negative wave, which goes in the upstream direction, and a reflection of this wave, which goes in the downstream direction. Thus, the water depth at any selected location plunges rapidly when the first negative wave arrives. It then remains nearly constant with slight fluctuations for a period of time before it starts to plunge again with the arrival of the reflected wave. After that the water depth drops slowly.

The experimental oscillations with a relatively small amplitude and period that are particularly noticeable at x=-11.20 m in figure 6.1 for t>11 seconds are surface waves that cannot be modelled with the St. Venant equations.

The time at which the water depth drops rapidly at any selected location in the channel is predicted accurately by the explicit method-of-characteristics (MOC) model. At any selected location, the computed depth hydrograph is in close agreement with the measured depth hydrograph. Thus, the explicit MOC model is able to describe closely the wave formations caused by a dam-break.

The initial condition of experimental model I causes values of the coefficients of the linearized system equations (equations (4.15) and (4.16)) to be equal for every grid point. In this case, the equations are poorly conditioned since only one independent equation exists, and numerical problems arise in the iteration procedure used by the implicit method-of-characteristics (MOC) model. To avoid this numerical problem, a very small bed slope (S_0=0.000004) was introduced as input data for the implicit MOC model.

At any selected location, the water depth computed by the implicit MOC model

is in close agreement with the measured water depth at any time except in the neighbourhood of a steep wave. In this region, the water depth computed by the implicit MOC model drops earlier and more slowly than the measured depth. Thus, the implicit MOC model predicts the arrival of the upper part too early and the arrival of the lower part of a steep negative wave too late. Although flow depths calculated from the implicit MOC model are noticeably less accurate than those calculated from the explicit MOC model in the neighbourhood of a steep negative wave, outflow hydrograph calculations are relatively insensitive to these inaccuracies.

The computed water depth by the linearized implicit finite-difference model is in a good agreement with the measured water depth when the water depth change slowly with time. However, this model cannot simulate the propagation of the steep wave as accurately as the explicit MOC model. The steep wave is always smeared over or diffused in the x-direction. Thus, the computed water depth drops earlier and more slowly than the measured water depth as a steep wave approaches any selected location.

6.3 Experimental Model II

Experimental model II was a prismatic channel with a sloping bed. The channel was 0.56 m wide, 12.52 m long, had a Manning n of 0.009 and a bed slope of 0.02069. The reservoir had a maximum depth of 0.259 m before part of the dam was removed instantaneously. Three test conditions, i.e., test conditions 2.1, 2.2, and 2.3, were used in this model by varying the breach opening in the model dam. The breach parameters are shown in table 5.1.

Figures 6.4, 6.5 and 6.6 are computed and measured depth hydrographs at four selected locations for test conditions 2.1, 2.2 and 2.3, respectively. At locations $x = -0.36$ m and $x = -1.00$ m behind the dam, the water surface drops rapidly

when the steep negative wave arrives. Then it drops gradually for a period of time before it starts to drop slowly with the arrival of the reflected wave. From these figures, it is obvious that the reflected wave on the sloping bed was much smaller than the reflected wave on the horizontal bed (experimental model I).

The slope of the steep negative wave gradually decreases as this wave travels upstream since the upper part of the negative wave travels faster than the lower part. This is because of their differences in their water depths and the resistance of the accelerated water moving downstream in the lower part.

Because the celerity of the leading edge of the negative wave gradually decreases as the water depth decreases in the upstream direction, the flow rate at this leading edge decreases correspondingly with time. Thus, after the steep negative wave passes any location in the downstream region, the water surface drops more gradually to satisfy the continuity equation. As this process continues, it forms a second long gradually-varied negative wave. Thus, for a reservoir on a sloping bed, two types of negative waves are formed after a dam break: a steep negative wave followed by a long gradually-varied negative wave.

A surge will occur in a reservoir with a sloping bed if the breach opening is big enough. This is shown in figure 6.4 at x = - 5.50 m by an abrupt change in water surface levels.

The explicit method-of-characteristics (MOC) model predicts accurately the arrival of the steep negative wave, the reflected wave and the surge front. At any selected location, the computed water depth is in close agreement with the measured depth at any time. In the neighbourhood of the surge, the computed water depth compares favourably with the measured water depth. This strongly suggests that the model is able to describe closely the wave formations caused by a dam-break in a prismatic channel with a sloping bed.

The depth hydrographs computed by the implicit method-of-characteristics (MOC) model show that this model has a relatively large amount of numerical diffusion in the neighbourhood of either the steep negative wave or the surge. The steep wave is always diffused in the x-direction, and a surge solution is not included in this model. In the downstream region, the implicit MOC model predicts too early the arrival of the reflected wave as shown in figure 6.4 (x=-0.36 m and x=-1.00 m).

Since a steep wave is always diffused in the x-direction by the linearized implicit finite-difference model, this model predicts the arrival of the upper part too early and the arrival of the lower part of the steep negative wave too late.

The water depth computed by the linearized implicit finite-difference model does not give an indication of the reflection of the steep negative wave at any location. This is because the simulation of the steep negative wave does not reach the upstream end of the reservoir. Since a water depth less than the normal depth at the upstream region will cause a computational problem, the location of the upstream boundary condition is shifted downstream one node at a time until the upstream depth is greater than the normal depth.

The computed water depth for the finite-difference solution is always lower than the measured water depth before the arrival of the reflected wave. Since the reflected wave does not appear in this numerical model, the computed water depth is always higher than the measured water depth after the reflected wave arrives at any location.

6.4 Experimental Model III

Experimental model III used on a nonprismatic channel with a sloping bed. The channel was 11.90 m long, had a width which varied linearly from 0.543 m at the downstream end to 0.026 m at the upstream end, had a Manning n of 0.009 and a bed slope of 0.02069. Before part of the dam was removed instantaneously, the maximum depth of the reservoir was 0.2462 m. Three test conditions, i.e., test conditions 3.1, 3.2, and 3.3, were used by varying the breach opening in the model dam. The breach parameters are shown in table 5.1.

Figures 6.7, 6.8 and 6.9 are computed and measured depth hydrographs at four selected locations for test conditions 3.1, 3.2 and 3.3, respectively. These figures show that the wave formations have the same pattern as those in experimental model II. Because the channel width decreases in the upstream direction, comparisons of these figures with those in experiment II show that: the water depth drops more gradually in experiment III after the steep negative wave passes any selected location in the downstream region (x=-0.36 m and x=-1.00); the reflected wave arrives earlier in the downstream region; and the surge occurs earlier, as shown in figure 6.7 for x = -4.50 m.

At any selected location, the water depth computed by the explicit method-of-characteristics model is in close agreement with the measured water depth at any time except in the neighbourhood of the surge. In this region, differences between the computed and measured water depths are slightly bigger than in the other regions, but they are still in a good agreement. This strongly suggests that the model is able to describe closely the propagation of a surge (which may or may not form), a steep negative wave and a long gradually-varied negative wave caused by a dam-break in a nonprismatic channel with a sloping bed.

The water depth computed by the implicit method-of-characteristics model drops earlier and more slowly than the measured depth as either the negative steep

wave or the reflected wave approaches any selected location. Thereafter, the water depth computed by the implicit MOC model agrees closely with the experiment result except in the neighbourhood of the surge. This suggests that the implicit MOC model is less accurate than the explicit MOC model.

The water depth computed by the linearized implicit finite-difference model drops earlier and more slowly than the measured depth as a steep wave approaches any selected location. Thereafter, the computed water depth is lower than the measured depth before the arrival of the reflected wave, and it is higher than the measured water depth after the reflected wave passes any selected location.

6.5 Experimental Model IV

In this model gradual breaches of a dam were simulated. The model used a nonprismatic channel with a sloping bed. The channel was 11.90 m long, had a width which varied linearly from 0.543 m at the downstream end to 0.026 m at the upstream end, had a Manning n of 0.009 and a bed slope of 0.02069. Four test conditions, i.e., test conditions 4.1, 4.2, 4.3 and 4.4, were used in the model by varying the breach opening and failure time interval in the model dam. The breach parameters and breach heights as a function of time are given in tables 5.1 and 5.2, respectively.

Figures 6.10, 6.11, 6.12 and 6.13 show both computed and measured depth hydrographs at four selected locations for test conditions 4.1, 4.2, 4.3 and 4.4, respectively. These figures show that at x = -0.36 m, the slope of the steep negative wave is not as steep as that in the instantaneous-partial breach of a dam (experiment model I, II and III). Thus, the slope of the steep negative wave

depends upon the failure time interval. Its slope decreases as the failure time interval increases, as shown in figures 6.10 and 6.11 or figures 6.12 and 6.13.

The depth hydrographs computed by the explicit method-of-characteristics (MOC) model show clearly the difference of the slope of steep negative wave for any test condition. The water depth computed by the explicit method-of-characteristics model agrees closely with the measured water depth at any selected location at any time except in the neighbourhood of the surge. In this region, differences between the computed and measured water depth are slightly bigger than in the other regions, but they are still in good agreement. These comparisons show that this model is able to describe closely water depth hydrographs of a gradual breach of a dam in a nonprismatic channel.

The accuracy of the slope of the steep negative wave computed by the implicit method-of-characteristics (MOC) model improves as the failure time interval increases, as shown in figures 6.10 and 6.11 for x=-0.36 m and x=-1.00 m. However, water depths computed by the implicit MOC model continue to be diffused in the neighbourhood of the negative wave and fail to agree closely with experiment near the surge.

In the steep negative wave region (figures 6.10 and 6.11 at x =-0.36 m), the water depth computed by the linearized implicit finite-difference model shows better agreement with the measured water depth for the longer failure time interval. However, numerical diffusion still persists near the negative wave, and poor accuracy still occurs in the neighbourhood of the surge.

6.6 Conclusions

An instantaneous-partial collapse of a dam creates a steep negative wave which goes in the upstream direction. In the downstream region, this steep negative wave is followed by a long gradually-varied wave for a period of time before the reflected wave arrives. After this reflected wave disappears, the remaining wave progressing in the reservoir is a long gradually-varied wave.

For gradual partial collapse of a dam, the slope of the steep negative wave decreases as the failure time increases. If the failure time interval is very large, a steep negative wave may not be formed. In this case, a long gradually-varied wave is the only wave which is formed in a reservoir after the dam-break.

Comparisons between model results and experiments show that:

(1) The water depth hydrographs computed by the explicit method-of-characteristics (MOC) model always agree closely with the experiments at any predetermined location. This strongly suggests that the explicit MOC model is able to describe closely the formation and propagation of the steep negative wave, the gradually-varied wave, the surge and the reflected wave caused by partial collapse of a dam in a reservoir.

(2) The implicit method-of-characteristics model displays a relatively large amount of numerical diffusion in the neighbourhood of the steep negative wave. In addition, the surge that appeared in some of the experimental results cannot be included in this model since both families of characteristics slope downstream in supercritical flow.

(3) The implicit finite-difference model always diffuses the steep negative wave. In addition, this model does not include a surge, and the appearance of a surge in the experimental solution causes relatively large differences between

calculated and measured flow depths. This model is unable to accurately model the relatively small negative wave that is reflected from the upstream end of the reservoir.

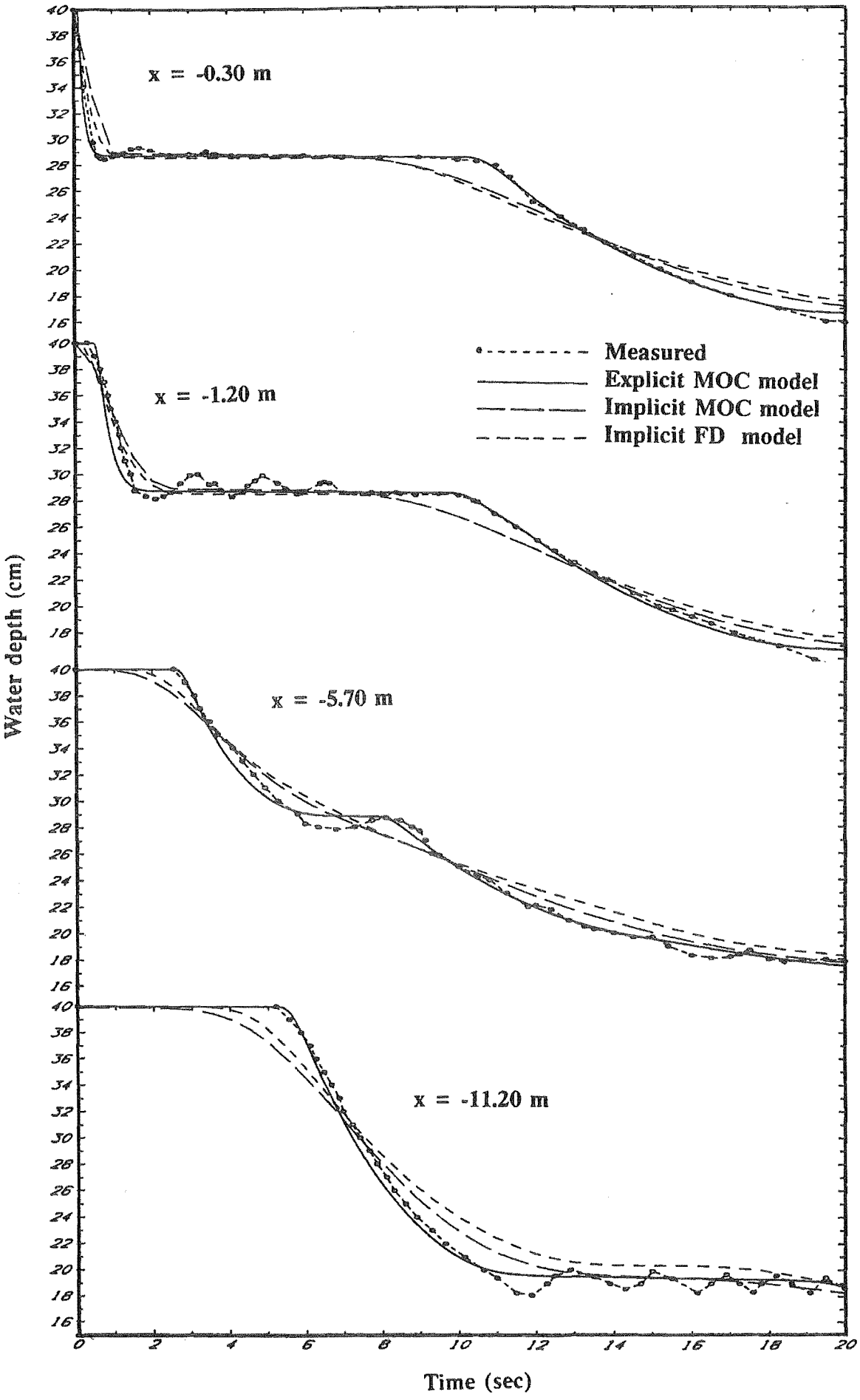

Fig. 6.1 Computed and measured depth hydrographs for test condition 1.1

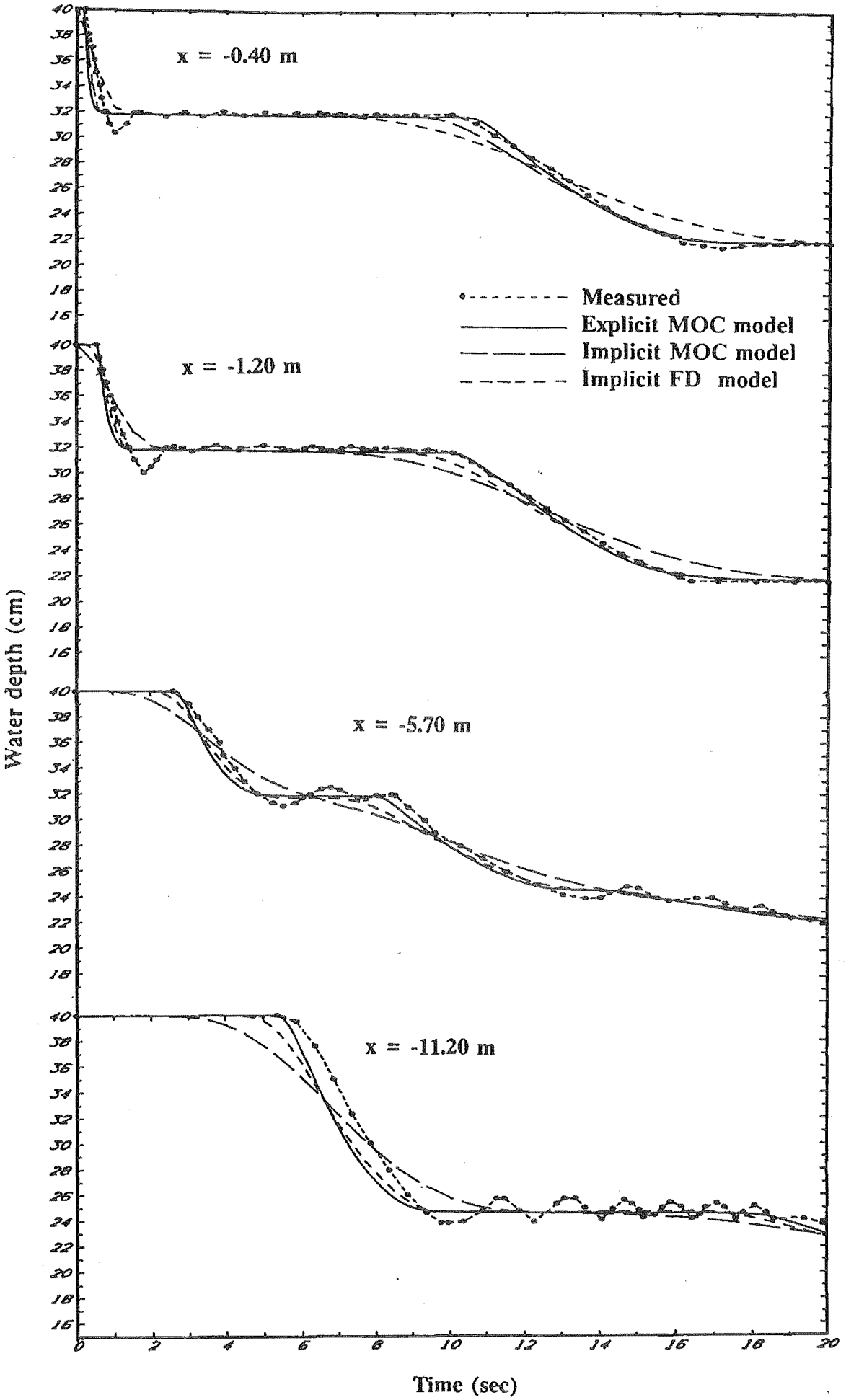

Fig. 6.2 Computed and measured depth hydrographs for test condition 1.2

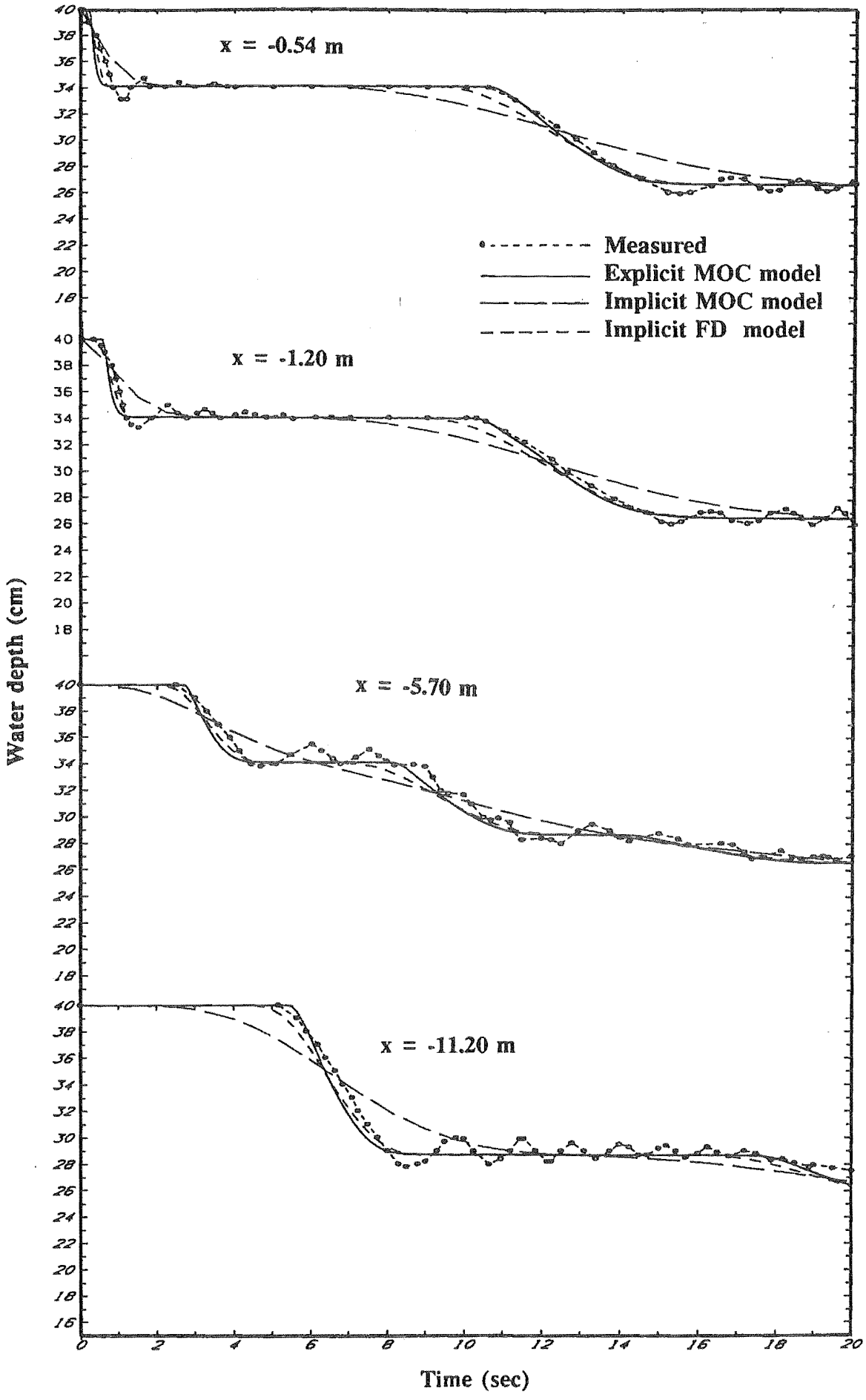

Fig. 6.3 Computed and measured depth hydrographs for test condition 1.3

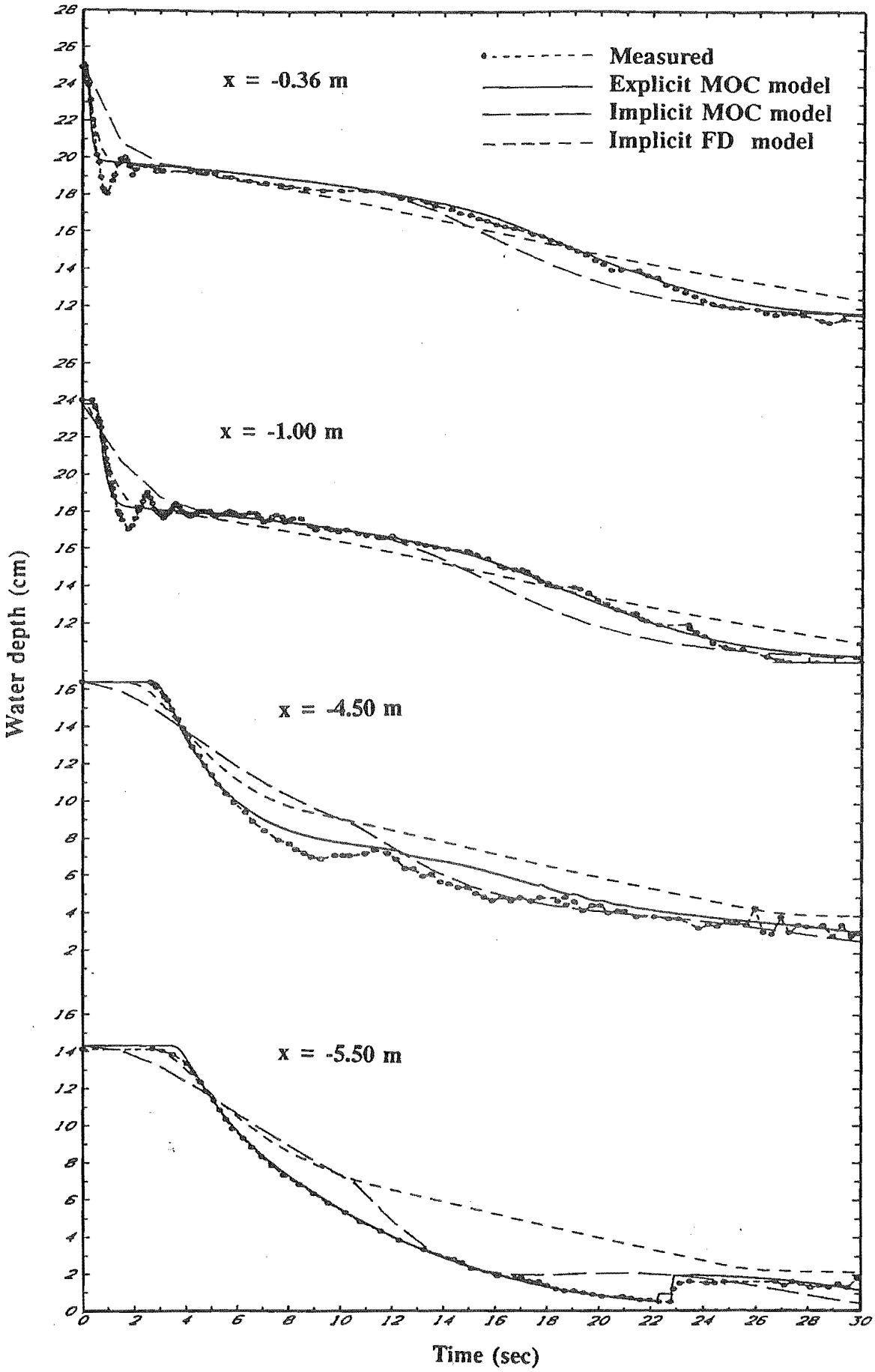

Fig. 6.4 Computed and measured depth hydrographs for test condition 2.1

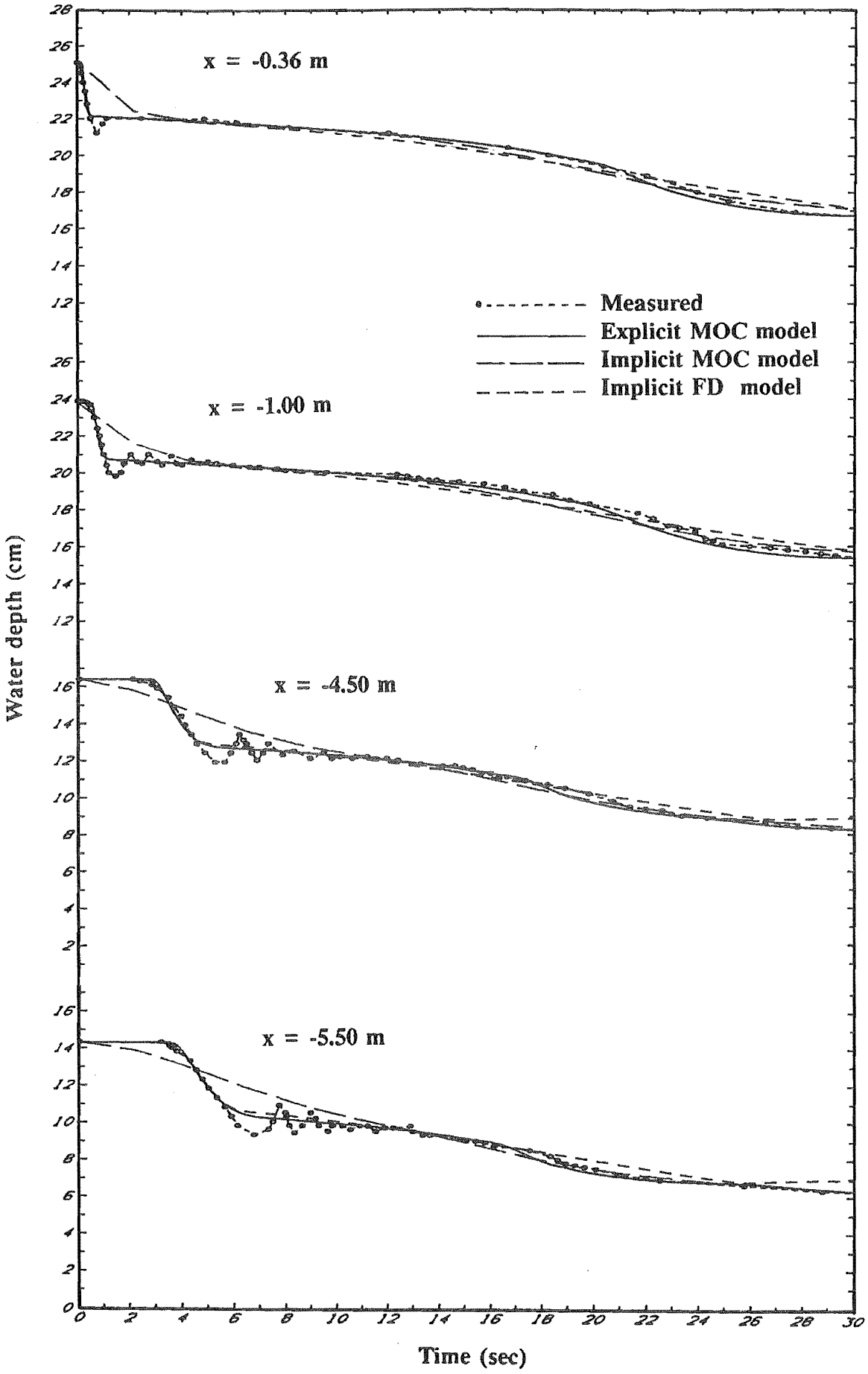

Fig. 6.5 Computed and measured depth hydrographs for test condition 2.2

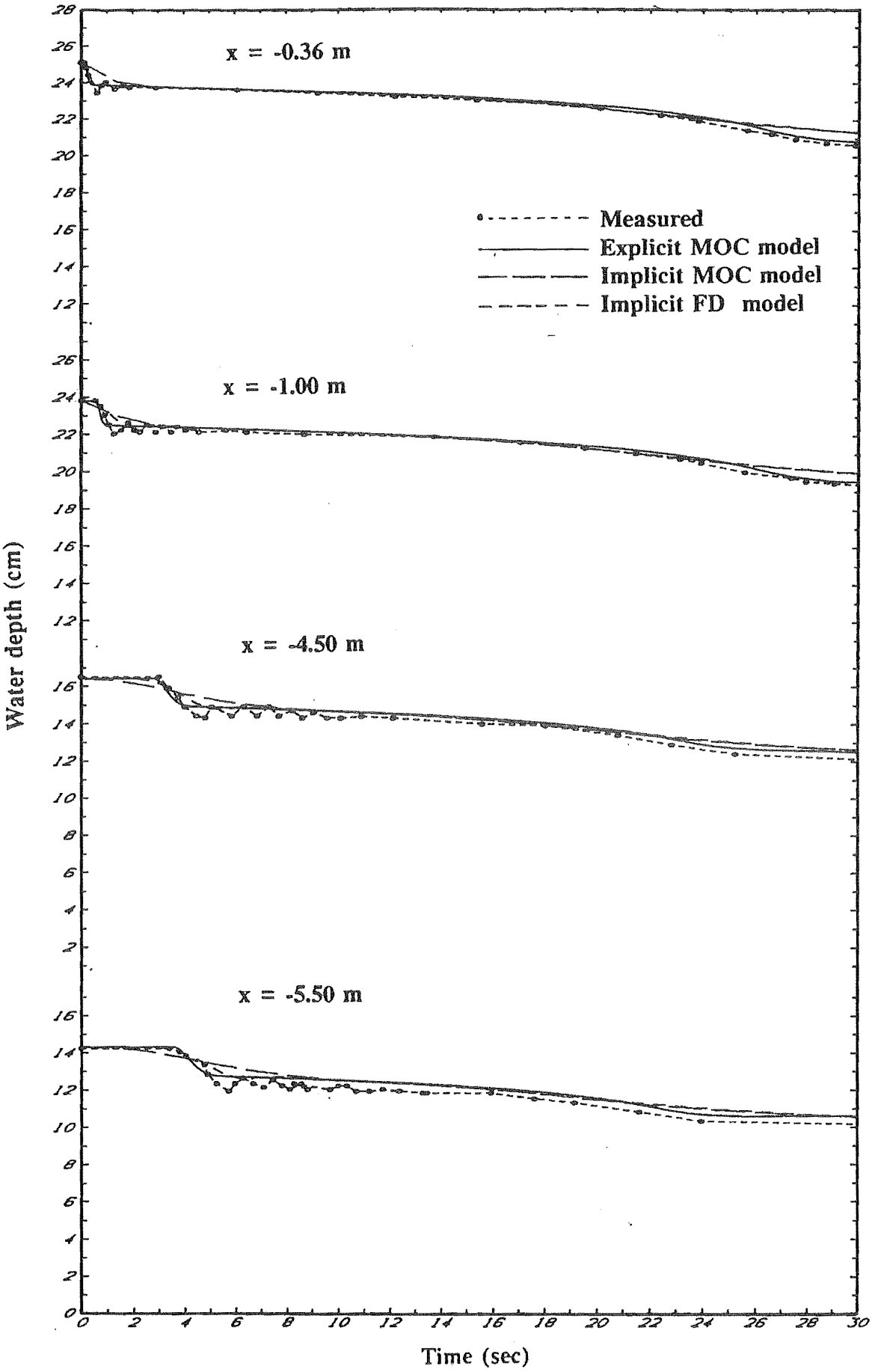

Fig. 6.6 Computed and measured depth hydrographs for test condition 2.3

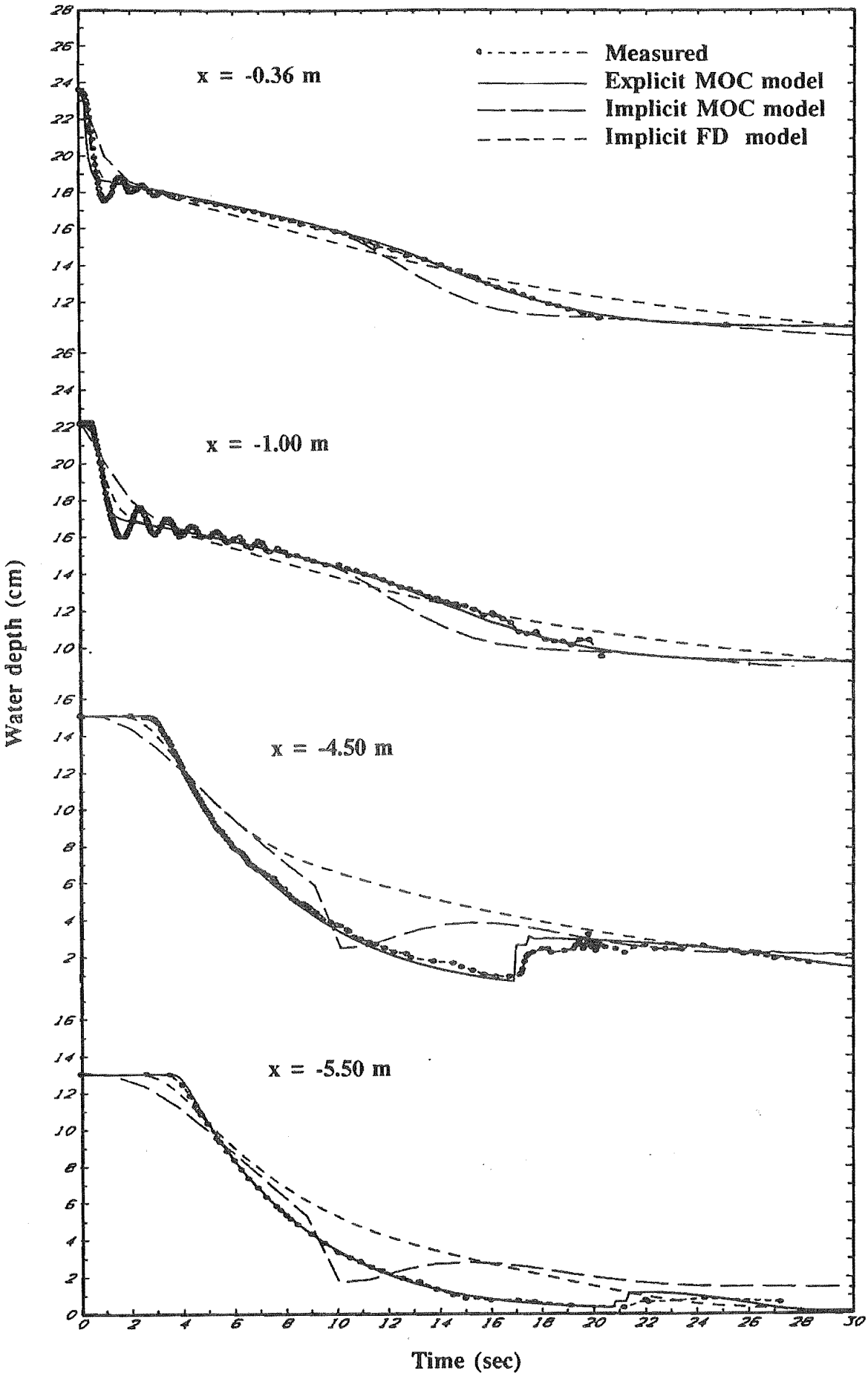

Fig. 6.7 Computed and measured depth hydrographs for test condition 3.1

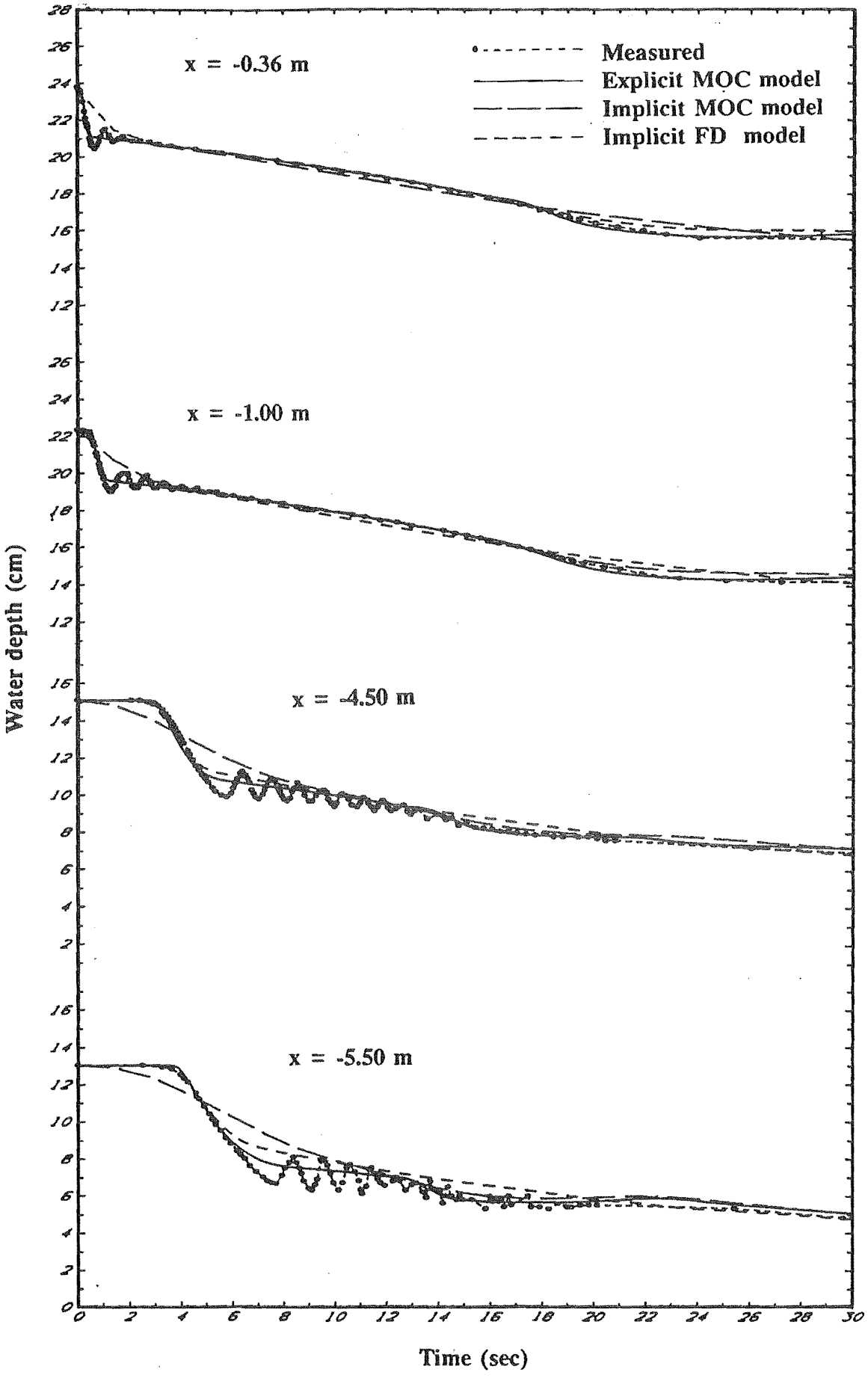

Fig. 6.8 Computed and measured depth hydrographs for test condition 3.2

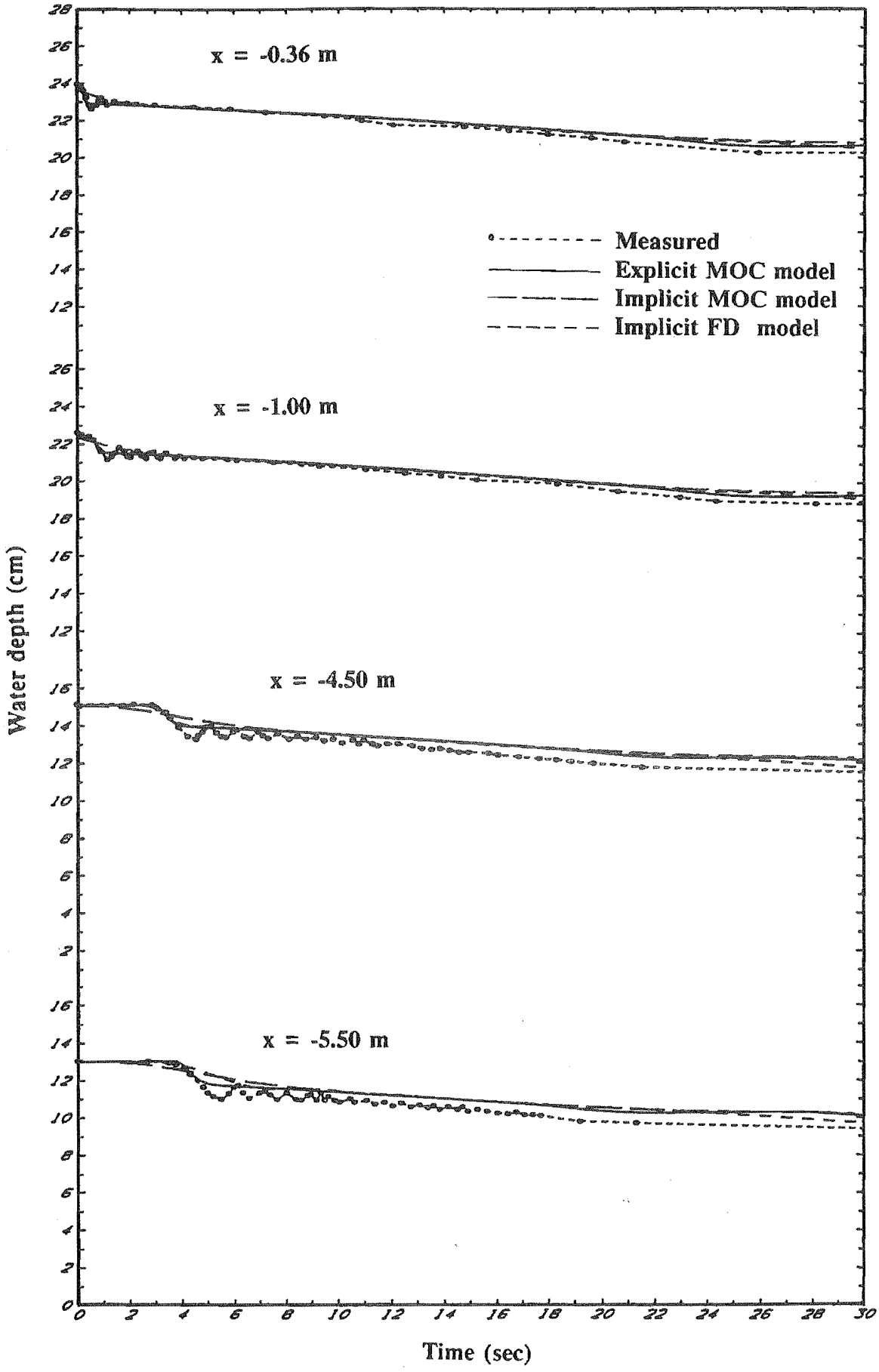

Fig. 6.9 . Computed and measured depth hydrographs for test condition 3.3

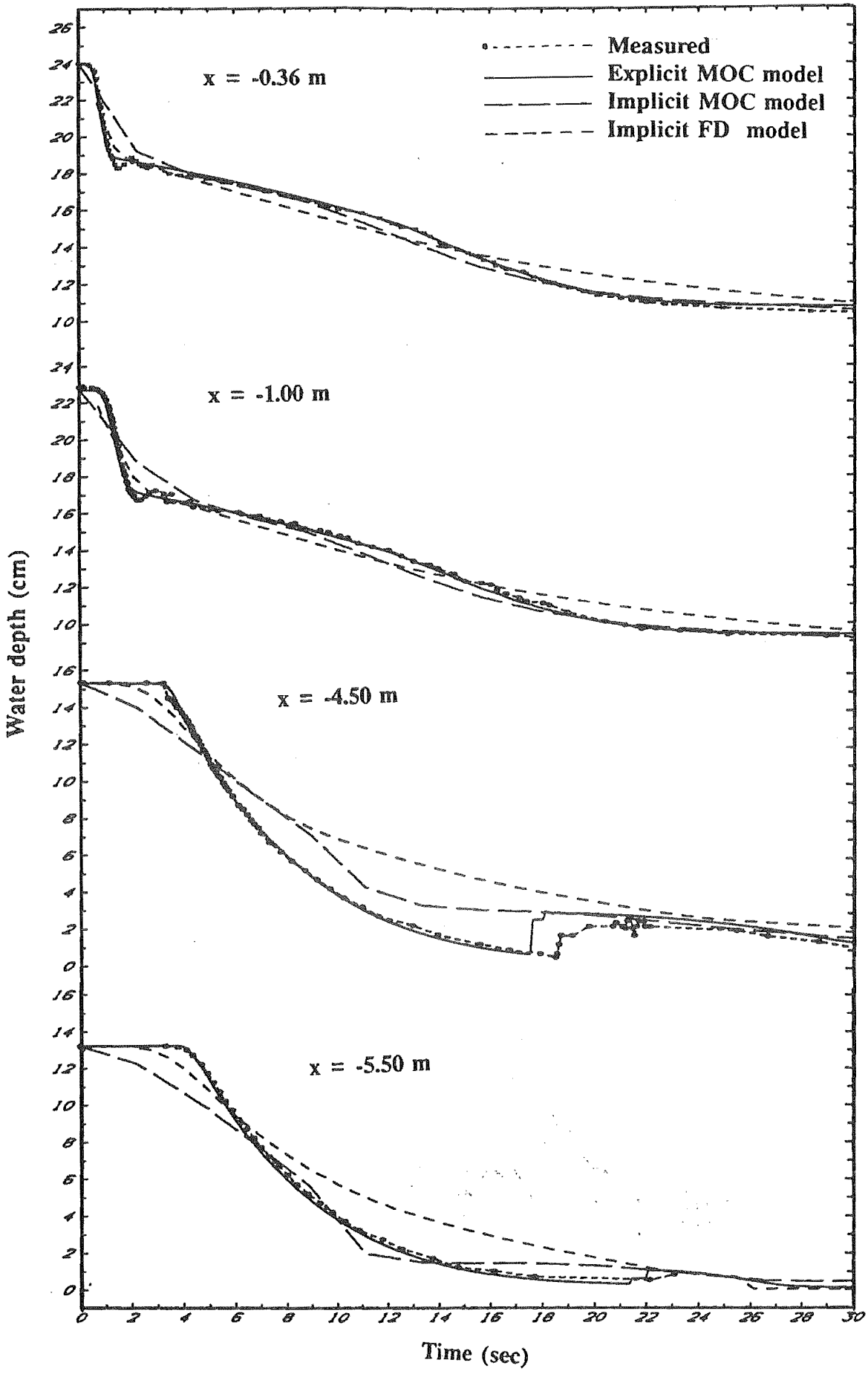

Fig. 6.10 Computed and measured depth hydrographs for test condition 4.1

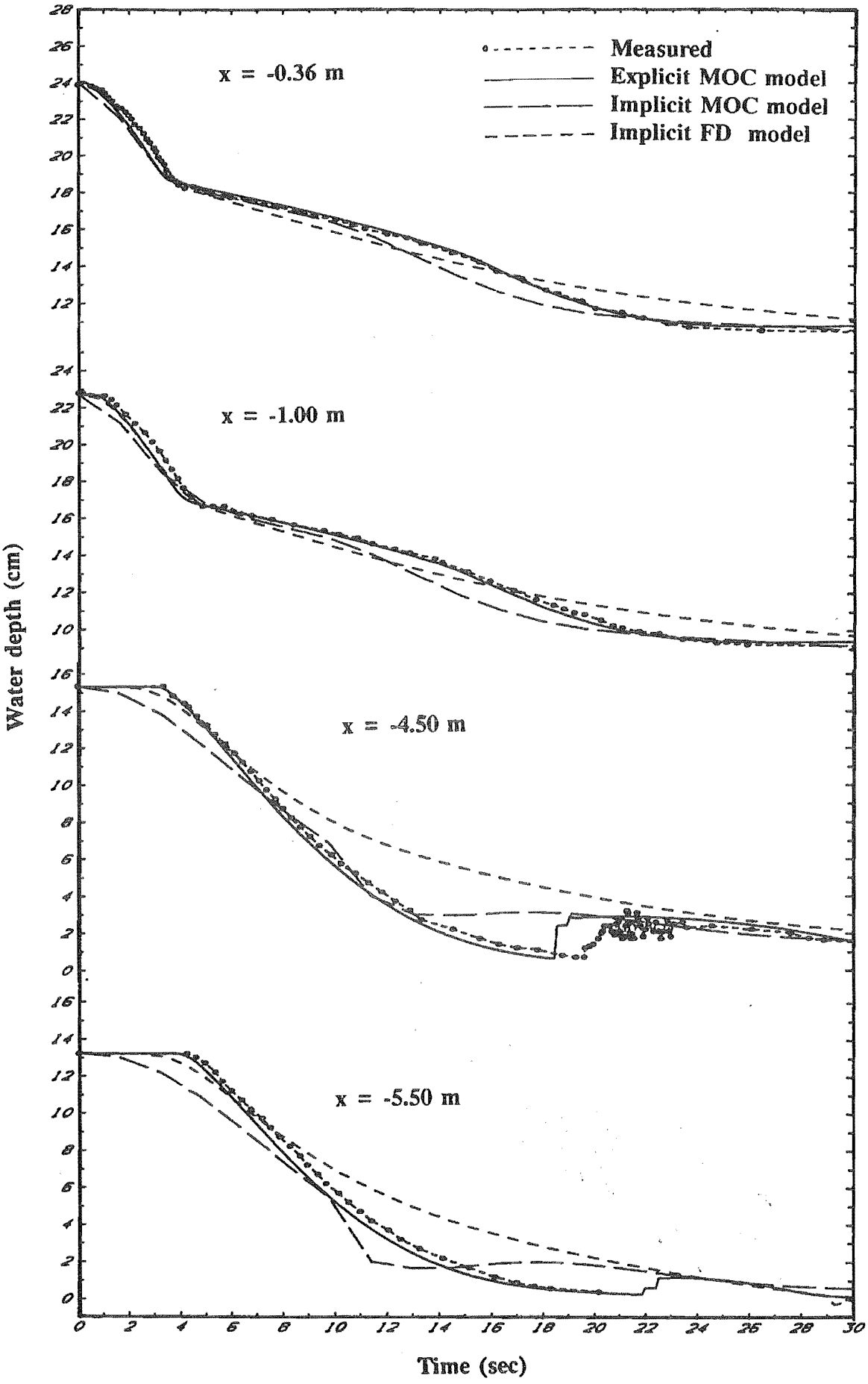

Fig. 6.11 Computed and measured depth hydrographs for test condition 4.2

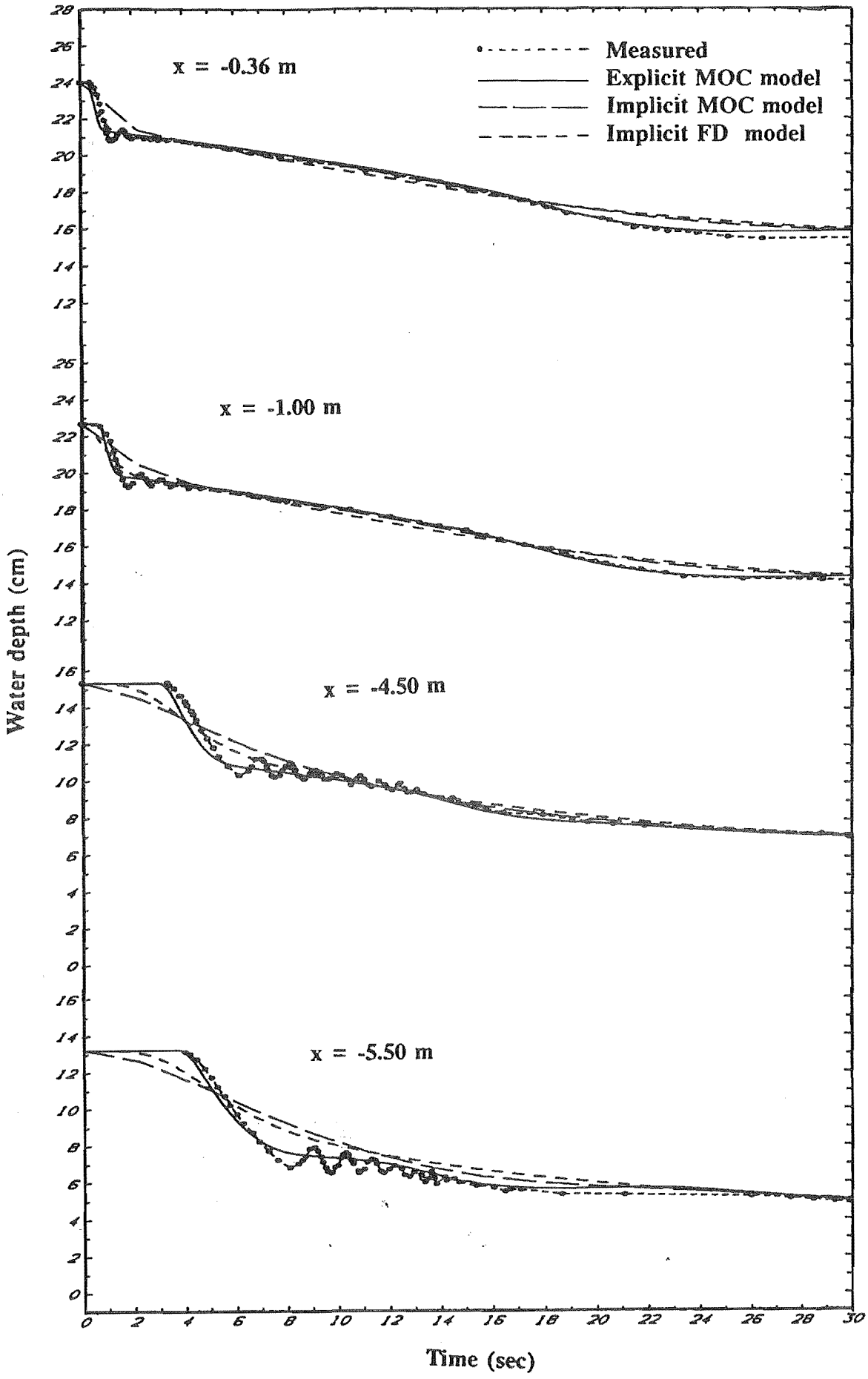

Fig. 6.12 Computed and measured depth hydrographs for test condition 4.3

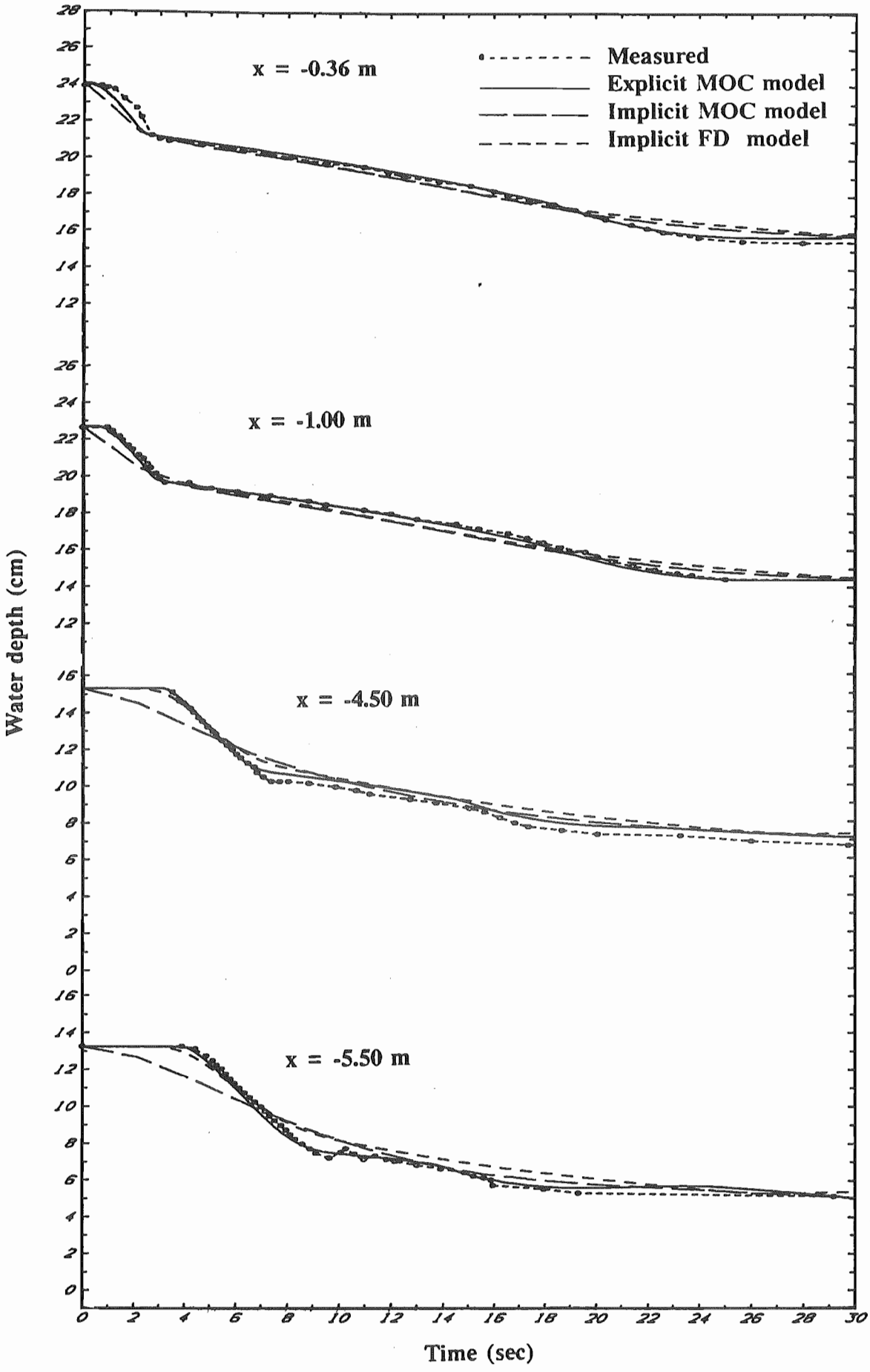

Fig. 6.13 Computed and measured depth hydrographs for test condition 4.4

CHAPTER 7

EVALUATION OF THE NUMERICAL MODELS

7.1 Introduction

In order to get a comprehensive numerical model for forecasting dam-break outflow hydrographs caused by partial collapse of a dam, four numerical models are evaluated. The models are the level-reservoir-approximation model, the explicit method-of-characteristics (MOC) model, the implicit method-of-characteristics (MOC) model and the implicit finite-difference model.

Comparisons between measured and computed water depth hydrographs show the ability of each model to simulate the wave formations in a reservoir. Since water depths directly upstream from the breach determine outflows from the reservoir, it is assumed that a model which simulates accurately depth hydrographs in the reservoir will also give an accurate prediction for outflow hydrographs. Thus, the reservoir outflow hydrographs computed by the explicit (MOC) model is assumed to be more accurate than values computed by the other models. Reservoir outflow hydrographs computed by the explicit MOC model are used as a reference to assess the accuracy of the outflow hydrographs computed by the other models.

Besides the accuracy and ability of the models to compute dam-break outflow hydrographs, computational problems, computer requirements and robustness of the models are evaluated to assess ease-of-use of the models.

7.2 The Level-Reservoir-Approximation Model

The level-reservoir-approximation model is the simplest and quickest model to use. It uses the storage form of continuity equation with an assumption of a horizontal free surface. It will give a good approximation for the outflow hydrograph if the slope of the reservoir water surface is not significant.

Because the reservoir water surface caused by a dam-break is never level, and because the level-reservoir-approximation model assumes the reservoir water surface is level, a comparison between computed and measured water depths cannot be used to evaluate the accuracy of this model. The computed reservoir outflow hydrograph is used to assess the capability of the model.

The discharge through the breach is a function of the reservoir water surface elevation. For large breach sizes (Figs. 7.1-7.4), the initial discharges are relatively large after the dam-break. These large discharges cause the reservoir water surface to drop rapidly and, in turn, cause the discharges to decrease rapidly. After a period of time, the discharges become relatively small and decrease gradually as the reservoir water surface drops more slowly. For smaller breach sizes (Fig. 7.5), the discharges are relatively small and drop gradually with time.

The computed reservoir outflow hydrographs (Figs. 7.1-7.5) show that: (1) For relatively large breach sizes, the initial discharge computed by the level-reservoir-approximation model does not agree with values computed by the other models. Later, as the discharge becomes relatively small, the discharge computed by the level-reservoir-approximation model agrees more closely with values computed by the other models; (2) Better agreement between the discharge computed by the level-reservoir-approximation model and values computed by the other models is obtained as the breach size decreases; (3) The level-reservoir-approximation model is as reliable as the other models when the computed discharge drops gradually with time.

For a dam breach with constant area and shape, the calculated solution for the discharge rating curve can be used to judge whether or not the assumption of a horizontal free surface is valid. Significant changes of the slope of the calculated discharge rating curve show that the reservoir water surface drops rapidly. In this case an assumption of a horizontal free surface is not valid, and relative errors in the computed discharges will be appreciable. Insignificant changes of the slope of the discharge rating curve show that the reservoir water surface drops slowly. Then an assumption of a horizontal free surface is valid, and relative errors in the computed discharge are likely to be negligible. A perturbation approach (Hunt, 1989) can be used to estimate the error involved in the level-reservoir-approximation model.

Since computations for the iterative solution of the non-linear equation (Eq. 4.6) always converge, the level-reservoir-approximation model does not have computational problems. The model only needs a little memory and computer time to obtain a reservoir outflow hydrograph.

The level-reservoir-approximation model gives a very quick and convenient method for estimating a reservoir outflow hydrograph. It gives a more accurate approximation for either small breaches or larger gradual breaches with no substantial reservoir inflow hydrographs. The maximum discharge computed by this model is always larger than maximum discharges computed by the other models. Differences between these maximum discharges increase as the breach size increases. Thus, if the slope of the reservoir water surface is significant, the level-reservoir-approximation model always gives a conservative forecast for the maximum discharge in a dam-break flood.

7.3 The Explicit Method-of-Characteristics Model

The explicit method-of-characteristics (MOC) model uses an explicit scheme of the method of characteristics to obtain approximate solutions of the dynamic equations. In order to obtain an accurate simulation of flow with a surge, a surge

solution is included in the explicit MOC model. Thus, the explicit MOC model can simulate a surge as well as both negative and positive waves, and it calculates water surface profiles as well as the reservoir outflow hydrograph.

Comparisons between computed and measured water depth hydrographs which were described in chapter 6 show that: the explicit MOC model simulates closely the formation and propagation of the steep negative wave, the reflected wave, the long gradually-varied wave and the surge; the water depth hydrographs computed by this model always agreed closely with the measured water depth hydrographs; results calculated with the explicit MOC model always gave closer agreement with experiment than the corresponding results calculated with both the implicit method-of-characteristics and finite-difference models.

For a partial-instantaneous breach, the maximum discharge is obtained almost instantaneously. Then the discharge decreases gradually as the water depth drops gradually due to the long gradually-varied negative wave which follows the steep negative wave. After a period of time, the discharge drops rapidly as the reflected negative wave approaches the dam. After this wave has disappeared, the discharge becomes relatively small and decreases very slowly. Thus, in general, there are three distinct slopes of the outflow rating curve computed by the explicit MOC model, as shown in Figs. 7.1-7.3.

The discharge computed by the explicit MOC model is believed to be more accurate than values computed by the implicit models. This is because the formation and propagation of waves are simulated more closely by the explicit MOC model than by the implicit models, as shown in chapter 6. Thus, the outflow hydrographs computed by the explicit MOC model can be used to assess the accuracy of the implicit models.

The explicit MOC model requires about the same effort to develop the input data as the implicit models. However, due to stability and convergence of its solution, it is much easier to use than the implicit models, especially in rapidly varied flows.

Relatively more computer memory is needed by the explicit MOC model to include the simulation of either a surge or a mixed flow condition (subcritical and supercritical flow occurring simultaneously). The explicit MOC model usually uses more computer time than the implicit models because its time step is subject to the Courant condition. However, for rapidly varied flow, the implicit models have to use a relatively small time step to prevent computational problems with accuracy and non-convergence. Thus, computer time used by the explicit MOC model is comparable with the implicit models.

The explicit MOC model is easy to use because it incorporates the Courant condition that prevents computational instability and non-convergence. Thus, it will give accurate solutions for a reasonable range of values for the input data. For a large breach size with a small failure time interval, which causes rapidly varied flow, the explicit MOC model is superior to the implicit models. Thus, the explicit MOC model gives more accurate solutions, its computer time is comparable to that required for the other models and it does not have computational problems.

For a small breach size, which causes gradually varied flow, the reservoir outflow hydrographs computed by the implicit models are as accurate as values computed by the explicit MOC model, as shown in Fig. 7.5. In this case the implicit models can use larger time steps without computational problems. Thus, in this case, the explicit MOC model is inferior to the implicit models because the explicit MOC model time steps are subject to the Courant condition.

7.4 The Implicit Method-of-Characteristics Model

The implicit method-of-characteristics (MOC) model uses the implicit scheme of the method of characteristics to obtain approximate solutions of the dynamic equations. In contrast to the explicit model, the implicit model requires that Courant numbers be greater than one. Because the implicit model can not deal with a mixed flow condition (subcritical and supercritical flow occurring

simultaneously), the flow is simulated without any consideration of surge existence. Thus, if a surge occurs in the channel, the water surface profiles calculated with this model will not be as good as the profiles calculated with explicit MOC model.

Comparisons between computed and measured water depth hydrographs, as described in chapter 6, show that: the steep negative wave and the reflected wave are always diffused in the x-direction; because the Courant number used by the implicit MOC model must be greater than one, the slope of the negative wave computed by this model is much more gradual than values computed by the other models; after the steep negative wave passes any selected location, the water depths computed by the implicit MOC model are as accurate as values computed by the explicit MOC model.

For a large breach size, the discharges computed by the implicit MOC model agree closely with values computed by the explicit method for a period of time after the dam-break. Then they drop earlier and more gradually than values computed by the explicit MOC model as the reflected wave approaches the dam. After the reflected wave disappears, however, the discharge becomes relatively small and agrees closely with values computed by the explicit MOC model. For a small breach size, the first negative wave is relatively small so that the reflected wave becomes insignificant as it approaches the dam. In this case, the discharges computed by the implicit MOC model always agree closely with values computed by the explicit MOC model.

A comparison of reservoir outflow hydrographs computed by the dynamic routing models, as shown in Figs. 7.1-7.5, indicates that: for large breach sizes, the discharges computed by the implicit MOC model are more accurate than values computed by the implicit finite-difference model, but they are not as accurate as values computed by the explicit MOC model; differences between the discharges computed by the explicit MOC and implicit MOC models become insignificant as the breach sizes decrease; for small breach sizes, the reservoir outflow hydrographs computed by either the implicit MOC model or the finite-

difference model are nearly the same as those computed by the explicit MOC model.

The implicit MOC model is easy to use for gradually varied flow, but it is difficult to use for rapidly varied flow. This is because rapidly varied flow computations with this model sometimes terminate without obtaining solutions due to the calculation of negative flow depths. This computational problem can be overcome by varying the distance and time steps used in the model.

In general, the implicit MOC model needs less memory and processing time than the explicit MOC model. However, for rapidly varied flow, varying the distance and time steps to overcome the computational problem are very time-consuming. Thus, in this case, the implicit MOC model uses more processing time than the explicit MOC model.

For gradually varied flow, the implicit MOC model is superior to either the explicit MOC model or the finite-difference model. However, because the Courant number used in the implicit MOC model must be greater than one, it becomes inferior for rapidly varied flow.

7.5 The Linearized Implicit Finite-Difference Model

The implicit finite-difference model uses the Preissmann scheme to obtain approximate solutions of the dynamic equations. The primary advantage of this scheme lies in the high efficiency of the computation since the time steps used in the implicit finite-difference model can be a few times larger than the Courant condition. However, this model can not deal with subcritical and supercritical flow occurring simultaneously. Thus, if this mixed-flow condition occurs, the water surface profiles calculated with this model will not be as good as the profiles calculated with the explicit method of characteristics model

Comparison of the finite-difference model results with experiment, as described

in chapter 6, shows that : the steep negative wave is always diffused in the x-direction; for a large breach size, the propagation of the gradually-varied negative wave is not simulated accurately; for a small breach size, the finite difference model simulates the gradually-varied negative wave more closely.

For large breach sizes (Figs. 7.1-7.4), the discharges computed by the finite-difference model agree closely with values computed by method of characteristic models for a period of time after the dam-break. Then, they decrease earlier and more gradually than values computed by the method of characteristic models. Thereafter, the discharges become relatively small and agree closely with values computed by the method of characteristic models. In this case the discharges computed by the finite-difference model are as accurate as values computed by the method of characteristic models except when the reflected negative wave approaches the dam. However, as the breach size decreases, the initial height of steep negative wave decreases so that the reflected wave becomes insignificant as it approaches the dam. Thus, for small breach sizes (Fig.7.5), the discharges computed by the finite-difference model agree more closely with values computed by the method-of-characteristic models.

Rapidly varied flows, such as simulations of dam-break waves, can cause computational problems (accuracy and non-convergence) when applied to the implicit finite-difference scheme. However, these computational problems can be reduced by reducing the time step (Δt) and by increasing the weighting coefficient (θ).

The finite-difference model requires memory and processing times that are comparable to those for the implicit MOC model. However, dynamic routing computational problems in an implicit scheme are overcome easier by the finite-difference model than by the implicit method of characteristics model. This is because these problems can be overcome by reducing the time step in the finite-difference model, whereas varying both distance and time steps are the only way to overcome these problems in the implicit MOC model. Thus, in this case the

finite-difference model requires less processing time than the implicit MOC model.

For a large breach size, the time step used by the implicit finite-difference model is often smaller than the Courant condition, and the accuracy of the computation decreases as the weighting coefficient increases. In this case, the finite-difference model is inferior to the explicit MOC model since the processing time is comparable and results calculated by the explicit MOC model are more accurate. .

As the breach size decreases, the time step used in the finite-difference model can be increased without causing computational problems. Thus, for a small breach size, the finite-difference model can use the time step a few times larger than the Courant condition. In this case, the finite-difference model is superior to the explicit MOC model.

7.6 Accuracy Test of the Dynamic Models

Accuracy of results computed by the numerical models have been checked by analyzing results of numerical experiments. In general, the accuracy depends on the selection of intervals Δx and Δt. The accuracy increases as the distance Δx decreases, but there is a limit beyond which we cannot decrease Δx further.

For the explicit MOC model, the time interval Δt was determined by keeping the Courant numbers less or equal than one. The interval Δx was chosen by decreasing Δx to the point where further decreases in Δx caused insignificant changes in the depth hydrographs.

For the implicit MOC model, a series of computation was carried out by maintaining Δt constant and by decreasing Δx to the point where small values of Δx caused negative depths to be calculated. A similar computation was repeated for smaller and smaller Δt.

A similar accuracy test described above was carried out for the implicit FD model. In this model, the weighting coefficient (θ) was maintained constant for a series of ratio $\Delta t/\Delta x$. The calculations were repeated for different values of θ.

7.7 Conclusions

The level-reservoir-approximation model becomes more reliable as the computed discharge drops slowly with time. The maximum discharge computed by this model is always larger than the maximum discharge computed by the other models. Thus, the level-reservoir-approximation model always gives a conservative forecast for the maximum discharge in a dam-break flood.

The explicit method-of-characteristics model is superior to the implicit models for a large breach size. This is because it gives a more accurate solution and its computer time is comparable to that required for the implicit models. However, for a small breach size, the implicit models give about the same accuracy as the explicit MOC model and require less computational time. In this case, the explicit MOC model is inferior to the implicit models.

The implicit method-of-characteristics model is more accurate than the finite-difference model. However, for a large breach size, the finite-difference model is more convenient to use than the implicit MOC model. This is because the implicit finite-difference model can use the Courant number less than one to overcome the computational problems in rapidly varied flow.

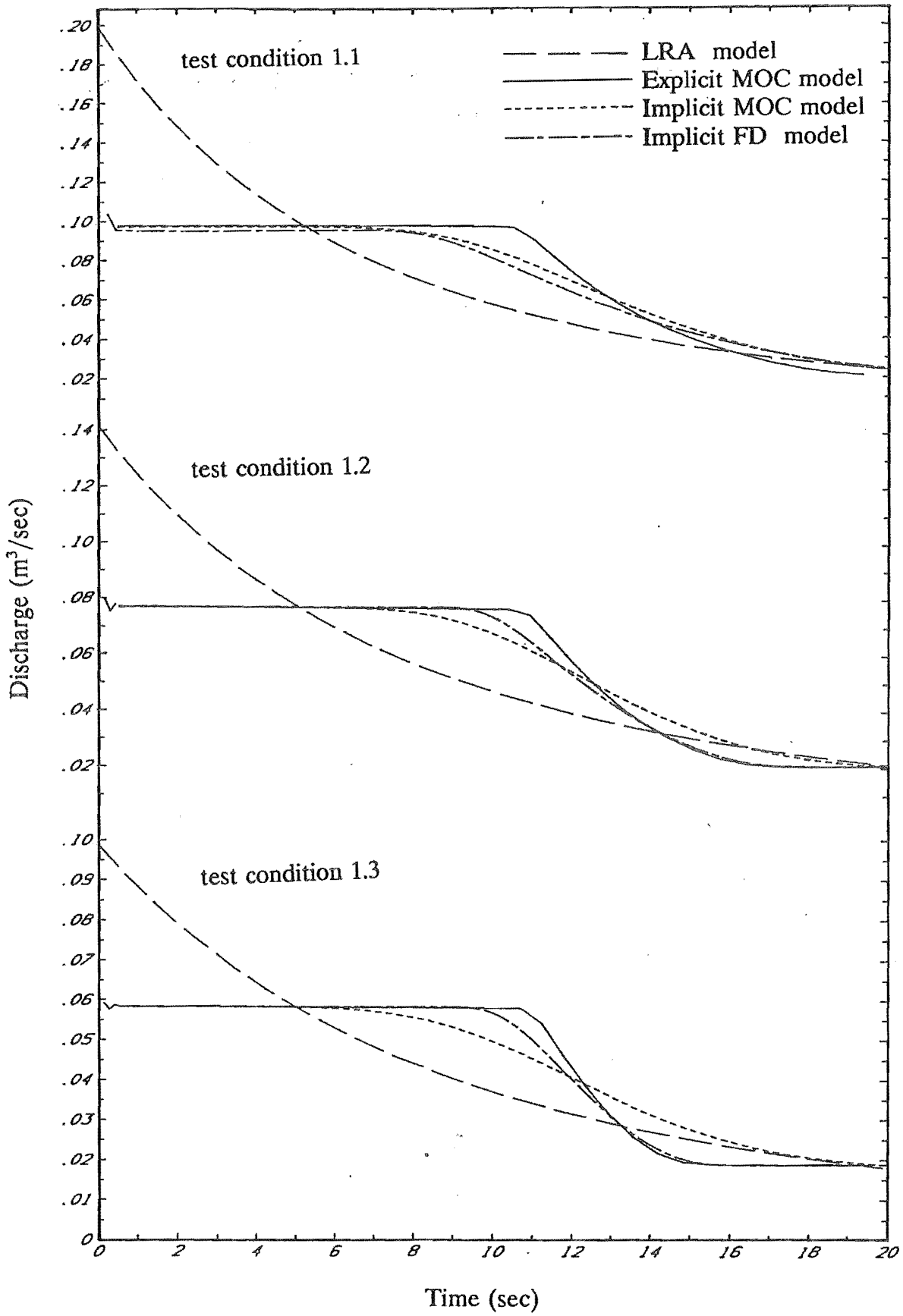

Fig. 7.1 Reservoir outflow hydrographs computed by the numerical models for experimental model I

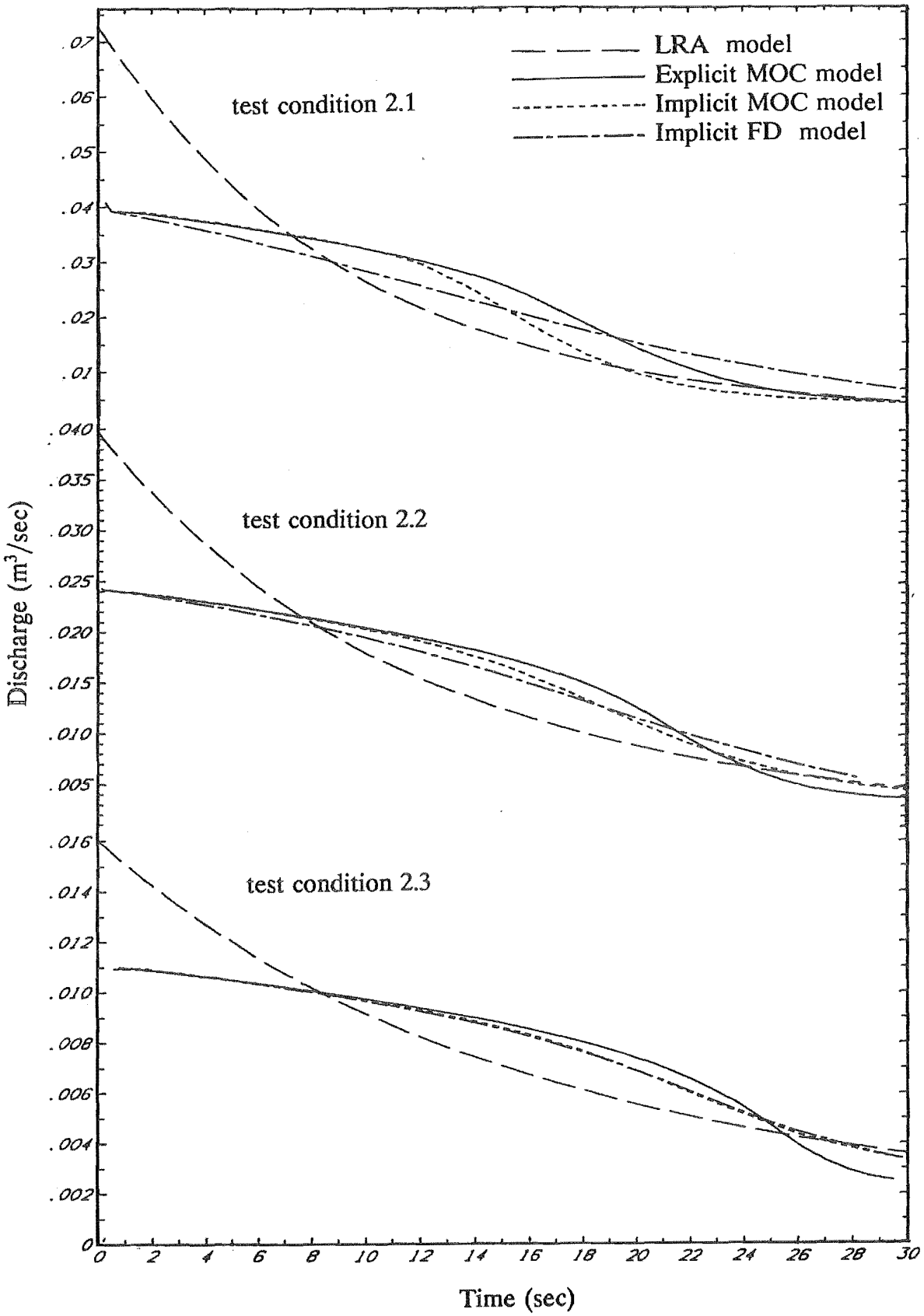

Fig. 7.2 Reservoir outflow hydrographs computed by the numerical models for experimental model II

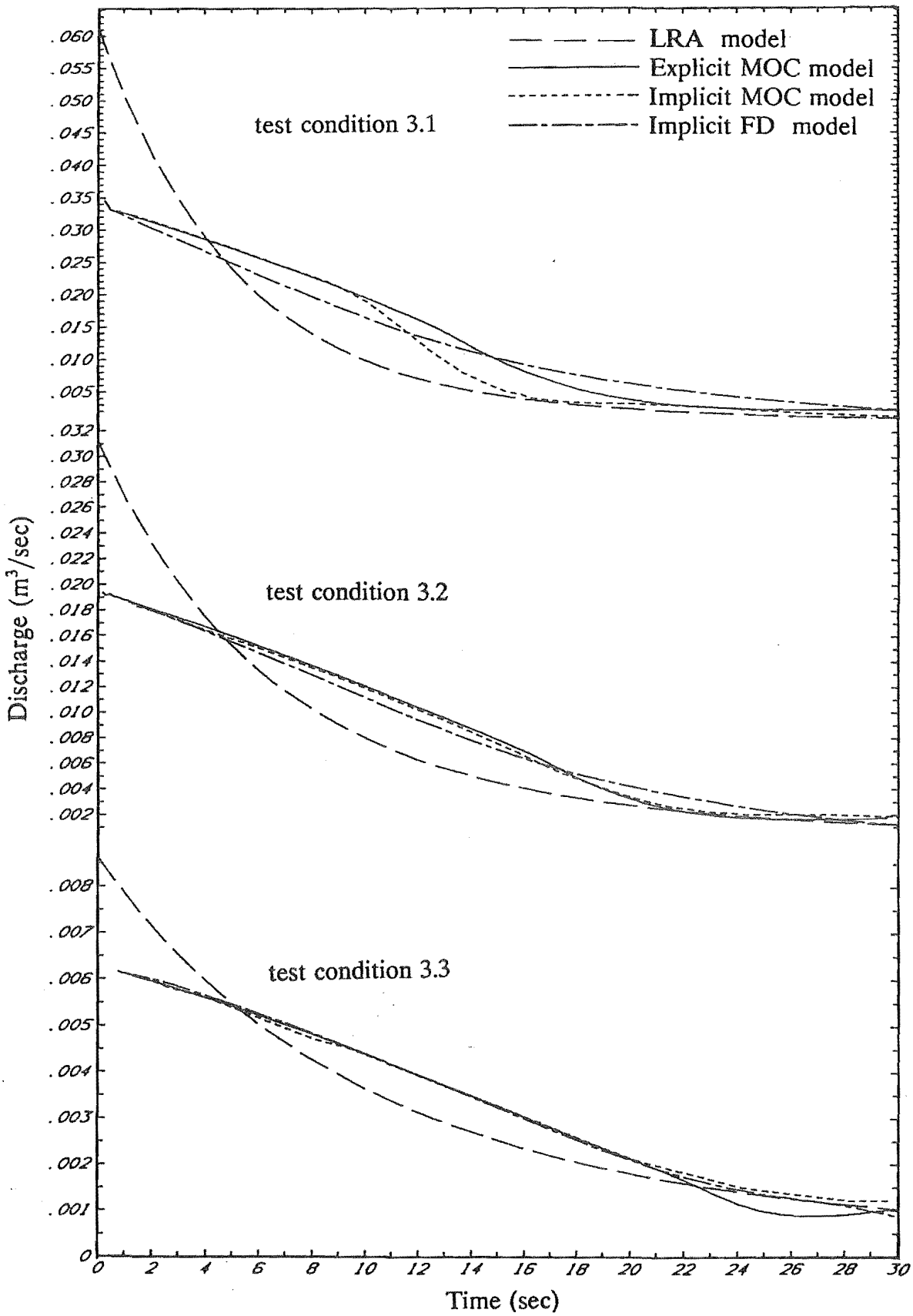

Fig. 7.3 Reservoir outflow hydrographs computed by the numerical models for experimental model III

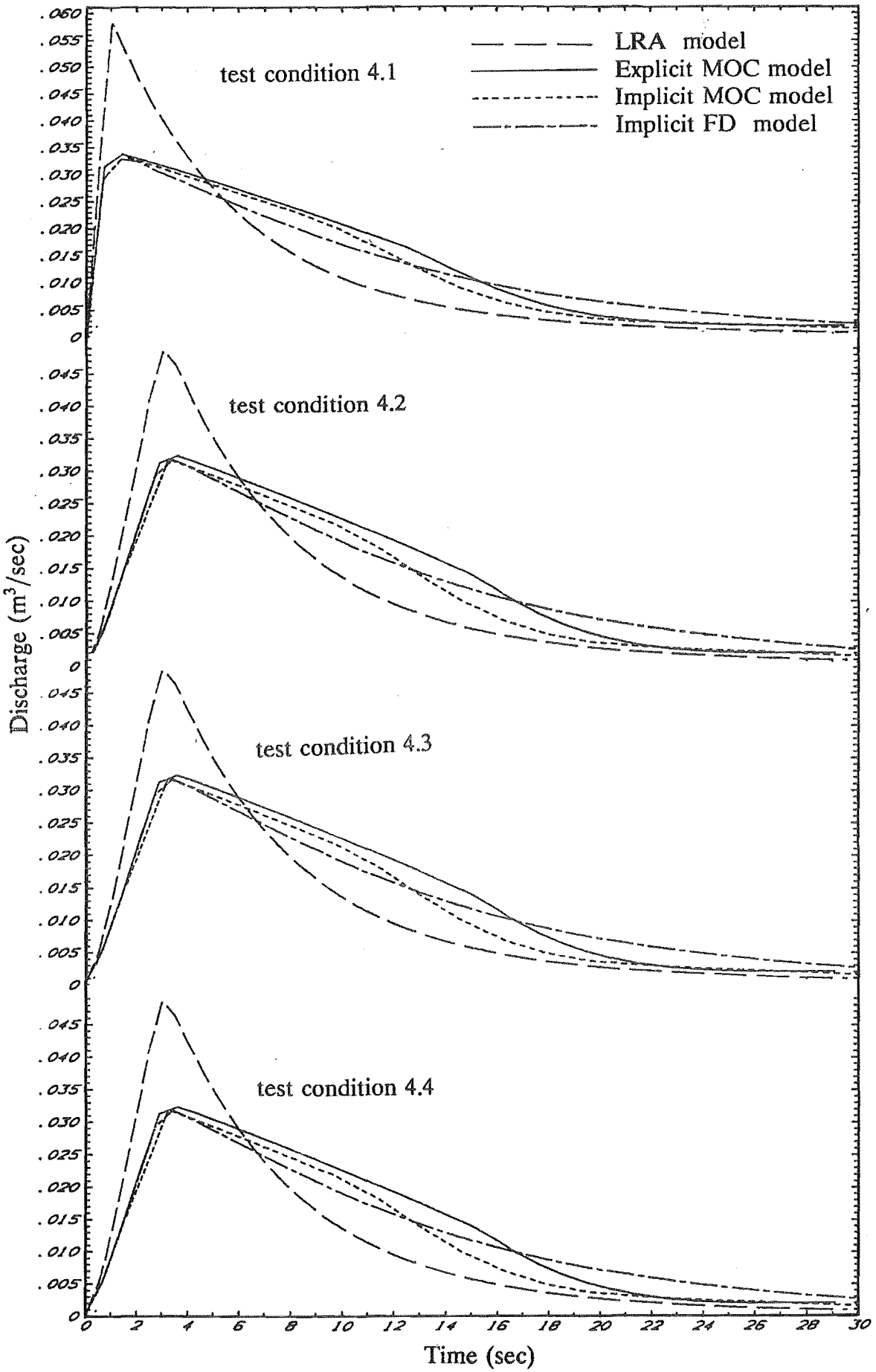

Fig. 7.4 Reservoir outflow hydrographs computed by the numerical models for experimental model IV

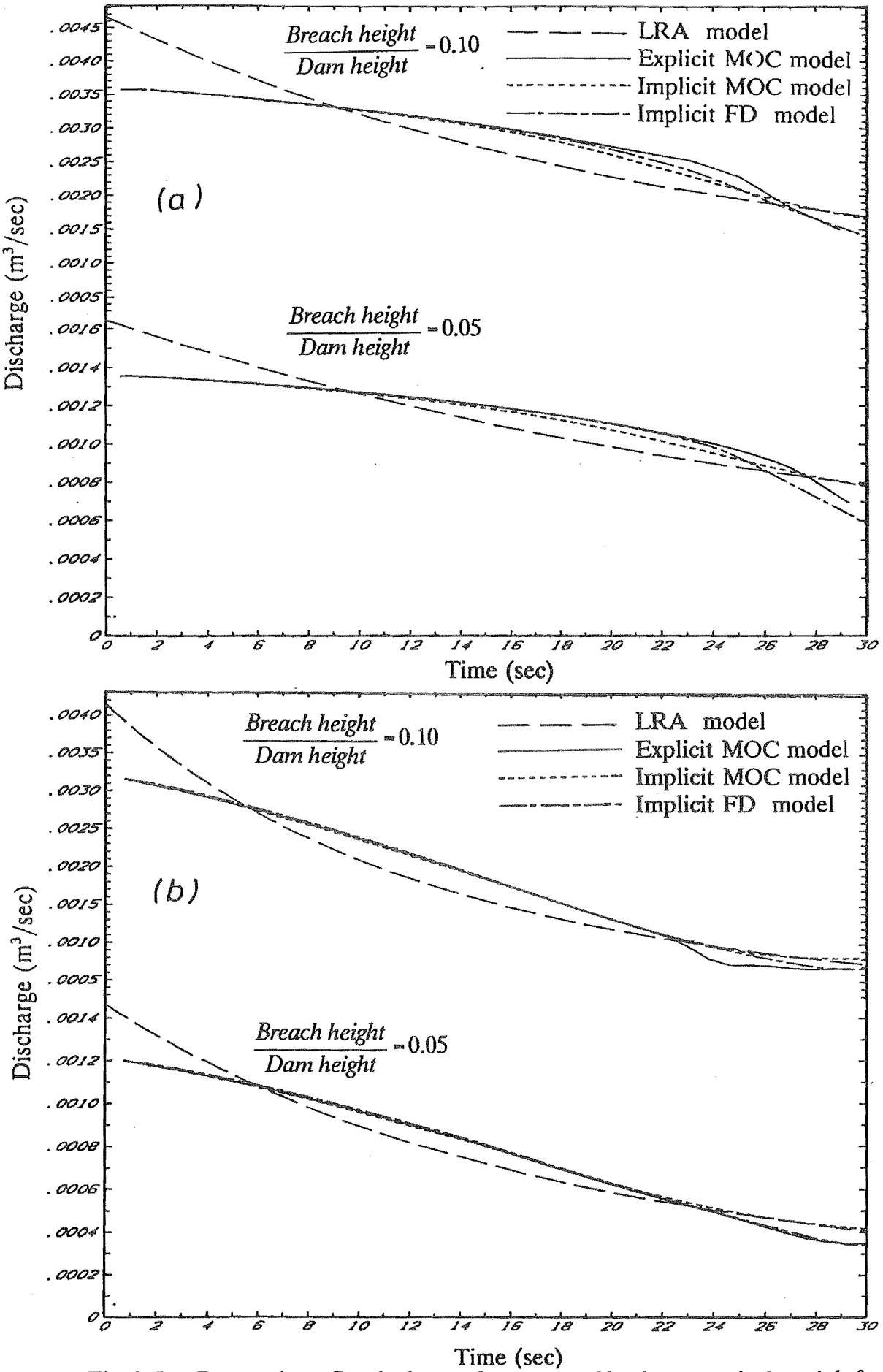

Fig. 7.5 Reservoir outflow hydrographs computed by the numerical models for small breach sizes: (a) assumed a reservoir of experimental model II; (b) assumed a reservoir of experimental model III

CHAPTER 8

APPROXIMATE SOLUTIONS

8.1 Introduction

In a dam-breach flood wave, the extreme rapidity of variation of water stages and velocities can cause computational problems when applied to numerical approximations of the unsteady flow equations. These computational problems are the reason that dynamic routing methods are more complicated to use than hydrologic routing methods. Although present-day technology of digital computers makes more complete dam-breach flood wave simulations possible, the price for utilizing the more complete simulations is generally complex, time consuming and expensive solution procedures. Therefore, for practical solutions, approximate hydrologic routing solutions may still be preferred, even though the dynamic routing methods are now feasible for organizations engaged in dam-breach flood forecasting.

Dam-break outflow hydrographs are a function of water depths directly upstream from the breach. At this location, variation of water depths and velocities are determined mainly by the combination of the movement of both steep and long gradually-varied negative waves which are formed after a dam-break. Therefore, practical and relatively accurate outflow hydrograph solutions can be obtained only by taking into consideration the effects of the movement of these two negative waves.

The speed of movement and shape of both the steep and long gradually varied negative waves are determined by the initial breach discharges and flow resistance. A practical procedure to compute initial breach discharges is

investigated in section 8.2, and the effect of flow resistance on the outflow hydrographs is described in section 8.3.

The level reservoir approximation based on hydrologic storage routing is widely used for routing floods through reservoirs. This approximation will give an accurate solution if the slope of the water surface is insignificant. Because the slope of the water surface caused by a dam-break is significant in many cases, the level reservoir approximation cannot be used to forecast dam-break outflow hydrographs for a wide range of breach sizes. In order to get a practical and robust model for computing dam-break outflow hydrographs, a numerical model using hydrologic storage routing and taking into consideration the effect of the movement of the negative waves and flow resistance is investigated.

8.2 Initial Breach Discharges

Initial breach discharges are functions of the initial breach geometry and the instantaneous upstream hydraulic head. Since little is understood about predicting the likely size and shape of the incipient breach, the initial size and shape of the breach are specified, and the initial breach is assumed to occur instantaneously. This type of failure forms a distinct steep negative wave which has a significant effect on the accuracy of outflow hydrographs.

Values of the hydraulic head (h_2) can be determined by using equation (3.16) along the forward characteristic 1-2 and a breach discharge equation along the line $x=0$, as shown in Fig. 8.1.

In many cases, deposited sediments in reservoirs tend to cause reservoir beds to become horizontal near the dam. At this location, for a small increment of length Δx, the reservoir can be assumed as a prismatic channel with a horizontal bed, and at $t \approx 0$ the friction loss can be neglected since values of mean water velocity are relatively small. Thus, in this case, values of the right hand side in equation (3.16) equal zero, and integration of this equation gives :

$$U_2 + \frac{2\,g\,H_2}{C_1 + C_2} - U_1 - \frac{2\,g\,H_1}{C_1 + C_2} = 0 \qquad (8.1)$$

in which $C = \sqrt{gA/B} = \sqrt{gD}$ is the celerity and D is hydraulic depth. The subscripts 1 and 2 indicate values at time $t = 0$ and $t = \Delta t$, respectively.

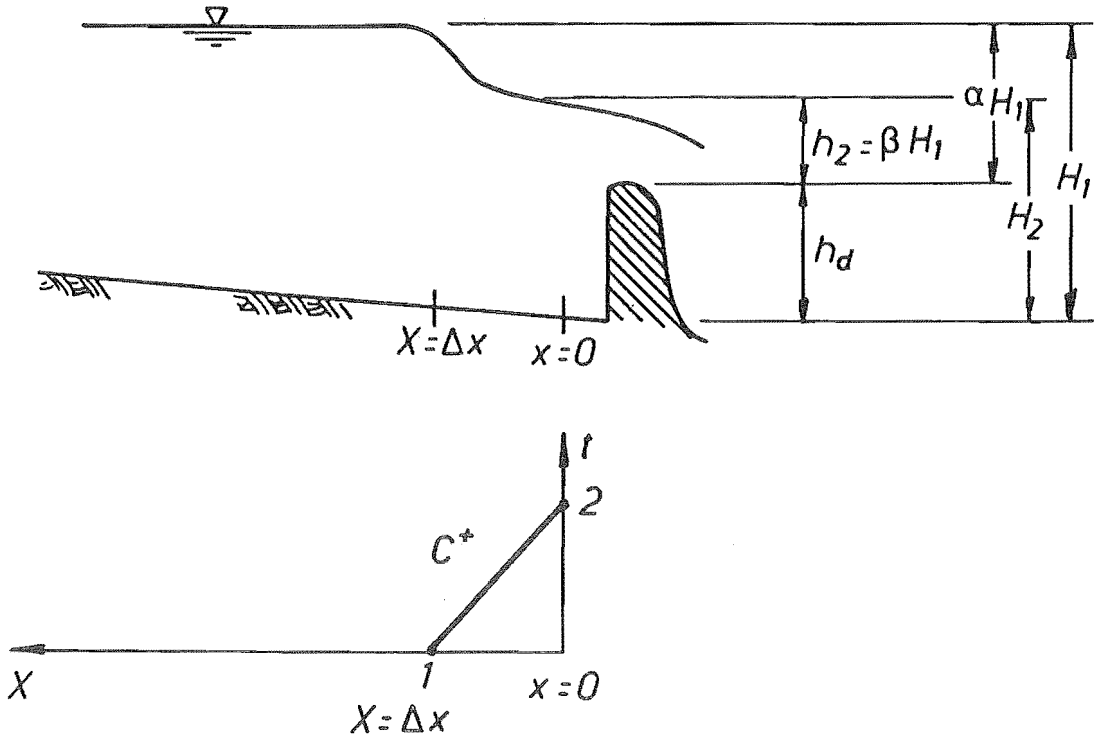

Fig. 8.1 Scheme for the derivation of initial breach discharge equation

In general, the discharge and velocity immediately upstream from the breach dam can be expressed in the following form:

$$Q_2 = U_2 A_2 = U_2 B_2 D_2 = \zeta h_2^n$$
$$U_2 = \frac{\zeta}{B_2} \frac{h_2^n}{D_2} \qquad (8.2)$$

where h_2 is the reservoir water surface elevation above the breach bottom at $t = \Delta t$, and the coefficient ζ and exponent n depend on the breach characteristics. It is assumed that the discharge at the breach and immediately upstream from the breach are the same. Inserting equation (8.2) in equation (8.1) gives

$$\frac{\zeta}{B_2}\frac{h_2^n}{D_2} - U_1 + 2\sqrt{g}\ \frac{h_2 + h_d - H_1}{\sqrt{D_1} + \sqrt{D_2}} = 0 \qquad (8.3)$$

Since $D_2 = D_2(h_2)$ and $B_2 = B_2(h_2)$ are known, and since all variables except h_2 are known, a value for h_2 can be calculated by using the Newton-Raphson iteration to solve equation (8.3).

Dimensionless relationships between the ratios $(H_1\text{-}h_d)/H_1$ and h_1/H_1 can be obtained by introducing the following dimensionless variables :

$$\begin{aligned} \alpha &= \frac{H_1 - h_d}{H_1} \\ \beta &= \frac{h_2}{H_1} \\ d_1 &= \frac{D_1}{H_1} \\ d_2 &= \frac{D_2}{H_1} \end{aligned} \qquad (8.4)$$

Thus, inserting equation (8.4) in equation (8.3) gives

$$\frac{\zeta H_1^{n-1.5}\beta^n}{B_2\sqrt{g}} - \frac{U_1}{\sqrt{g H_1}} + \frac{2(\beta - \alpha)}{\sqrt{d_1} + \sqrt{d_2}} = 0 \qquad (8.5)$$

A family of curves of $\beta = f(\alpha)$ can be developed for particular geometries such as triangular, rectangular, trapezoidal, parabolic and elliptic breach openings. For example, for a rectangular cross section near the dam with a zero initial velocity ($U_1=0$) and a breach geometry that can be assumed to be rectangular, equation (8.5) becomes :

$$E^{1.5} + (1 + \alpha - \beta)^{1.5} - (1 + \alpha - \beta) = 0 \qquad (8.6)$$

in which $E = \frac{1}{3}\frac{B_b}{B} C_d \sqrt{\frac{2}{3}}$ is a constant, B_b is effective breach width and C_d is the coefficient of discharge, values of which are in the range 0.848 to 1.052 for broad-crested weirs. Figure 8.2 gives curves of $\beta = f(\alpha)$ for five values of C_d with $B_b/B = 1.0$. These curves can be fitted to parabolas with coefficients that are given in table 8.1.

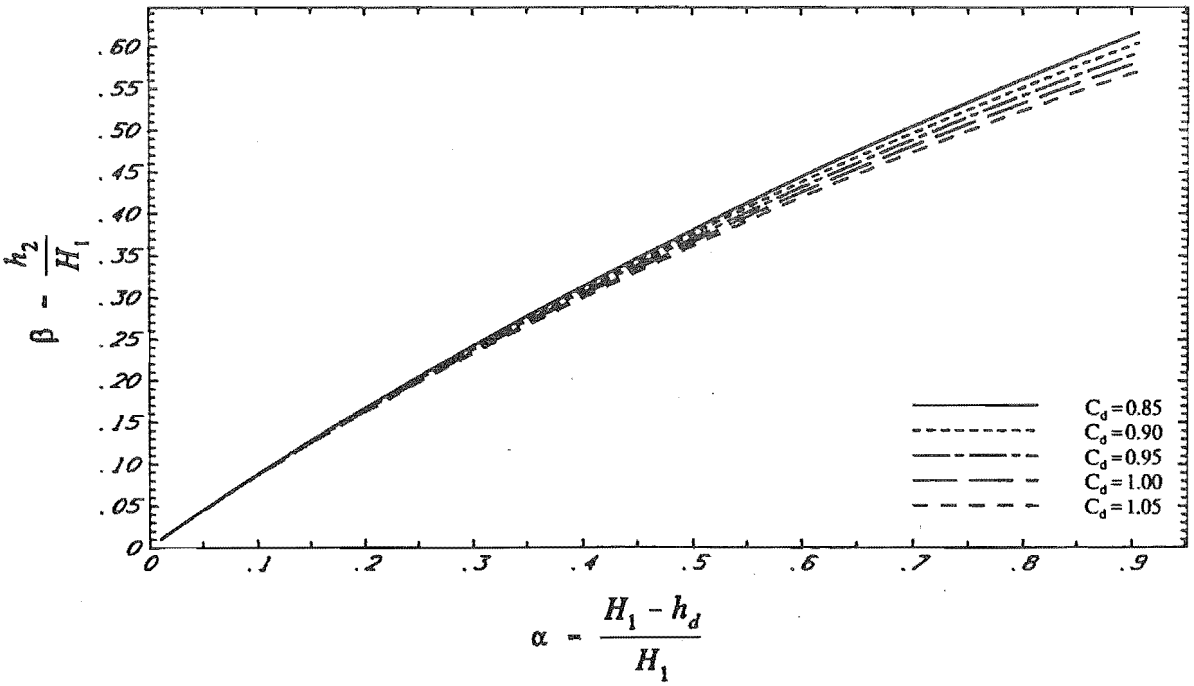

Fig. 8.2 Relationship of the relative height of the initial hydraulic head (β) to the relative of opening height (α) of rectangular breaches of the same width as the reservoir

Table 8.1

No	C_d	$\beta = a\,\alpha^3 + b\,\alpha^2 + c\,\alpha$		
		a	b	c
1	0.085	0.1662	-0.4226	0.9282
2	0.090	0.1741	-0.4407	0.9250
3	0.095	0.1781	-0.4538	0.9208
4	0.100	0.1852	-0.4699	0.9173
5	0.105	0.1895	-0.4826	0.9132

Having ß = f(α), initial breach discharges can be determined by using a discharge equation. For a rectangular broad-crested weir :

$$Q = C_d B_b \frac{2}{3}\sqrt{\frac{2}{3}g}\,\left[(a\alpha^3 + b\alpha^2 + c\alpha)\,H_1\right]^{1.5} \qquad (8.7)$$

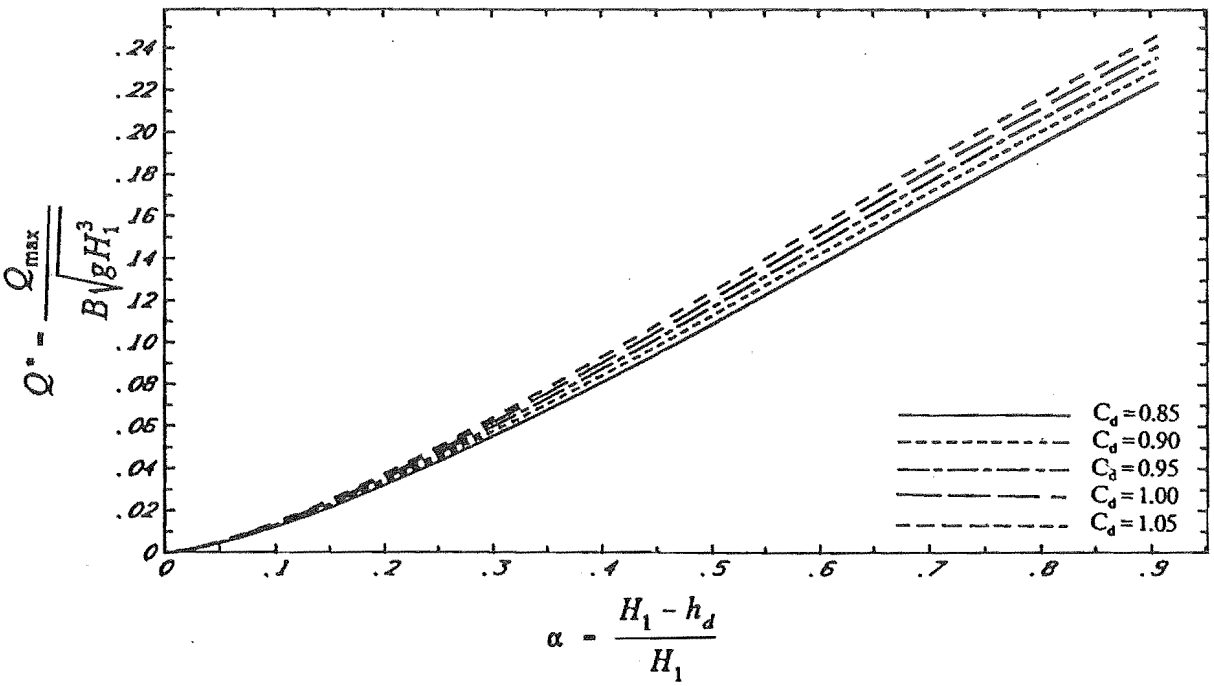

Fig. 8.3 Relationship of the initial breach discharges to the relative of opening height of rectangular breaches of the same width as the reservoir

Initial breach discharges computed by this method are based on assumptions that near the dam the reservoir channel can be assumed prismatic with horizontal bed, and friction loss can be neglected (Fig. 8.3).

Comparisons of initial breach discharges computed by the above method with the explicit method-of-characteristics model are shown in Fig. 8.4. These comparisons show that initial breach discharges are mainly a function of the breach size and shape and that the effects of bed slope, bed roughness and nonprismatic channels can be neglected. Thus, the initial breach discharges computed by this method are as reliable as those computed by the explicit MOC model.

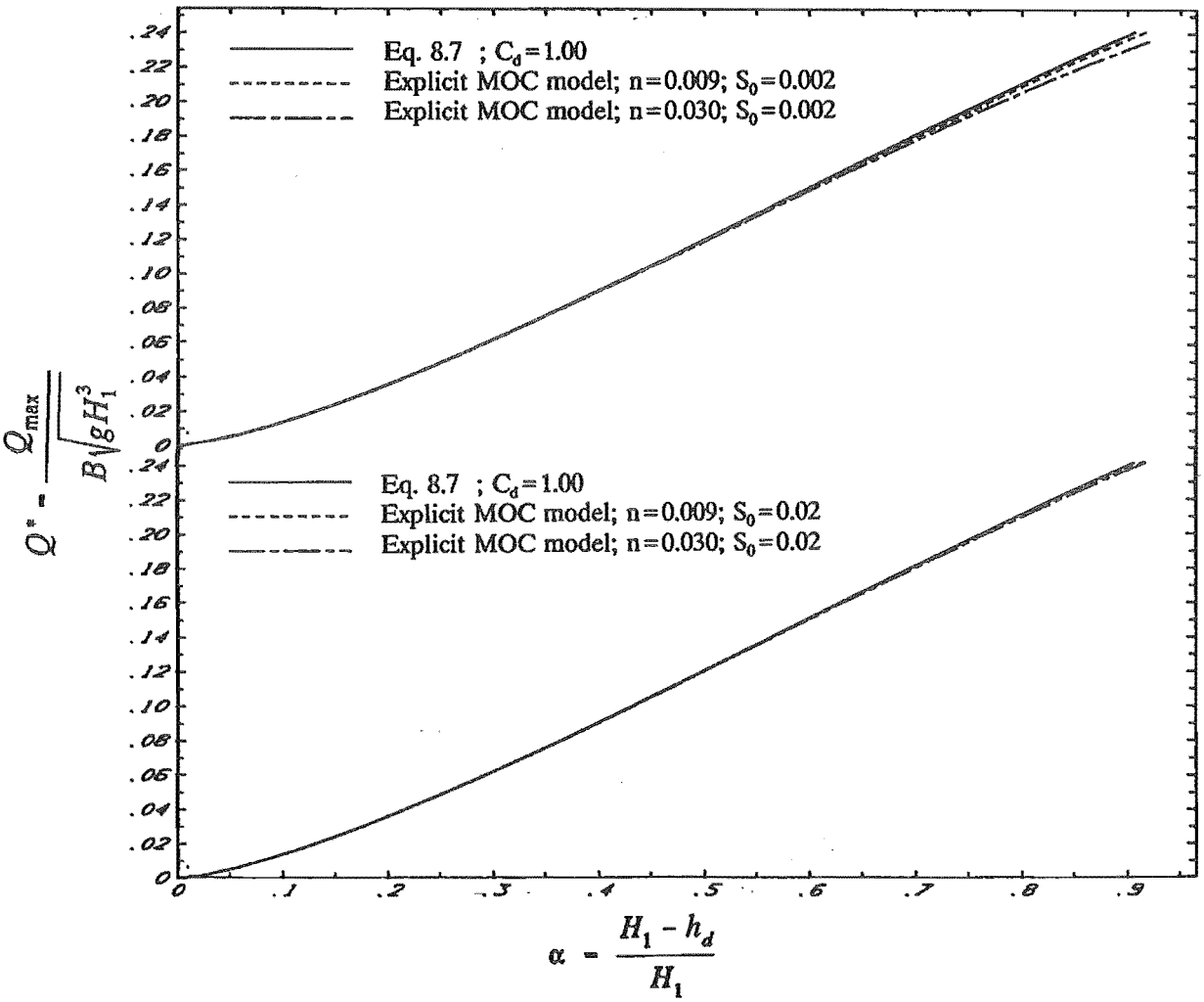

Fig. 8.4 Comparison of initial breach discharges computed by Eq. 8.7 with the corresponding results computed by the explicit MOC model, for rectangular breaches of the same width as the reservoir

8.3 Effect of Flow Resistance Within the Reservoir on the Outflow Hydrograph

The flow resistance is a shear along the bottom and sides of a channel. This force is included in the dynamic equation by introducing the friction slope, which can be evaluated by using either the Manning's or Chezy's formula. Since the friction slope is proportional to the square of the velocity, its effects on the outflow hydrographs depend on flow velocities in the channel.

A dam-break causes water within a reservoir to be accelerated. The initial accelerated discharges depend only on the initial breach sizes, and they are independent of the bed roughness and reservoir characteristics, as shown in section 8.2. Thereafter, discharges are affected by the bed roughness when water velocities become large enough to cause the flow resistance term to become significant.

The leading-negative-wave propagation speed is independent of the bed roughness. However, the height of this steep negative wave is decreased by flow resistance as it moves upstream. Its height decreases as the negative wave progress upstream. This is because the flow depths increase in the downstream region due to the flow resistance.

The effect of flow resistance on the steep negative wave can be approximated by assuming that the discharge at any cross section between the wave and the breach changes only with time. In this case, the gradually-varied steady-flow equation (equation 4.7) can be used to compute the flow depth immediately downstream from the negative wave. For a constant discharge, equation (4.7) shows that increasing the friction slope causes the depth gradient to increase and, in turn, causes the wave height to decrease.

Since the height of the steep negative wave gradually decreases with time, the accelerated flow per unit time caused by this wave decreases correspondingly in the upstream direction. This causes discharges at the breach to decrease with

time, and the water surface at the breach drops more gradually to satisfy the continuity equation.

Increasing Manning's n causes the breach discharge to decrease more rapidly for a period of time. Thereafter, the discharge decreases more gradually as flow velocities become relatively small. For a reservoir with a specific breach size and shape, the total volume depleted from the reservoir is a constant. Thus, the time needed to drain the reservoir increases as Manning's n increases, as shown in Fig. 8.5.

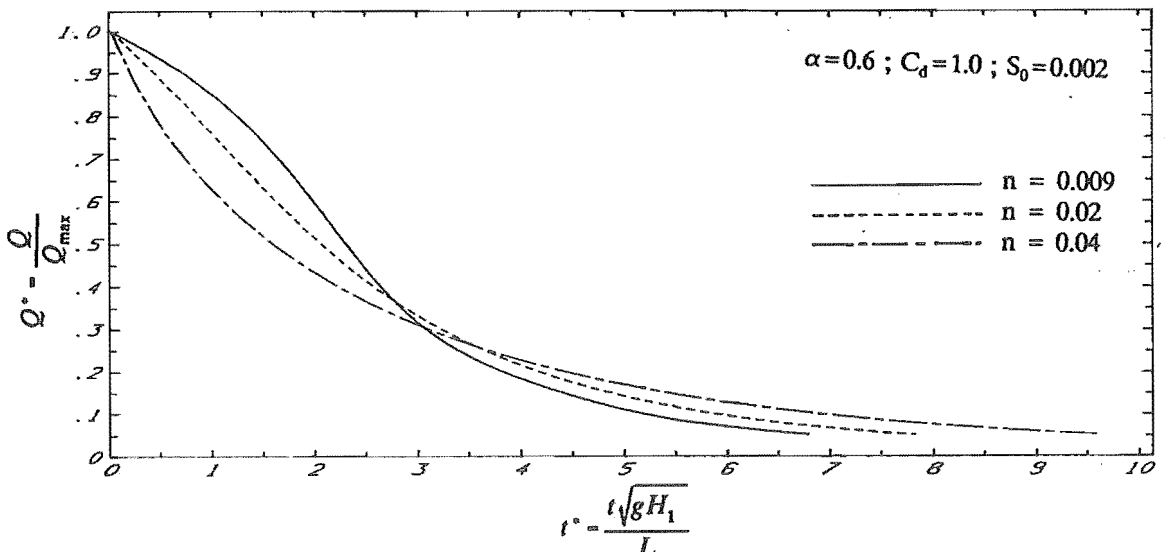

Fig. 8.5 Effect of bed roughness on the outflow hydrographs, assumed for a prismatic-rectangular channel with a sloping bed and a rectangular breach of the same width as the channel

The speed of accelerated-flow within the reservoir is a function of the height of the steep negative wave. The flow velocity is relatively slow for a small negative wave, and it is relatively fast for a large negative wave. For a small breach size, the first negative wave is relatively small. In this case, the flow resistance is small, and its effects on the outflow hydrographs are less pronounced. For a large breach size, the first negative wave is relatively large. In this case, the flow velocity within the reservoir is relatively large, and the effects of flow resistance on the outflow hydrograph are more pronounced, as shown in Fig. 8.6. Thus, the effects of the flow resistance on the outflow hydrographs depend on the breach size and become more pronounced as the breach size increases.

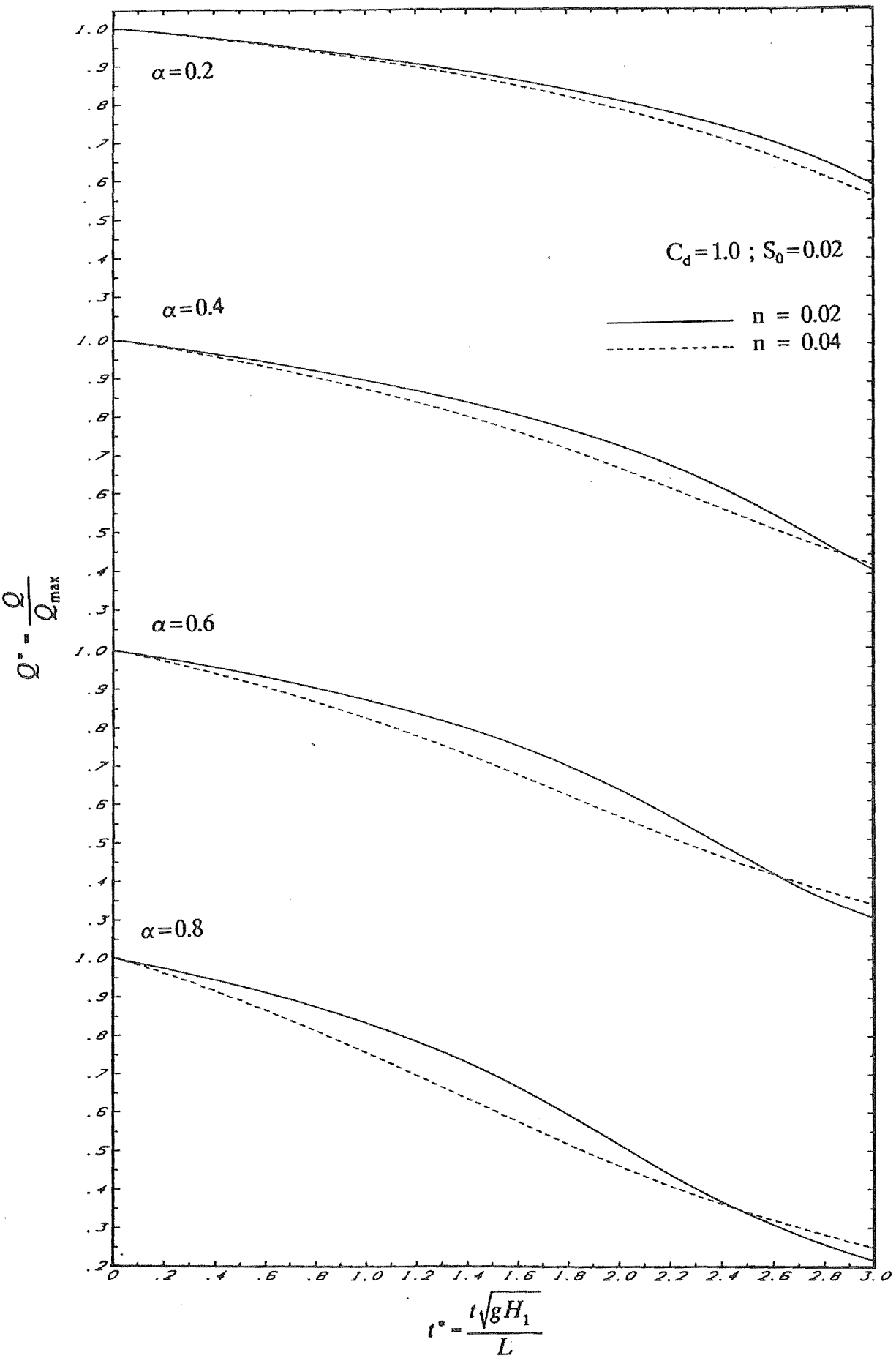

Fig. 8.6 Effect of bed roughness and breach sizes on the outflow hydrographs, assumed for a prismatic-rectangular channel with a sloping bed and rectangular breaches of the same width as the channel

8.4 Dam-Break Outflow Hydrographs

Dam-break outflow is a function of water surface elevation at a short distance upstream from the breach. Because an outflow causes a negative wave to travel upstream, this outflow tends to cause the discharge to decrease. On the other hand, increase at the upstream end tends to cause the discharge to increase. In order to determine the outflow as a function of time, a reservoir routing technique must be used to account for the simultaneous effects of reservoir inflow and reservoir storage characteristics.

Either hydrologic routing or dynamic routing methods can be used to determine dam-break outflow hydrographs. Dynamic routing methods are accurate in many situations, but they are generally complex, time-consuming and expensive solution procedures. Hydrologic routing methods are generally easier to use than dynamic routing methods and are accurate in many typical situations in which the basic assumptions are valid. Therefore, for practical solution, a numerical model may still be preferred using hydrologic routing than dynamic routing methods.

Hydrologic routing methods are based on the storage form of the continuity equation (Eq. 4.1). Reservoir volume computed by the level reservoir approximation is based on the assumption that the water surface within the reservoir is level. This approach is widely used for routing floods through reservoirs. The level reservoir approximation will give an accurate solution if the slope of the water surface is insignificant. However, if there is a significant steep wave progressing within the reservoir, this method will not give an accurate solution. Thus, the application of the level reservoir approximation is limited only to small breach sizes.

In order to get a practical method which can be used for a wide range of breach sizes, a variation of hydrologic routing methods is investigated. These methods differ from the level reservoir approximation, as described in section 4.4.1, in expressing the storage versus discharge relationships. In this proposed method,

the change in the water surface profile caused by the movement of waves within the reservoir is used to approximate the difference in the reservoir volume during the time interval Δt, as shown in figure 8.7. In order to obtain the water surface profile, the reservoir geometry is described by cross-sections and Manning roughness coefficients.

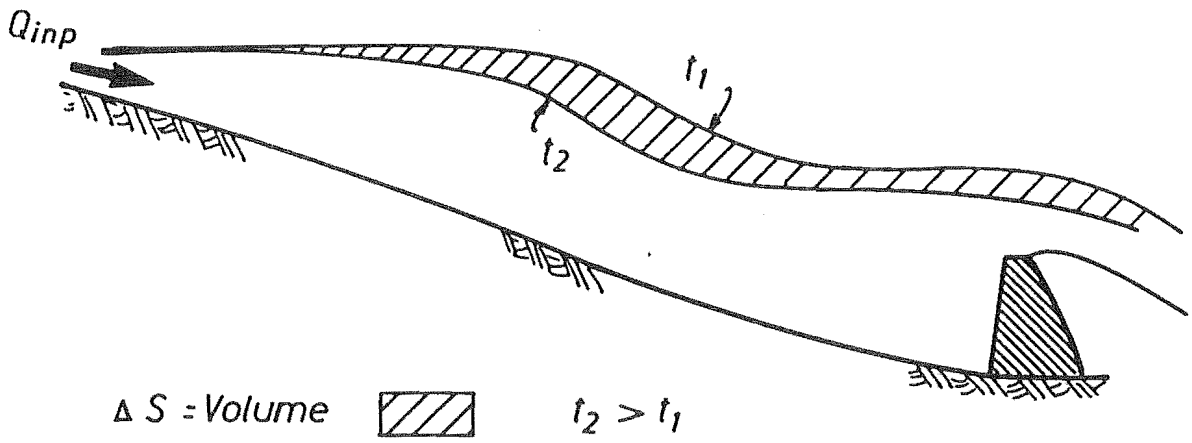

Fig. 8.7 Scheme to approximate the difference in the reservoir volume during the time interval Δt

Water surface profiles are approximated by tracing waves caused by the dam-break outflow. The type of waves progressing within the reservoir is a function of the failure time interval of the breach. Usually, it is a steep negative wave followed by a long gradually-varied negative wave. The slope of this steep negative wave decreases as the wave travels upstream. This is because the upper part of the wave travels faster than the lower part.

The movement of the steep negative wave is affected by changes in both the celerity and the inflow. For the lower part of the negative wave, its movement is also affected by the accelerated flow due to the movement of the steep negative wave. Thus, during the time Δt the negative wave travels upstream a distance :

$$\Delta x_1 = \left(C_1 - \frac{Q_{inp}}{A_1} \right) \Delta t \tag{8.8}$$

for the leading edge and

$$\Delta x_2 = \left(C_2 - \frac{Q_{inp} + Q_{acc}}{A_2} \right) \Delta t \tag{8.9}$$

for the lowest part, as shown in Fig.8.8

in which Q_{acc} is the accelerated flow caused by the movement of the steep negative wave and Q_{inp} is a specified reservoir inflow.

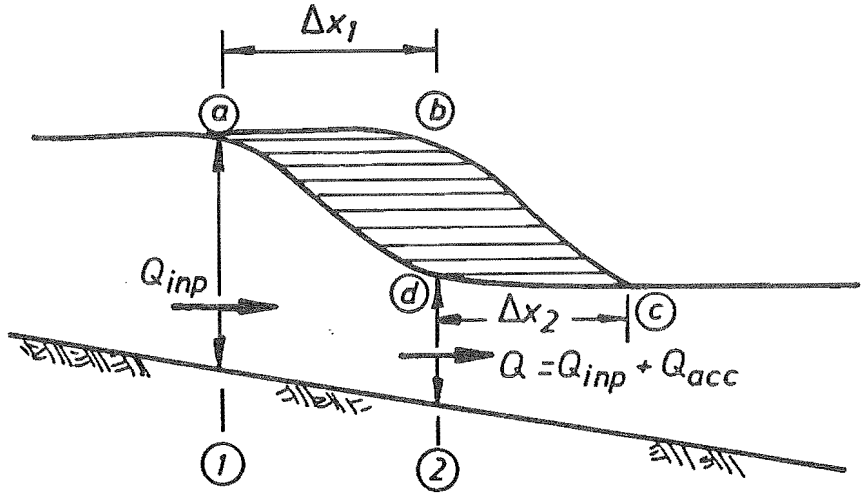

$$Q_{acc} = \frac{Volume\ (a\text{-}b\text{-}c\text{-}d)}{\Delta t}$$

Fig. 8.8 Scheme for derivation of the discharge Q_{acc} in case of movement of the steep negative wave

For a small time interval Δt the propagation celerity (C_1 or C_2) can be assumed constant in the vicinity of the cross section X_1 or X_2. For simplicity, the steep negative wave free surface is approximated with a straight line joining points 1

and 2. In this way, the accelerated flow Q_{acc} can be approximated by using equations (8.8) and (8.9) for a given height of the steep negative wave, as shown in Fig. 8.8.

The celerity (C), the flow area (A) and the accelerated flow (Q_{acc}) are functions of cross-sectional characteristics and the wave height. Values of C, A and Q_{acc} can be determined for a given cross-section, initial water depth and wave height.

For a given breach size, the initial wave height can be approximated by using equation (8.5). Having the wave height, the progression of the leading edge and the lowest part of the steep negative wave can be determined by integrating equations (8.8) and (8.9), respectively.

A steep negative wave is usually followed by a long gradually-varied negative wave after part of a dam collapse. This is because a continuous lowering of level occurs at the downstream region as the accelerated flow rate decreases with time.

Discharges and water depths between the steep negative wave and the breach are calculated by applying boundary conditions at the lowest part of the steep negative wave as a moving upstream boundary and at the dam breach as a downstream boundary.

Water surface elevations associated with the gradually-varied flow are approximated by assuming that: values of the accelerated discharges at any cross-section can be expressed in terms of a linear relationship of the corresponding values at the steep negative wave and at the dam breach. Therefore, the gradually-varied steady-flow equation (Eq. 4.7) can be used to calculate water surface elevations in the gradually-varied flow region (i.e. $Q_0 = Q_0(x,t)$ with t as a parameter).

After part of the dam collapse, water surface elevations associated with the gradually-varied flow are computed by solving equation (4.7). This equation is

solved using the Newton-Raphson method by starting at a specified elevation at the dam breach and solving the adjacent upstream elevation step by step until the upstream boundary is reached.

Water surface elevations and discharges at the dam breach are known for all time (t-Δt) prior to the current time (t) from earlier calculations or from initial boundary conditions. Because water surface profiles and the breach discharges are functions of water surface elevations at the dam breach, the difference in the reservoir volume during the time interval Δt ($\Delta S/\Delta t$) is a function of water surface elevation at the dam breach. Thus, values of the dependent variables in the storage form of continuity equation (Eq. (3.8)) can be expressed in terms of known and unknown values of water depths at the dam-breach at time t-Δt and t, respectively. This equation can be solved by using the Newton-Raphson iteration method to determine the value of water depth at the dam-breach at time (t).

A simplified model for computing dam-break outflow hydrographs, using the storage form of continuity equation (Eq. (3.8)) and taking into consideration the effect of the movement of a steep negative wave and flow resistance, consists of following steps :

(1) Compute the initial height of the steep negative wave and the initial breach discharge by using equations (8.5) and (3.2), respectively;

(2) Locate the leading of the steep negative wave with equation (8.8). Calculate an approximate location for the lowest part of the steep negative wave by using the previous estimate for C_2 and Q_{acc} in equation (8.9). Then use this result to recalculate Q_{acc} from Q_{acc}=(storage change)/Δt for use in the next iteration.

(3) Compute water depths for the gradually-varied flow region by starting with the downstream elevation calculated from the previous iteration. This assumed elevation gives a breach discharge, and Q_0 in equation (4.7) is assumed to vary linearly with x from this breach discharge to $Q_{inp}+Q_{acc}$ at the downstream end

of the steep negative wave. The depth calculated at the beginning of the steep negative wave is retained for use in step 2 in the next iteration.

(4) Integration of the flow depths computed in steps 2 and 3 gives a change in reservoir storage that is inserted in equation (3.8) to recalculate the breach discharge. If this newest breach discharge differs significantly from the value used in step 3, then the iteration is repeated by starting again with step 2.

The reservoir outflow hydrograph is developed by computing the breach discharge for each time, which goes from zero to a terminating value.

In order to assess the accuracy of the simplified model, outflow hydrographs computed by the simplified model are compared with the corresponding results from the explicit MOC model, as shown in figures 8.9 and 8.10. These comparisons show that: (1) for small breach sizes, the outflow hydrographs computed by the simplified model agree closely with the corresponding results computed by the explicit MOC model; and (2) for large breach sizes, the discharge computed by the simplified model agree relatively closely with the corresponding results computed by the explicit MOC model at any time except after the leading edge of the steep negative wave arrives at the upstream boundary at dimensionless time $t^* > 2$, in which $t^* = t\sqrt{gH_1/L}$. This is because after the leading edge arrives at the upstream boundary, the complex reflection of the steep negative wave cannot be simulated by the simplified model. Therefore, the shapes of outflow hydrographs computed by the simplified model have a slight kink at $t^* = 2$ and differ slightly with the corresponding results computed by the explicit MOC model. However, they are still in good agreement, which suggests that the simplified model maintains its accuracy for any dam breach size, reservoir bed slope and Manning roughness coefficient.

The simplified model is relatively easy and quick to use. Since it can be used for a wide range of breach sizes and gives a maximum practical level of accuracy with minimal computer time, it is an optimal choice to approximate dam-break outflow hydrographs for practical purposes.

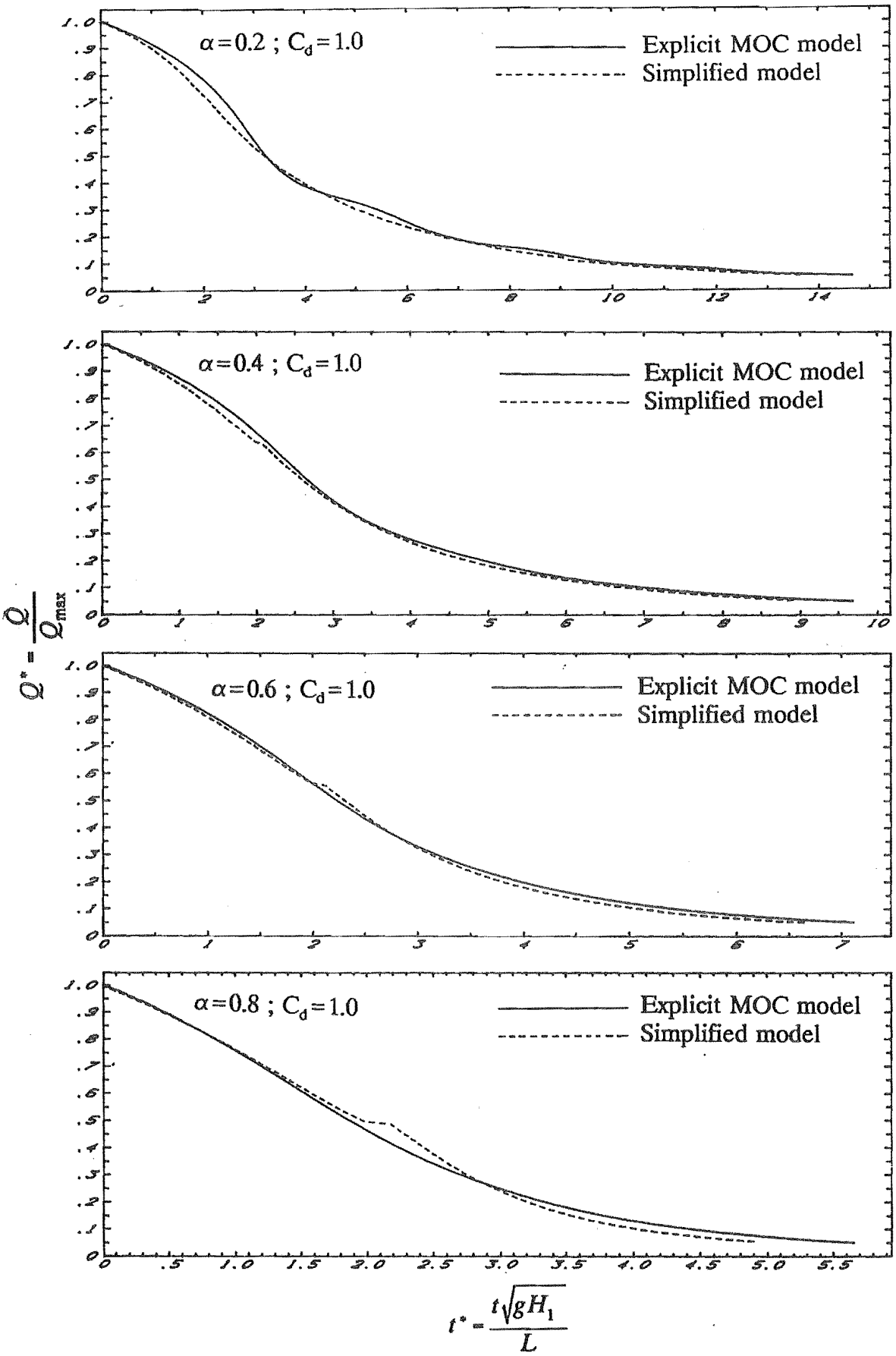

Fig. 8.9 Comparisons between reservoir outflow hydrograph computed by the simplified model and the corresponding result computed by the explicit MOC model, assumed for a prismatic-rectangular channel with $S_0=0.02$, $n=0.04$ and rectangular breaches of the same width as the channel

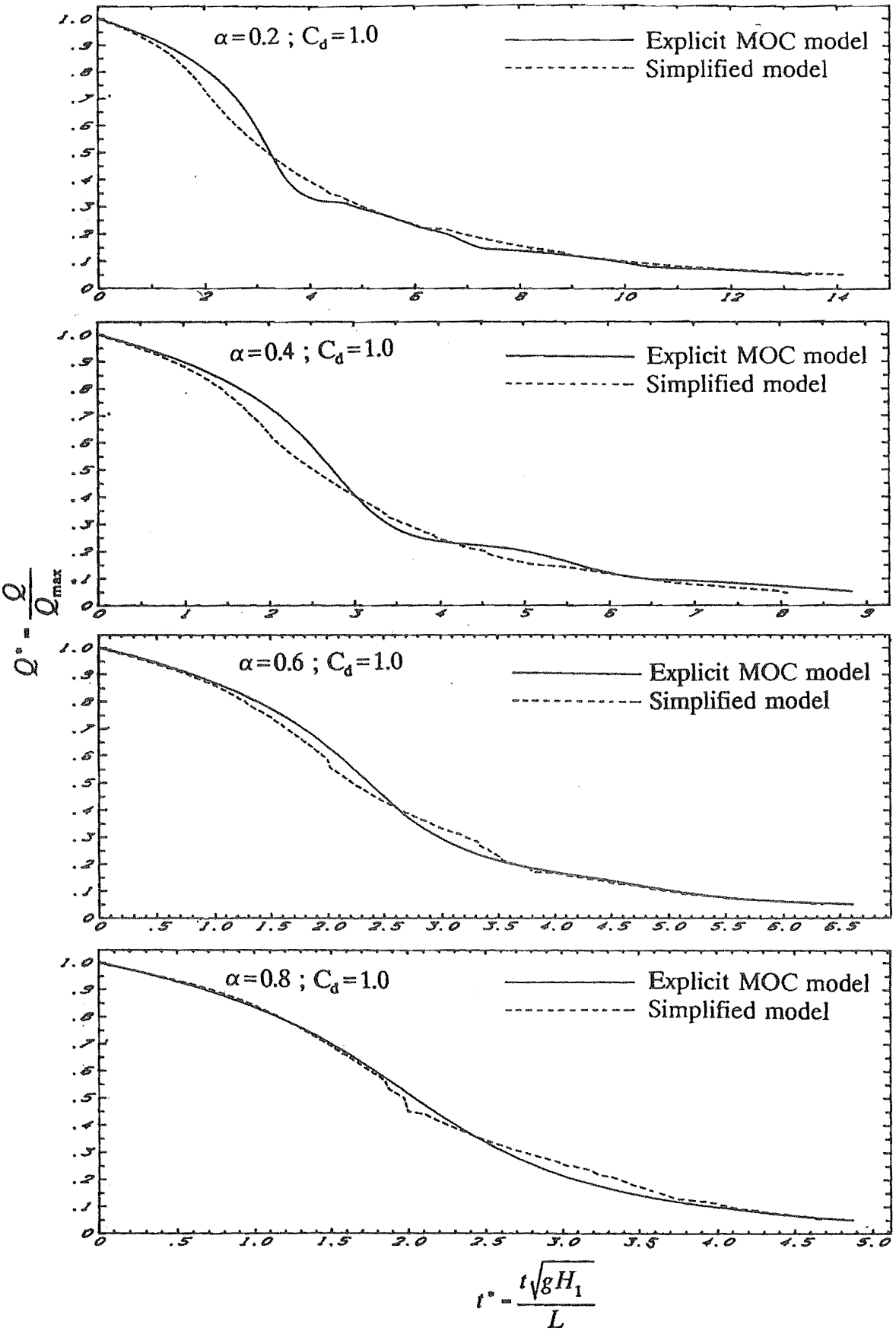

Fig. 8.10 Comparisons between reservoir outflow hydrograph computed by the simplified model and the corresponding result computed by the explicit MOC model, assumed for a prismatic-rectangular channel with $S_0=0.02$, $n=0.02$ and rectangular breaches of the same width as the channel

8.5 Conclusions

Initial breach discharges are mainly functions of the initial breach geometry and the instantaneous upstream hydraulic head. The effects of bed slope, bed roughness and nonprismatic channels on initial breach discharges can be neglected. Therefore, initial breach discharges can be expressed in terms of breach sizes for given shapes.

The effect of flow resistance on the outflow hydrographs depends on flow velocities and bed roughness along the reservoir. Because the speed of accelerated-flow increases as the breach size increases, the effect of flow resistance on the outflow hydrographs becomes more pronounced as the breach size increases. The flow resistance causes the flow velocities to decrease and, in turn, causes the breach discharge to decrease. Therefore for a reservoir with a specific breach size and shape, the time needed to drain the reservoir increases as Manning's n increases.

Dam-break outflow hydrographs are determined mainly by the movement of both the steep and the long gradually-varied waves. A relationship between initial breach discharge and breach geometry can be used to approximate the initial height of the steep negative wave, and the approximate wave height then allows the progression of the steep negative wave to be determined. The movement of the long gradually-varied negative wave, for a small distance (Δx), can be approximated by using the gradually-varied steady-flow equation.

The outflow hydrographs computed by the simplified model described above agree relatively closely with the corresponding results computed by the explicit MOC method for any breach size. Thus, a simplified model using hydrologic storage routing and taking into consideration the effect of movement of the negative waves and flow resistance can be used for a wide range of breach sizes and gives a maximum practical level of accuracy.

CHAPTER 9

GENERAL CONCLUSIONS

The major objective of this investigation has been to simulate numerically the flow resulting from either partial or gradual collapse of a dam. Four numerical models have been developed to simulate this wave. Laboratory experiments have been conducted to verify the validity of the numerical models. The numerical models have been evaluated in order to assess the accuracy, advantages and disadvantages of each model. Based on these numerical studies, approximate solutions have been developed to compute the reservoir outflow hydrograph. The major conclusions of this investigation will be divided into three sections, each reflecting a different aspect of the study.

9.1 Wave Propagation

It is very important to understand wave propagation in a reservoir caused by a dam-break. This information has been used to assess the accuracy of each of the numerical models. Based on the experimental results, the following conclusions can be drawn:

(1) A partial collapse of a dam creates a steep negative wave.

(2) The slope of the steep negative wave decreases as the failure time increases for a gradual collapse. If the failure time is very large, a steep negative wave may not be formed.

(3) The steep negative wave is followed by a long gradually-varied wave.

(4) A gradually-varied flow is the only flow in the reservoir after the reflection of the steep negative wave disappears in the downstream region.

(5) Large breach discharges may cause supercritical flow in the upstream region, in this case a surge will be formed within the reservoir.

9.2 The Numerical Models

Four numerical models have been developed to estimate dam-break flood waves. Based on comparison of model results with experiment and evaluation of the numerical models, the following conclusions can be drawn:

(1)The level-reservoir-approximation model is the simplest and quickest model. Its solution is reliable only when the computed discharge drops slowly with time, and this model always overestimates for the maximum discharge in a dam-break flood.

(2) In general, the explicit method-of-characteristics (MOC) model simulates more closely the formation and propagation of waves than either the linearized implicit finite-difference model or the linearized implicit method-of-characteristics (MOC) model . For rapidly-varied flow, the explicit MOC model gives more accurate solutions and its computer time is comparable to that required for the implicit models. In this case, the explicit MOC model is superior to the implicit models. However, for gradually-varied flow the implicit models give about the same accuracy as the explicit model and require less computational time. In this case, the explicit MOC model is inferior to the implicit models.

(3) The implicit MOC model is able to describe wave progression more closely than the implicit finite-difference model. However, the finite-difference model is more convenient to use than the implicit MOC model for rapidly-varied flow.

(4) The implicit finite-difference model, in general, simulates reasonably closely the wave formations within a reservoir. Therefore, the implicit finite-difference model is able to compute reasonably accurately outflow hydrographs caused by partial collapse of a dam.

(5) For obtaining the best resolution of a practical problem, both the method-of-characteristics models can be linked. The explicit MOC model can be used to simulate the flood wave immediately after the dam-break. After the rapidly-varied flow has dissipated, the results of the explicit MOC can be used as initial conditions for subsequent computations by using the implicit MOC model.

9.3 The Approximate Solutions

Approximate solutions have been developed to compute the reservoir outflow hydrographs. Results computed by the explicit MOC model have been used to assess the accuracy of these approximate solutions. The following conclusions can be drawn from this numerical study:

(1) Initial breach discharges can be expressed in terms of breach sizes for given shapes for an instantaneous failure of a dam.

(2) A simplified model using hydrologic storage routing and taking into consideration the upstream movement of the steep negative wave, the gradually-varied negative wave that follows this steep negative wave and flow resistance can approximate relatively accurately the outflow hydrograph for a wide range of breach sizes.

(3) The reflection of both the steep and gradually-varied negative waves and the propagation of a surge within a reservoir have a very small effect on the outflow hydrograph. Thus, they can be neglected in the computation.

REFERENCES

Abbot, M.B. (1975).
Method of Characteristics.
Unsteady Flow in Open Channels, K. Mahmood and V. Yevjevich, eds., Vol. 1, Water Resources Publications, Fort Collins, Colorado, pp. 63-88.

Abbot, M.B. (1975).
Weak Solutions of the Equations of Open Channel Flow.
Unsteady Flow in Open Channels, K. Mahmood and V. Yevjevich, eds., Vol. 1, Water Resources Publications, Fort Collins, Colorado, pp. 283-312.

Abbot, M.B. (1979).
Computational Hydraulics.
Pitman Publishing Limited, London.

Ackers, P., et al. (1978).
Weirs and Flumes for Flow Measurement.
John Wiley & Sons Ltd., New York.

Amein, M. and Fang, C.S. (1970).
Implicit Flood Routing in Natural Channels.
Journal of the Hydraulics Division, ASCE, Vol. 96, No. HY12, Proc. Paper 7773, pp. 2481-2500.

Amein, M. and Chu, H.L. (1975).
Implicit Numerical Modelling of Unsteady Flows.
Journal of the Hydraulics Division, ASCE, Vol. 101, No. HY6, pp. 717-731.

Ballofet, A., et al. (1974).
Dam Collapse Wave in a River.
Journal of the Hydraulics Division, ASCE, Vol. 100, No. HY5, pp. 645-665.

Ballofet, A. (1977).
Simulation of Dam Break Flooding Under Normal and Probable Maximum Flood Conditions.
Proceedings, Dam-Break Flood Modelling Workshop, U.S. Water Resources Council, Washington, D.C., pp. 384-401.

Baltzer, R.A. and Lai, C. (1968).
Computer Simulation of Unsteady Flows in Waterways.
Journal of the Hydraulics Division, ASCE, Vol. 94, No. HY4, pp. 1083-1117.

Bellos, C.V. and Sakkas, J.G. (1987).
1-D Dam-Break Flood-Wave Propagation on Dry Bed.
Journal of Hydraulic Engineering, ASCE, Vol. 113, No. 12, pp. 1510-1524.

Bos, M.G. (1976).
Discharge Measurement Structures.
Publications No. 20, International Institute for Land Reclamation and Improvement/ILRI, Wageningen, The Netherlands, 464 pp.

Bos, M.G., Replogle, J.A. and Clemmens, A.J. (1984).
Flow Measuring Flumes for Open Channel Systems.
John Wiley & Sons Ltd., New York

Brater, E. (1959).
Hydraulics
Civil Engineering Hand-book, edited by L.C. Urquhart, Section 4, Mc. Graw-Hill Book Co., New York, pp. 4.44-4.60.

Brown, R.J. and Rogers, D.C. (1977).
A Simulation of the Hydraulic Events During and Following the Teton Dam Failure.
Proceedings, Dam-Break Flood Modelling Workshop, U.S. Water Resources Council, Washington, D.C., pp. 131-163.

Chaudhry, Y.M. and Contractor, D.N. (1973).
Application of the Implicit Method to Surges in Open Channels.
Water Resour. Res., 9, No. 6, pp.1605-1612.

Chaudhry, M.H. and Miller, S (1989)
Dam-Break Flows in Curved Channel.
Journal of Hydraulic Engineering, ASCE, Vol. 115, No. 11, pp. 1465-1478.

Chen, C.L. and Druffel, L.A. (1977).
Dam-Break Flood Wave Computation by Method of Characteristics and Linearized Implicit Schemes.
Proceedings of Dam-Break Flood Routing Model Workshop, U.S. Water Resources Council, Washington, D.C., pp. 312-345.

Chen, C.L. and Armbruster, J.T. (1980).
Dam-Break Wave Model: Formulation and Verification.
Journal of the Hydraulics Division, ASCE, Vol. 106, No. HY5, pp. 747-767.

Chen, C.L. (1987).
Discharge and Depth behind a Partially Breached Dam.
Proceedings of the 1987 National Conference on Hydraulic Engineering, ed. by R.M. Ragan, ASCE, Williamsburg, Virginia, pp. 648-654.

Chow, V.T. (1959).
Open-Channel Hydraulics.
McGraw-Hill Book Company, New York, 680 pp.

Cunge, J.A. (1975).
Rapidly Varying Flow in Power and Pumping Canals.
Unsteady Flow in Open Channels, K. Mahmood and V. Yevjevich, eds., Vol. 2, Water Resources Publications, Fort Collins, Colorado, pp. 539-586.

Cunge, J.A., Holly, F.M.Jr. and Verwey, A. (1980).
Practical Aspects of Computational River Hydraulics.
Pitman Publishing Limited, London

De Saint-Venant, Barre (1871).
Theory of Unsteady Water Flow, With Application to River Floods and to Propagation of Tides in River Channels.
Acad. Sci. (Paris) Comptes Rendus, 73, pp. 237-240.

Dressler, R.F. (1952)
Hydraulic Resistance Effect Upon the Dam-Break Functions.
Journal of Research, National Bureau of Standards, Washington, D.C., Vol. 49, No.3, pp. 217-225.

Dressler, R.F. (1954).
Comparison of Theories and Experiments for the Hydraulic Dam-Break Wave.
Internat. Assoc. Sci. Pubs., 3, No. 38, pp. 319-328.

Fletcher, A.G. and Hamilton, W.S. (1967).
Floode Routing in an Irregular Channel.
Journal of the Engineering Mechanics Division, ASCE, Vol. 93, No. EM3, pp. 45-62.

Fread, D.L. and Harbaugh, T.E. (1973).
Transient Hydraulic Simulation of Breached Earth Dams.
Journal of the Hydraulics Division, ASCE, Vol. 99, No. HY1, pp. 139-154.

Fread, D.L. (1977).
The Development and Testing of a Dam-Break Flood Forecasting Model.
Proceedings of Dam-Break Flood Routing Model Workshop, U.S. Water Resources Council, Washington, D.C., pp. 164-197.

Fread, D.L. and Smith, G.F. (1978).
Calibration Technique for 1-D Unsteady Flow Models.
Journal of the Hydraulics Division, ASCE, Vol. 104, No. HY7, pp. 1027-1043.

Fread, D.L. (1984).
Dambrk: The NWS Dam-Break Flood Forecasting Model.
National Weather Service, Office of Hydrology, Silver Spring, Md.

French, R.H. (1985).
Open-Channel Hydraulics.
McGraw-Hill Book Company, New York

Garrison, J.M., Granju, J.P. et al (1969).
Unsteady Flow Simulation in Rivers and Reservoirs.
Journal Hydraulics Division, ASCE, Vol. 95, No. HY5, pp. 1559-1576.

Gozali, S. and Hunt, B. (1989).
Water Waves Generated by Close Landslides.
Journal of Hydraulic Research, Vol. 27, No.1, pp. 49-60.

Goldberg, D.E. and Wylie, E.B. (1983).
Characteristics Method Using Time-Line Interpolations.
Journal of Hydraulic Engineering, ASCE, Vol. 109, No. 5, pp. 670-683.

Hartree, D.R. (1952)
Some Practical Methods of Using Characteristics in the Calculation of Non-Steady Compressible Flows.
U.S. Atomic Energy Commission Report AECU-2713, Los Alamos, N.M., 44 pp.

Henderson, F.M. (1966).
Open Channel Flow.
The Macmillan Company, New York

Hunt, B. (1982).
Asymptotic Solution for Dam-Break Problem.
Journal of the Hydraulics Division, ASCE, Vol. 108, No. HY1, pp. 115-125.

Hunt, B. (1983).
Asymptotic Solution for Dam Break on Sloping Channel.
Journal of Hydraulic Engineering, ASCE, Vol. 109, No. 12, pp. 1698-1706.

Hunt, B. (1984).
Dam-Break Solution.
Journal of Hydraulic Engineering, Vol. 110, No. 6, pp. 675-685.

Hunt, B. (1984).
Perturbation Solution for Dam-Break Floods.
Journal of Hydraulic Engineering, ASCE, Vol. 110, No. 8, pp. 1058-1071.

Hunt, B. (1987).
An Inviscid Dam-Break Solution.
Journal of Hydraulic Research, Vol. 25, No. 3, pp. 313-327

Hunt, B. (1989).
The Level-Reservoir Approximation for Unsteady Flows on Sloping Channels
Journal of Hydraulic Research, Vol. 27, no.3, pp. 347-354

Ikegawa, M. and Washizu, K. (1973).
Finite Element Method Applied To Analysis of Flow Over a Spillway Crest.
Int. Journal for Numerical Methods in Engineering, Vol. 6, pp. 179-189.

Johnson, F.A., and Illes, P. (1976).
A Classification of Dam Failures.
Water Power and Dam Construction, Dec., pp. 43-45.

Katopodes, N.D. (1980).
Divergent Flow in the Vicinity of a Breached Dam.
Computer and Physical Modelling in Hydraulic Engineering, Proceeding of the Specialty Conference on American Society of Civil Engineers, New York, pp. 310-321.

Keefer, T.N. and Simons, R.K. (1977).
Qualitative Comparison of Three Dam-Break Routing Models.
Proceedings, Dam-Break Flood Modelling Workshop, U.S. Water Resources Council, Washington, D.C., pp. 292-311.

Lai, C. (1982).
Flow Computation Using Extrapolation Procedures.
Journal Hydraulics Division, ASCE, Vol. 108, No. HY11, pp. 1374-1380

Lai, C. (1986).
Numerical Modelling of Unsteady Open Channel Flow.
Advances in Hydroscience, V. T. Chow and B. C. Yen, eds., Vol. 14, Academic Press, Orlando, Fla., pp. 161-333.

Lai, C. (1988).
Comprehensive Method of Characteristics Models for Flow Simulation.
Journal of Hydraulic Engineering, ASCE, Vol. 114, No. 9, pp. 1074-1097.

Liggett, J.A. (1975).
Basic Equations of Unsteady Flow.
Unsteady Flow in Open Channels, K. Mahmood and V. Yevjevich, eds., Vol. 1, Water Resources Publications, Fort Collins, Colorado, pp. 29-62.

Liggett, J.A. and Cunge, J.A. (1975).
Numerical Methods of Solution of the Unsteady Flow Equations.
Unsteady Flow in Open Channels, K. Mahmood and V. Yevjevich, eds., Vol. 1, Water Resources Publications, Fort Collins, Colorado, pp. 89-179.

Lister, M. (1960)
The Numerical Solution of Hyperbolic Partial Differential Equations by the Method of Characteristics.
Mathematical Methods for Digital Computers, A. Ralston and H.S. Wilf, eds., John Wiley & Sons, Inc. New York.

Martin, C.S. and Zovne, J.J. (1971).
Finite-Difference Simulation of Bore Propagation.
Journal Hydraulics Div., ASCE, Vol. 97, No. HY7, pp. 993-1010.

Menendez, A.N. and Navarro, F. (1990).
An Experimental Study on the Continuous Breaking of a Dam.
Journal of Hydraulic Research, Vol. 28, No. 6, pp. 753-772.

Ponce, V.M. and Tsivoglou, A.J. (1981).
Modelling Gradual Dam Breaches.
Journal Hydraulics Division, ASCE, 107(7), pp. 829-838.

Preissmann, A. (1961)
Propagation of Translatory Waves in Channels and Rivers.
Paper presented at First Congress of French Assoc. for Computation, Grenoble, Sept. 14-16, Proceedings, AFCAL, pp. 433-442.

Preissmann, A. and Cunge, J.A. (1961).
Calcul des intumescences sur machines e'lectronique.
IX meeting of the IAHRE, Dubrovnik.

Price, J.J., Lowe, G.W. and Garrison, J.M. (1974).
Hydralic Transients Generated by Partial and Total Failures of Large Dams.
Paper Presented at August 1974 Hydraulics Division Specialty Conference, Knoxville, Tennessee.

Price, R.K. (1974)
Comparison of Four Numerical Methods for Flood Routing.
Journal of the Hydraulics Division, ASCE, Vol. 100, No. HY7, pp. 879-899.

Price, J.T., Lowe, G.W. and Garrison, J.M. (1977).
Unsteady Flow Modelling of Dam-Break Waves.
Proceedings, Dam-Break Flood Modelling Workshop, U.S. Water Resources Council, Washington, D.C., pp. 90-130.

Rajar, R. (1978).
Mathematical Simulation of Dam-Break Flow.
Journal of the Hydraulics Division, ASCE, Vol. 104, No. HY7, pp. 1011-1026.

Ritter, A. (1892).
The Propagation of Water Waves.
Ver. Deutsch Ingenieure Zeitschr. (Berlin),36, Pt. 2, No. 33, pp. 947-954.

Sakkas, J.G. and Strelkoff, T. (1973).
Dam-Break Flood in a Prismatic Dry Channel.
Journal of the Hydraulic Division, ASCE, Vol. 99, No. HY12, pp. 2195-2216.

Sakkas, J.G. and Strelkoff, T. (1976).
Dimensionless Solution of Dam-Break Flood Waves.
Journal of the Hydraulics Division, ASCE, Vol. 102, No. HY2, pp. 171-184.

Schmitz, G. and Edenhofer, G. (1983).
Flood Routing in the Danube River by the New Implicit Method of Characteristics (IMOC).
Proc. 3 rd Int. Conf. on Applied Mathematical Modelling, Mitteil., Inst. fur Meereskunde, University of Hamburg, Hamburg, FRG, 1-13.

Schocklithsch, A. (1917)
On Waves Created by Dam Breaches.
Akad. Wiss. (Vienna) Proc., 126, Pt. 2A, pp. 1489-1514.

Serafim, J.L. and Coutinho-Rodrigues, J.M. (1989).
Statistics of Dam Failures: A Preliminary Report.
Water Power and Dam Construction, April, pp. 30-34.

Singer, J. (1964).
Square-edged broad-crested weir as a flow measurement device.
Water and Water Engineering, Vol. 28, No. 820, pp 229-235.

Singh, V.P. and Scarlatos, P.D. (1988).
Analysis of Gradual Earth-Dam Failure.
Journal of Hydraulic Engineering, ASCE, Vol. 114, No. 1, pp. 21-42.

Singh, V.P. and Quiroga, C.A. (1987).
Dimensionless Analytical Solutions for Dam-Breach Erosion.
Journal of Hydraulic Research, Vol. 26, No. 2, pp. 179-197.

Stoker, J.J. (1957).
Water Waves.
Interscience Publishers, New York.

Streeter, V.L. and Wylie, E.B. (1975).
Fluid Mechanics.
McGraw-Hill Book Company, New York

Strelkoff, T. (1970).
Numerical Solution of Saint-Venant Equations.
Journal of the Hydraulics Division, ASCE, Vol. 96, No. HY1, pp. 223-252.

Su, S.T. and Barnes, A.H. (1970).
Geometric and Frictional Effects on Sudden Releases.
Journal of the Hydraulics Division, ASCE, Vol. 96, No. HY11, Proc. Paper 7670, pp. 2185-2200

Teton Dam Verdict (1977).
Teton Dam Verdict: A Foul-up by the Engineers.
Science, American Association for the Advancement of Science, Vol. 195, pp. 270-272.

Terzidis, G. and Strelkoff, T. (1970).
Computation of Open Channel Surges and Shocks.
Journal Hydraulics Division, ASCE, Vol. 96, No. HY12, pp. 2581-2610.

Tous Dam (1982).
Storm Ferocity Wipes Out Tous Dam.
New Civil Engineer International, Dec., pp. 23-24.

Townson, J.M. and Al-Salihi, A.H. (1989)
Models of Dam-Break Flow in R-T Space.
Journal of Hydraulic Engineering, ASCE, Vol. 115, No. 5, pp. 561-575.

U.S. Army Corps of Engineers (1960).
Floods Resulting from Suddenly Breached Dams: Conditions of Minimum Resistance.
Hydraulic Model Investigation, Miscellaneous Paper No. 2-374, Report No. 1, Waterways Experiment Station, Vicksburg, Mississippi

U.S. Army Corps of Engineers (1961).
Floods Resulting from Suddenly Breached Dams: Conditions of High Resistance.
Miscellaneous Paper No. 2-374, Report No. 2, Waterways Experiment Station, Vicksburg, Mississippi

Varoglu, E. and Finn, W.D.L. (1978).
Variable Domain Finite Element Analysis of Free Surface Gravity Flow.
Computer and Fluids, Vol. 6, pp. 103-114

Whitham, G.B. (1955).
The Effects of Hydraulic Resistance in the Dam-Break Problems.
Proceedings, Royal Society of London, Series A, Vol. 227, No. 1170, pp. 399-407.

Wortman, R.T. (1989).
Spillway Discharge Calculations in NWS DAMBRK.
Journal of Hydraulic Engineering, Vol. 115, No. 7, pp. 975-981.

Wylie, E.B. (1970).
Unsteady Free-Surface Flow Computations.
Journal of the Hydraulics Division, Vol. 96, No. HY11, pp. 2241-2251.

Wylie, E.B. (1980).
Inaccuracies in the Characteristics Method.
Proc. of the Specialty Conference on Computer and Physical Modelling in Hydraulic Engineering, August 6-8. George A., Editor, ASCE, New York, pp. 165-176

Wurbs, R.A. (1987).
Dam-Breach Flood Wave Models.
Journal of the Hydraulics Division, ASCE, Vol. 113, No. 1, pp. 29-46.

Yevjevish, V. (1975).
Sudden Water Release.
Unsteady Flow in Open Channels, K. Mahmood and V. Yevjevich, eds., Vol. 2, Water Resources Publications, Fort Collins, Colorado, pp. 587-665.

APPENDIX A

DERIVATION OF THE CHARACTERISTIC EQUATIONS

Unsteady flow in nonprismatic channel can be expressed by the continuity and the conservation of momentum equations, respectively:

$$B\frac{\partial h}{\partial t} + U\left(\frac{\partial A}{\partial x}\right)_h + UB\frac{\partial h}{\partial x} + A\frac{\partial U}{\partial x} = 0 \qquad \text{(A.1)}$$

$$\frac{\partial U}{\partial t} + U\frac{\partial U}{\partial x} + g\frac{\partial h}{\partial x} = g(S_0 - S_f) \qquad \text{(A.2)}$$

Multiplying equation (A.1) by λ and adding to equation (A.2) result in

$$\left[(\lambda A + U)\frac{\partial U}{\partial x} + \frac{\partial U}{\partial t}\right] + \lambda\left[U\left(\frac{\partial A}{\partial x}\right)_h + UB\frac{\partial h}{\partial x} + \frac{g}{\lambda}\frac{\partial h}{\partial x} + B\frac{\partial h}{\partial t}\right] = g(S_0 - S_f) \qquad \text{(A.3)}$$

or

$$\left[(\lambda A + U)\frac{\partial U}{\partial x} + \frac{\partial U}{\partial t}\right] + \lambda B\left[U\left(\frac{\partial A}{\partial x}\right)_h + \left(\frac{\lambda U + \frac{g}{B}}{\lambda}\right)\frac{\partial h}{\partial x} + \frac{\partial h}{\partial t}\right] = g(S_0 - S_f) \qquad \text{(A.4)}$$

Let

$$\frac{dx}{dt} = \lambda A + U = \frac{\lambda U + \frac{g}{B}}{\lambda} \qquad \text{(A.5)}$$

The solution of the quadratic equation (A.5) for λ is

$$\lambda = \pm \sqrt{\frac{g}{A\,B}} \tag{A.6}$$

Thus, inserting equation (A.6) in equation (A.5) gives

$$\frac{dx}{dt} = U \pm \sqrt{\frac{g\,A}{B}} = U \pm C \tag{A.7}$$

in which C = celerity of a disturbance in the fluid when U = 0. Inserting equation (A.7) in equation (A.4) leads to the characteristic equations:

$$\frac{dU}{dt} + \frac{g}{C}\frac{dh}{dt} = g\,(S_0 - S_f) - \frac{U}{A}\,C\left(\frac{\partial A}{\partial x}\right)_h \tag{A.8}$$

along the forward characteristic C^+

$$\frac{dx}{dt} = U + C \tag{A.9}$$

and

$$\frac{dU}{dt} - \frac{g}{C}\frac{dh}{dt} = g\,(S_0 - S_f) + \frac{U}{A}\,C\left(\frac{\partial A}{\partial x}\right)_h \tag{A.10}$$

along the backward characteristic C^-

$$\frac{dx}{dt} = U - C \tag{A.11}$$

APPENDIX B

THE TWO COMPABILITY EQUATIONS IN THE IMPLICIT MOC MODEL

For any pair of grid points (j,j+1) as shown in Fig. 4.7, the two compability equations along the forward (C^+) and the backward (C^-) characteristics can be written as:

$$\frac{g}{C_{L_{j+1}M_{j+1}}}\left(h_{M_{j+1}}-(\tau_j h_{N_j}+\tau_j' h_{M_j})\right)+U_{M_{j+1}}-(\tau_j U_{N_j}+\tau_j' U_{M_j})$$

$$=\left(g(S_0-S_f)\ -\ \frac{U}{A}C\left(\frac{\partial A}{\partial x}\right)_h\right)_{L_{j+1}M_{j+1}}\tau_j\Delta t \qquad \text{(B.1)}$$

$$\frac{g}{C_{R_jM_j}}\left(-h_{M_j}+(\eta_{j+1}h_{N_{j+1}}+\eta_{j+1}' h_{M_{j+1}})\right)+U_{M_j}-(\eta_{j+1}U_{N_{j+1}}+\eta_{j+1}' U_{M_{j+1}})$$

$$=\left(g(S_0-S_f)\ +\ \frac{U}{A}C\left(\frac{\partial A}{\partial x}\right)_h\right)_{R_jM_j}\eta_{j+1}\Delta t \qquad \text{(B.2)}$$

These equations can be written symbolically as :

$$A' h_{j+1}^{i+1}\ +\ B' U_{j+1}^{i+1}\ +\ C' h_j^{i+1}\ +\ D' U_j^{i+1}\ +\ G' = 0 \qquad \text{(B.4)}$$

$$A\,h_{j+1}^{i+1} + B\,U_{j+1}^{i+1} + C\,h_j^{i+1} + D\,U_j^{i+1} + G = 0 \tag{B.3}$$

where

$$A = \frac{g}{C_{L_{j+1}M_{j+1}}} \tag{B.5}$$

$$B = 1 \tag{B.6}$$

$$C = -\frac{g}{C_{L_{j+1}M_{j+1}}}\,\tau_j' \tag{B.7}$$

$$D = -\tau_j' \tag{B.8}$$

$$G = -\left[\frac{g}{C_{L_{j+1}M_{j+1}}}h_j^i + U_j^i - \left(g(S_0 - S_f) - \frac{U}{A}C\left(\frac{\partial A}{\partial x}\right)_h\right)_{L_{j+1}M_{j+1}}\Delta t\right]\tau_j \tag{B.9}$$

$$A' = \frac{g}{C_{R_jM_j}}\,\eta_{j+1}' \tag{B.10}$$

$$B' = -\eta'_{j+1} \tag{B.11}$$

$$C' = -\frac{g}{C_{R_jM_j}} \tag{B.12}$$

$$D' = 1 \tag{B.13}$$

$$G' = -\left[-\frac{g}{C_{R_jM_j}} h^i_{j+1} + U^i_{j+1} - \left(g(S_0 - S_f) + \frac{U}{A} C \left(\frac{\partial A}{\partial x}\right)_h\right)_{R_jM_j} \Delta t\right] \eta_{j+1} \tag{B.14}$$

APPENDIX C

THE TWO LINEAR EQUATIONS IN THE IMPLICIT FINITE-DIFFERENCE MODEL

The implicit finite-difference model is based on the two non-linear algebraic equations in terms of z_j^{i+1}, Q_j^{i+1}, z_j^i, Q_j^i (Eqs. (3.53) and (3.54)). Substituting $z_j^{i+1}=z_j^i+\Delta z$ and $Q_j^{i+1}=Q_j^i+\Delta Q$ in equations (3.53) and (3.54) leads to a system of two non-linear algebraic equations in terms of Δz_j, ΔQ_j, Δz_{j+1} and ΔQ_{j+1}. The equations can be linearized in terms of unknowns Δz_j and ΔQ_j, $j=1,2,..,N$ as described by Liggett and Cunge (1975). For any pair of grid points $(j,j+1)$, the system of two linearized algebraic equations can be written as follows:

$$A\,\Delta z_{j+1} + B\,\Delta Q_{j+1} + C\,\Delta z_j + D\,\Delta Q_j + G = 0 \qquad \text{(C.1)}$$

$$A'\Delta z_{j+1} + B'\Delta Q_{j+1} + C'\Delta z_j + D'\Delta Q_j + G' = 0 \qquad \text{(C.2)}$$

where

$$A = 1 - \frac{4\theta\Delta t}{\Delta x}\,\frac{Q_{j+1}-Q_j}{(B_{j+1}+B_j)^2}\,\frac{dB_{j+1}}{dz_{j+1}} \qquad \text{(C.3)}$$

$$B = \frac{4\theta\Delta t}{\Delta x}\frac{1}{B_{j+1}+B_j} \tag{C.4}$$

$$C = 1 - \frac{4\theta\Delta t}{\Delta x}\frac{Q_{j+1}-Q_j}{(B_{j+1}+B_j)^2}\frac{dB_j}{dz_j} \tag{C.5}$$

$$D = -\frac{4\theta\Delta t}{\Delta x}\frac{1}{B_{j+1}+B_j} \tag{C.6}$$

$$G = \frac{4\Delta t}{\Delta x}\frac{Q_{j+1}-Q_j}{B_{j+1}+B_j} \tag{C.7}$$

$$A' = -\frac{1}{2}\left(\frac{Q_{j+1}B_{j+1}}{A_{j+1}}+\frac{Q_jB_j}{A_j}\right)+\theta\frac{\Delta t}{\Delta x}\left\{(Q_{j+1}-Q_j)\left(\frac{Q_{j+1}}{A_{j+1}}\frac{d\alpha_{j+1}}{dz_{j+1}}-\frac{Q_{j+1}B_{j+1}\alpha_{j+1}}{A_{j+1}^2}\right)\right.$$

$$-B_{j+1}\left(\frac{\alpha_{j+1}Q_{j+1}^2}{A_{j+1}^2}+\frac{\alpha_jQ_j^2}{A_j^2}\right)-\frac{Q_{j+1}^2}{A_{j+1}^2}(A_{j+1}-A_j)\left(\frac{d\alpha_{j+1}}{dz_{j+1}}-\frac{2\alpha_{j+1}B_{j+1}}{A_{j+1}}\right)+gB_{j+1}(z_{j+1}-z_j)$$

$$\left.-\frac{Q_{j+1}^2B_{j+1}}{2A_{j+1}^2}(\alpha_{j+1}-\alpha_j)+g(A_{j+1}+A_j)+\frac{1}{2}\left(\frac{Q_{j+1}^2}{A_{j+1}}+\frac{Q_j^2}{A_j}\right)\frac{d\alpha_{j+1}}{dz_{j+1}}\right\}$$

$$-g\theta\Delta t\frac{Q_{j+1}|Q_{j+1}|}{K_{j+1}^2}\left(B_{j+1}-\frac{2A_{j+1}}{K_{j+1}}\frac{dK_{j+1}}{dz_{j+1}}\right) \tag{C.8}$$

$$B' = 1 + \frac{\theta \Delta t}{\Delta x}\left(\frac{\alpha_{j+1} Q_{j+1}}{A_{j+1}} + \frac{\alpha_j Q_j}{A_j} + (Q_{j+1} - Q_j)\frac{\alpha_{j+1}}{A_{j+1}} - (A_{j+1} - A_j)\frac{2\alpha_{j+1} Q_{j+1}}{A_{j+1}^2} \right.$$

$$\left. + (\alpha_{j+1} - \alpha_j)\frac{Q_{j+1}}{A_{j+1}} \right) - 2g\theta \Delta t \frac{A_{j+1}|Q_{j+1}|}{K_{j+1}^2} \qquad \text{(C.9)}$$

$$C' = -\frac{1}{2}\left(\frac{Q_{j+1} B_{j+1}}{A_{j+1}} + \frac{Q_j B_j}{A_j} \right) + \theta \frac{\Delta t}{\Delta x}\left\{ (Q_{j+1} - Q_j)\left(\frac{Q_j}{A_j}\frac{d\alpha_j}{dz_j} - \frac{Q_j B_j \alpha_j}{A_j^2} \right) \right.$$

$$- B_j\left(\frac{\alpha_{j+1} Q_{j+1}^2}{A_{j+1}^2} + \frac{\alpha_j Q_j^2}{A_j^2} \right) + \frac{Q_j^2}{A_j^2}(A_{j+1} - A_j)\left(\frac{d\alpha_j}{dz_j} - \frac{2\alpha_j B_j}{A_j} \right) - gB_j(z_{j+1} - z_j)$$

$$\left. + \frac{Q_j^2 B_j}{2A_j^2}(\alpha_{j+1} - \alpha_j) + g(A_{j+1} + A_j) + \frac{1}{2}\left(\frac{Q_{j+1}^2}{A_{j+1}} + \frac{Q_j^2}{A_j} \right)\frac{d\alpha_j}{dz_j} \right\}$$

$$- g\theta \Delta t \frac{Q_j|Q_j|}{K_j^2}\left(B_j - \frac{2A_j}{K_j}\frac{dK_j}{dz_j} \right) \qquad \text{(C.10)}$$

$$D' = 1 + \frac{\theta \Delta t}{\Delta x}\left(-\frac{\alpha_{j+1} Q_{j+1}}{A_{j+1}} - \frac{\alpha_j Q_j}{A_j} + (Q_{j+1} - Q_j)\frac{\alpha_j}{A_j} - (A_{j+1} - A_j)\frac{2\alpha_j Q_j}{A_j^2} \right.$$

$$\left. + (\alpha_{j+1} - \alpha_j)\frac{Q_j}{A_j} \right) - 2g\theta\Delta t \frac{A_j |Q_j|}{K_j^2} \qquad \text{(C.11)}$$

$$G' = \frac{\Delta t}{\Delta x}\left\{ (Q_{j+1} - Q_j)\left(\frac{\alpha_{j+1} Q_{j+1}}{A_{j+1}} + \frac{\alpha_j Q_j}{A_j} \right) - (A_{j+1} - A_j)\left(\frac{\alpha_{j+1} Q_{j+1}^2}{A_{j+1}^2} - \frac{\alpha_j Q_j^2}{A_j^2} \right) \right.$$

$$\left. + g(z_{j+1} - z_j)(A_{j+1} + A_j) + \left(\frac{Q_{j+1}^2}{2A_{j+1}} + \frac{Q_j^2}{2A_j} \right)(\alpha_{j+1} - \alpha_j) \right\}$$

$$- g\Delta t \left(\frac{Q_{j+1} |Q_{j+1}| A_{j+1}}{K_{j+1}^2} + \frac{Q_j |Q_j| A_j}{K_j^2} \right) \qquad \text{(C.12)}$$